# Antenna Design for Mobile Satellite Communications

June 2016

**Adriana M. Oprian**

Project report

Aalborg University
Department of Electronic Systems
Wireless Communication Systems
Fredrik Bajers Vej 7
DK-9220 Aalborg

**Electronics and IT**
Aalborg University
http://www.aau.dk

# AALBORG UNIVERSITY
## STUDENT REPORT

**Title:**
Antenna Design for Mobile Satellite Communications

**Theme:**
L-band handset antenna for satellite communication (with focus on the antenna design)

**Project Period:**
Spring Semester 2016

**Project Group:**
1055

**Participant(s):**
Adriana Mihaela Oprian

**Supervisor(s):**
Alexandru Tatomirescu
Gert Frølund Pedersen

**Copies:** 1

**Page Numbers:** 106

**Date of Completion:**
June 2, 2016

**Abstract:**

The aim of this study is to design an antenna for mobile satellite communication that can be integrated in a modular phone. The initial idea was to find a solution for mobile satellite communications that is more agreeable and manageable than the existing satellite phones. To design such a product it is important to understand the parameters and operation of an antenna, but also the requirements of a satellite link. Another important and challenging aspect of this study is that the antenna consists of an array of elements that will allow beam steering.

By choosing a mobile satellite communication operator, a set of requirements will be established for the operation of the antenna, which have a major impact on the design. The implementation is performed in an electromagnetic simulation software starting from the design of a single element and continuing with the implementation of a linear and eventually a planar array. Each form of implementation presents advantages and disadvantages which are presented and discussed throughout this project.

The results of the array performance in terms of gain and axial ratio were in agreement with the link budget requirements, but when steering the beam the performance worsens.

# Contents

# Chapter 1

# Introduction

Satellite systems have evolved considerably in the last years, making possible a relliable way of mobile communications. In the beginning the satellite performances in terms of resources and applications were reduced, requiring very large ground station antennas and offering limited services such as long distance telephony and television signals. Now that technology has evolved, satellites are more powerful and can fulfill a larger area of services with an improved quality, allowing direct transmission to users' terminals, without needing intermediary nodes. Through satellites, users can have wider coverage than the one offered by the cellular networks [1].

The existing phones for mobile satellite communications have a cluncky aspect with dimensions varying from 140x60x27mm to 170x54x39 mm (L x W x H), most of them having external antenna [2].The modern smartphones on the other hand have a slim design with dimensions in the range of 138 x 67 x 6.9 mm to 160 x 83 x 10 mm [3] [4]. In case of the smartphones, the antenna is almost always internal and its implementation is getting more difficult as the smartphones' functions are getting more advanced and diverse, having to keep a low profile design. Figure 1.1 shows the modern smartphones in the left side and the modern satellite phones in the right side.

New smartphones design adopt a custom design that changes to a certain degree according to each individual user known as modular phones. A modular phone is a mobile phone that can be assembled from individual parts that include a camera, processor, internal storage, battery and so on, as shown in Figure 1.2. In this way, the user is free to pick, replace and upgrade the parts according to his needs and preferences [6]. Although the modular phone is a good solution for the user, it represents a challenge for the engineers, who will have to limit the design of each function to the dimensions of the available tiles.

The challenge lies not only in the antenna low profile design but also in developing a product that takes into consideration the user implication. It has been shown that the way in which a user handles the phone impacts strongly the performances of the antenna [8]. Satellite phones have precise requirements regarding usability from handling the phone to background considerations. To assure a flexibility to these requirements and offer the user a less rigid solution, an antenna array with beam steering capabilities is intended. The benefits of the array beside flexibility in handling are also increased gain and easier reconfigurability in the case the user changes location or position of the phone [9].

The purpose of this study is to design a low profile antenna array for mobile satellite communications in L-band. The motivation of this project lies in implementing an user friendly solution for situations in which terrestrial mobile services are not available. Beside a reliable way of communications, this also represents a managable and

**Figure 1.1:** Smartphones compared to satellite phones (source: [5])

**Figure 1.2:** Modular smartphone Ara (source: [7])

simple solution for emercengy situations and disaster scenarios given the almost worlde wide coverage of the satellites constelation [10].

**Report structure**

Chapter 2 presents a brief introduction of the satellite communications parameters, system description and modular phone implementation. These will conclude in a description of the main purpose and expectations of the project. In Chapter 3 a theoretical presentation of the chosen solution is made, while the actual design is introduced in Chapter 4. Chapter 4 describes in detail the development process, starting from the design of a single element and continuing with a 1x2 array and 2x2 array implementation. The beam steering capabilities of the arrays are also included in this chapter, along with the performance of the antenna in the link budget. Chapter 5 deals with the implementation of the prototype and the implications of a beam forming network. Eventually, in Chapter 6, a conclusion of the project is drawn based on the information found and presented throughout the report. Various implementations and additional theory are added in the appendix.

# Chapter 2

# Prestudy

This chapter presents the fundamentals of satellite communications system. In the beginning of the chapter a presentation of the main link parameters is made, followed by a description of a mobile satellite communications provider and a description of a modular phone. The reason for these descriptions is to have a real case study and a definition of the ground requirements which together with the link parameters will lead to the design delimitation.

## 2.1 Satellite Communications System

### 2.1.1 Satellite Link Parameters

This section will describe a satellite link and the main parameters that define and affect the radio segment of the satellite link. All these paramteres represent the input for the link budget calculation, which reflects the performance of the link. The link budget accounts all losses from the transmitter to the receiver and shows the minimum requirements for achieving a certain performance level in terms of a chosen parameter [11].

Figure 2.1 describes the link itself, composed of two air links, *forward link* (Earth station A $\rightarrow$ Earth station B) and *return link* (Earth station B $\rightarrow$ Earth station A), each having an *uplink* (Earth station $\rightarrow$ Satellite) and *downlink* (Satellite $\rightarrow$ Earth station) [12]. As mentioned above, the main input parameters and their definition are further presented.

#### Free Space Path Loss

The free space path loss, as the name suggests, affects all radio waves which travel in free space or in a medium with characteristics close to those of free space, which is the case of earth's atmosphere. The free space path loss is defined as [12]:

$$L_{FS} = (\frac{4\pi r}{\lambda})^2 \tag{2.1}$$

which in dB can be written as:

$$L_{FS} = 20\log(\frac{2\pi r}{\lambda}) \text{ [dB]} \tag{2.2}$$

where $r$ is the distance between the transmitter and receiver and $\lambda$ is the wave length.

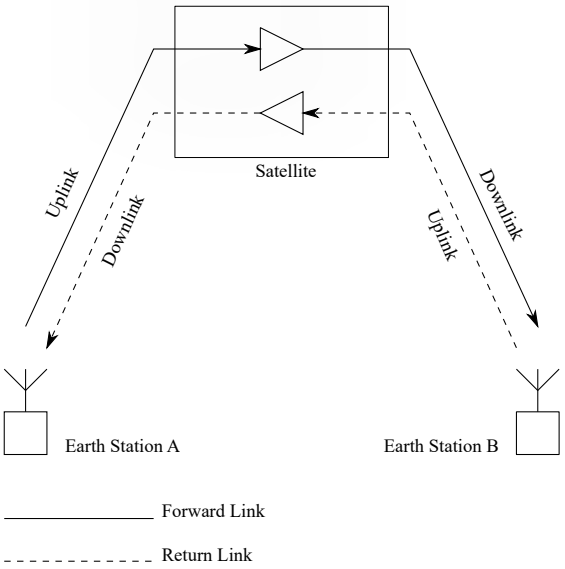


**Figure 2.1:** Satellite Link

### Effective Isotropic Radiated Power

The *EIRP* unifies the transmitter performance in a single parameter and is defined as [12]:

$$EIRP = P_t G_t \tag{2.3}$$

which in dB can be written as:

$$EIRP = P_t + G_t \text{ [dBW]} \tag{2.4}$$

where $P_t$ is the transmission power and $G_t$ is the gain of the transmitting antenna.

### Figure of Merit (G/T)

The *figure of merit* is a parameter that quantifies the efficiency of the receiver in a satellite communications link and is defined as the ratio between the receiver antenna gain and the receiver system noise temperature. The figure of merit is written as [12]:

$$M = \frac{G}{T} \tag{2.5}$$

which in dB can be written as:

$$M = G_r - T_r \text{ [dB/K]} \tag{2.6}$$

where $G_r$ is the gain of the receiver antenna and $T_r$ is the system noise temperature in K.

**Carrier to Noise Ratio**

The *carrier to noise ratio* defines the ratio of the average RF carrier power to the noise power. This parameter is one of the main parameters which define the overall system performance. The carrier to noise ratio at the receiver terminals is defined as [12] :

$$\frac{C}{N} = (\frac{EIRP_t}{KB})(\frac{G_r}{T_s})(\frac{1}{L_{FS}L_0}) \tag{2.7}$$

which in dB can be written as:

$$\frac{C}{N} = EIRP_t + \left(\frac{G}{T}\right) - L_{FS} - L_O - K - B \tag{2.8}$$

where $EIRP_t$ is the transmitter EIRP, $\frac{G}{T}$ is the figure of merit of the receiver, $L_{FS}$ is the free space loss, $L_O$ represents other losses(polarization losses(See Figure 3.8), atmospheric losses(A.3), etc), $K$ is the Boltzmann constant and $B$ is the bandwidth.

**Carrier to Noise Density**

The carrier to noise density is related to the carrier to noise ratio and also used as a performance defining parameter in the link budget calculations. This is written as [12] :

$$\frac{C}{N_0} = \frac{C}{N}B \tag{2.9}$$

which in dB can be written as:

$$\frac{C}{N_0} = \frac{C}{N} + B \text{ dBHz} \tag{2.10}$$

**Overall Carrier to Noise Density**

The carrier to noise ratio and density can be defined at any point in the link. In order to establish a total link performance which accounts for both uplink and downlink, an overall carrier to noise density has to be computed. The overall carrier to noise density for the link, comprising both uplink and downlink, is defined as [13]:

$$\frac{C}{N_0}_{overall} = \frac{1}{\frac{1}{\frac{C}{N_0}_u} + \frac{1}{\frac{C}{N_0}_d}} \tag{2.11}$$

where $\frac{C}{N_0}_u$ and $\frac{C}{N_0}_d$ are the uplink and downlink carrier to noise densities.

**Energy per Bit to Noise Ratio and Bit Error Rate**

The *energy per bit to noise ratio* is frequently used in digital communications for describing the link performance and stability. The energy per bit to noise ratio allows comparison between different modulations techniques and bit rates for the same link. This parameter is defined as [12] :

$$\frac{E_b}{N_0} = \frac{C}{N}\frac{B}{Br} \tag{2.12}$$

which in dB can be written as:

$$\frac{E_b}{N_0} = \frac{C}{N} + B - Br \text{ [dB]} \tag{2.13}$$

where $B$ is the bandwidth and $Br$ is the bit rate.
The *bit error rate* is the ratio between the eronated received bits and the total number of received bits. It can be approximted to the *bit error probability* which is definded according to the type of modulation [14]:

- For QPSK modulation

$$BER = Q\Big(\sqrt{2\frac{E_b}{N_0}}\Big) \tag{2.14}$$

- For Rectangular MQAM modulation (k even)

$$BER = \frac{2}{k}\frac{\sqrt{M}-1}{\sqrt{M}}Q\Big(\sqrt{\frac{3k\frac{E_b}{N_0}}{M-1}}\Big) \tag{2.15}$$

### 2.1.2 Inmarsat system description

The study is developed following the link parameters and requirements of Inmarsat, one of the biggest mobile satellite communcations provider. Inmarsat has a fleet of 12 geostationary satellites which serve various puproses from mobile satellite communications for small user terminals to vessel, vehicular and airborne mobile terminals [10].

Geostationary satellites are satellites operating in the geosynchronous orbit, which has the same revolution period as the Earth. This is ideally suited for communications due to its fixed Earth - satellite geometry and its large coverage area. The geosynchronous orbit altitude above Earth is 35786 km, which is rounded to 36000 km for calculations [12].

The following technical description is based on the Inmarsat 4F2 satellite , a geostationary satellite which provides mobile satellite services to small user terminals. The satellite has a full duplex system, using the 1525 - 1559 MHz band for satellite to earth transmissions and the 1626 - 1660 MHz band for earth to satellite transmissions. The two- way services are provided through spot beams. Global and regional beams are used solely for signaling carriers transmission. Right hand polarization is used for both uplink and downlink in L band, as described in tables 2.1 and 2.2 respectively. The L band links are channelized onto a 200 kHz grid across the available spectrum [15].

| | UPLINK | | |
|---|---|---|---|
| Description | Beam | Polarization | Frequency Band [MHz] |
| Forward Link | Global | RHCP | 6425 - 6515.8 |
| | Global | LHCP | 6425 - 6515.8 |
| Return Link | Spot and/or Regional | RHCP | 1626.5 - 1660.5 |
| | Spot and/or Regional | RHCP | 1626.5 - 1660.5 |

**Table 2.1:** Uplink frequency plan for the mobile satellite communication operator, Inmarsat [15]

| | DOWNLINK | | |
|---|---|---|---|
| Description | Beam | Polarization | Frequency Band [MHz] |
| Forward Link | Sport and/or Regional | RHCP | 1525 - 1559 |
| | Spot and/or Regional | RHCP | 1525 - 1559 |
| Return Link | Global | RHCP | 3551.4 - 3657.8 |
| | Global | LHCP | 3551.4 - 3657.8 |

**Table 2.2:** Downlink frequency plan for the mobile satellite communication operator, Inmarsat [15]

For the spot beams, the nominal peak gain ranges from 40 to 42 dBi and the maximum attainable EIRP is 70 dBW. The total effective noise temperature of the spot beam receiver is approximately 583 K, giving a G/T performance in the range of 12.3 dB/K to 14.3 dB/K.

### 2.1.3 Link Budget

As mentioned in the chapter introduction, the parameters from Section 2.1.1 are the input for the link budget calculation. The link budget in this project follows the example of the link budget from Inmarsat 4F [15] having as target the overall carrier to noise ratio and density.

| | Unit | |
|---|---|---|
| **UPLINK** | | |
| Frequency | GHz | 1.644 |
| MS EIRP | dBW | 8 |
| Path loss | dB | 187 |
| Athmospheric loss | dB | 0.1 |
| Polarization loss | dB | 0.15 |
| Satellite $G/T$ | dB/K | 12.7 |
| Boltzmann constant | dBW/K/Hz | -228.6 |
| Bandwidth | dBHz | 52.7 |
| Up-path $C/N_0$ | dBHz | 60 |
| **DOWNLINK** | | |
| Frequency | GHz | 1.544 |
| Satellite EIRP | dBW | 50 |
| Path loss | dB | 187 |
| Athmospheric loss | dB | 0.1 |
| Polarization loss | dB | 0.15 |
| MS $G/T$ | dB/K | -15 |
| Boltzmann constant | dBW/K/Hz | -228 |
| Bandwidth | dBHz | 52.7 |
| Down-path $C/N_0$ | dBHz | 75.75 |
| **TOTAL** | | |
| Mean overall $C/N_0$ | dBHz | 60 |
| Mean overall $C/N$ | dB | 7.3 |

**Table 2.3:** Example of link budget calculation following the example in [15]

For the link budget example given in Table 2.3 the following assumptions have been made:

- The *effective isotropic radiated power* is computed assuming a transmission power of 2 W, the maximum transmit power allowed for a user terminal in UMTS according to [16], and an antenna gain of 5 dBi.

| | QPSK | 4QAM | 16QAM | 64QAM |
|---|---|---|---|---|
| Voice | -1.15 | -1.15 | 2.11 | 5.87 |
| Data | 6.5 | 6.5 | 11.02 | 14.77 |

**Table 2.4:** Minimum $\frac{E_b}{N_0}$ values in dB for different types of modulation

| | QPSK | 4QAM | 16QAM | 64QAM |
|---|---|---|---|---|
| Voice | -20 | -20 | -16 | -13 |
| Data | -3 | -3 | 0.66 | 5 |

**Table 2.5:** Minimum $\frac{C}{N}$ values in dB for different types of modulation

- The *polarization loss* value corresponds to an axial ratio of 3.3 dB
- The *bandwidth* value in dB correspond to a value of 189 kHz
- The *figure of merit*, $\frac{G}{T}$, of the mobile station is computed according to Formula 2.6, assuming an antenna gain of 5 dBi and an antenna noise temperature of 100 K (See appendix A.1.1).

The values in the above link budget calculation were taken as an example. However, the maximum allowable transmit power for an UMTS terminal will be assumed as the transmit power for further calculations. The antenna noise temperature will also keep the same value and its deduction it explained in Appendix A.1.1.

According to [17], for Mobile Satellite Services(MSS), the channel Bit Error Ratio(BER) should be better than $4x10^{-2}$ for voice services and better than $1x10^{-5}$ for data services.

Following the specificiations from [18], the satellite phone produced by the Inmarsat operator, has a bit rate of 2.4 kbps for voice services and a bit rate of 20 kbps for data services. Using the Formulas 2.13, 2.14, 2.15, and the above mentioned threshold values for the BER, the values for the energy per bit to noise ratio and carrier to noise ratio that are obtained are given in Table 2.4 and 2.5. Coding is not taken into consideration in these computations, as this would lead to a more detailed calculation and this is not the purpose of the project.

### 2.1.4 Requirements of the radio link

The project will follow the Inmarsat system requirements for the mobile satellite communications. The antenna will operate in the L-band, using the frequency band 1525 - 1559 for space to Earth transmission (downlink) and the frequency band 1626 - 1660 for Earth to space transmission (uplink). Right hand circular polarization is used in both uplink and downlink transmissions. The satellite parameters will be considered for a spot beam, as described in [15] and the user terminal parameters will be considered as presented in Table 2.6. As previously mentioned, the transmission power of the user terminal is considered to be the maximum allowed for an UMTS terminal and the temperature is 100 K, base on calculations which can be seen in appendix A.1.1. The path loss is computed according to the formula 2.2 for a distance of 36000 km and a central frequency of 1.6 GHz. The atmospheric losses and the bandwidth are following the technical report of the Inmarsat satellite [15]. From Table 2.6 it can be concluded that the antenna gain will play an important role in the link budget calculation. This is one of the main parameters that the design will have as goal, and it has to suffice for the minimum required values of the carrier to noise ratio. The available Inmarsat phone for mobile satellite communications has a maximum gain of 2 dBi according to [19]. Another parameter that will influence the design is the axial ratio, which in the link budget is translated as polarization loss. The relation between the two is given in Figure 3.8. Although no

specific requirements are made on the axial ration of the user terminal, one of their products has an axial ratio of 6 dB [20], which is considered as guideline for this project.

| | |
|---|---|
| **User Terminal** | |
| EIRP | 3 + G [dBW] |
| G/T | G - 20 [dB/K] |
| **Satellite** | |
| EIRP | 50 |
| G/T | 12.7 [dBK] |
| **Common parameters** | |
| Path loss | 187 [dB] |
| Atmospheric loss | 0.1 [dB] |
| Bandwidth | 52.7 [dBHz] |

**Table 2.6:** Requirements of the radio link

## 2.2 Modular Phone

A modular phone is a mobile phone that can be assembled from individual parts that include a camera, processor, internal storage, battery and so on. In this way, the user is free to pick, replace and upgrade the parts according to his needs and preferences.

*Project Ara* launched by Google defines such a modular phone where all the parts are connected to a backbone, an aluminum skeleton called "endoskeleton". [21] This skeleton contains networking circuitry and a small back up battery. Everything else comes as a module: from processor to the screen. The phone will have three

**Figure 2.2:** Modular phone [22]

versions, each of a different size as described in Table 2.7 [23] [21].

Following the specifications of the Ara modular phone, the physical implementation of the antenna for mobile

| | Size of the frame W x L x H [mm] | # of 1x1 tiles 22 x 22 x 4[mm] | # of 1x2 tiles 22 x 44 x 4[mm] | # of 2x2 tiles 44 x 44 x 4[mm] |
|---|---|---|---|---|
| Small Ara phone | 45 x 118 x 9.7 | 1 | 4 | 0 |
| Medium Ara phone | 68 x 141 x 9.7 | 2 | 2 | 2 |
| Big Ara phone | 91 x 164 x 9.7 | 0 | 4 | 5 |

**Table 2.7:** ARA Phone dimensions

satellite communications is restrained to the dimensions of the available tiles, that is 22 x 22 x 4 mm , 22 x 44 x 4 mm or 44 x 44 x 4 mm.

## 2.3 Antenna challenges

Following the previous information about the satellite link for a geostationary satellite and about the modular phone, it can be concluded that the design of the antenna will have to combine two kinds of requirements: the satellite link requirements and performance targets, and the low profile design characteristic to a modular phone.

The satellite link defines the characteristics and the performance goals of the antenna in terms of circular polarization, frequency and carrier to noise ratio. The latter will translate into a requirement of the gain and transmission power which along with the other parameters have to suffice the carrier to noise thresholds. Also, from the link budget it can be observed that the limiting variable is the uplink which due to low levels of the handset antenna gain, exhibits low carrier to noise ratio.

Typical antennas used in mobile satellite communications are *quadrifilar helix antenna (QHA)* (Figure 2.3 A ), *crossed dipole antenna* (Figure 2.3 B ) and *microstrip patch antenna* [24] (Figure 2.3 C ). The helical antenna is usually used for the external antenna of the satellite phones as it can produce circular polarized waves and has a wide band characteristic. The drawbacks of this antenna is the height and wide ground plane requirements. In [25], a helix antenna for Inmarsat system is proposed. The height of the antenna is 50 mm, which is above the expectation of height for the nowadays handsets. In [26] a crossed dipole antenna is presented whose height exceeds 10 mm and goes up to 82 mm. The same pattern appears in [27], where the height is 40 mm. The patch antenna also represents and options for mobile satellite communications as it can exhibit circular polarization through different designs and has a low profile aspect [28]. They are widely use especially for GPS applications [29].

The modular phone limits the size of the antenna to the size of the available tiles. As stated previously, the largest tile of the presented modular phone measures 44 x 44 mm, while an L-band antenna operating at 1.6 GHz requires a length of approximately $\frac{\lambda_0}{2}$ = 93 mm (for a dipole and a patch antenna). Attempts have been made in the beginning of this project to implement an antenna for the screen tile, but with no success (See appendix B.1). This leads to a different solution, a smart phone cover which will incorporate the antenna array, as described in Figure 2.4. This would represent a compact and functional solution, that can be connected to a modular phone through an embedded tile.

Although the cover will provide a wider area, it will still have to follow the phone dimensions, keeping a low profile. Therefore its dimensions, according to the medium modular phone will be 140 mm x 80 mm (L x W). The height of the cover on the other side will not have the same "freedom". Measuring such a cover for a smartphone (see Figures A.1 and A.2 in appendix, the height of one layer measures approximately 2 mm, while the height of the second layer measures 2.98 mm. Having these figures, the height of the antenna considered for

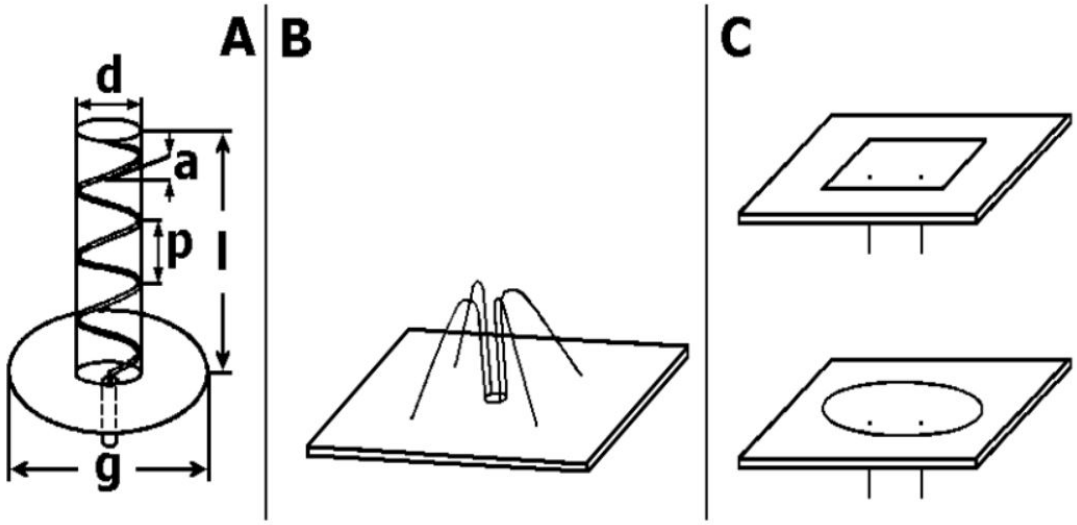


**Figure 2.3:** Types of antennas used in mobile satellite communications (Source: [24])

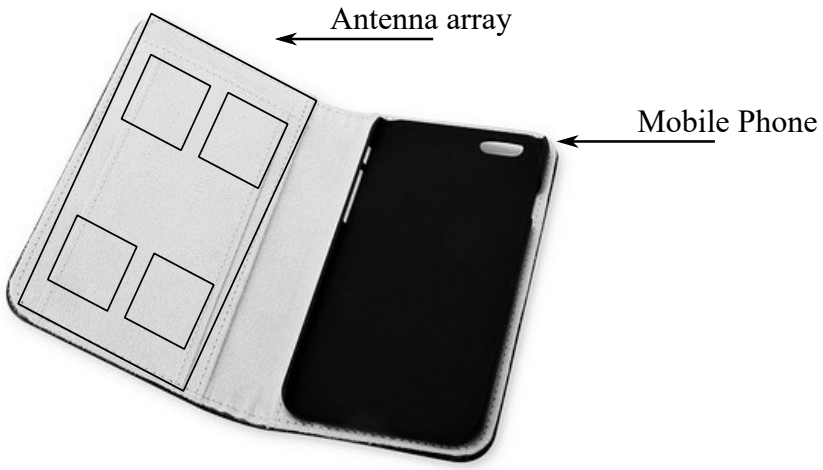


**Figure 2.4:** Placement of the array relative to the cover

this project will be close to 3 mm. No other references could be found about the thickness of a smart cover, but looking through the variety of options in [30], it can be noticed that they all keep the same thin height, similar to the one shown in this project.

Two major restrictions are defined now: the application of the antenna, mobile satellite communications, and the available area, 140 x 80 x 3 mm (L x W x H). By investigating the options of the antenna types, the proposed antenna for this project is a patch antenna array, mainly due to its low profile, but also due to other advantages like low cost, easy fabrication and robustness. As it will be further presented, the required dimension of the length of a patch antenna is close to $\frac{\lambda_0}{2}$ (93 mm at 1.6 GHz) and therefore the patch element will be miniaturized by optimum methods. This will also represent a challenge in designing the antenna, along with the dual band operation and the circular polarization. Circular polarization will limit the design of the patch, especially when it has to be present in both bands. Another problem is posed by the required bandwidth of 34 MHz in both uplink and downlink frequency band as the patch antenna has a narrow bandwidth.

# Chapter 3

# Proposed antenna characteristics

The previous chapter concluded that one of the main targets of the design is the low profile implementation which meets the requirements of the radio link. It also presented the types of antenna that are used in mobile satellite communications out of which the patch antenna showed the advantage of a low profile, light weight and easy implementation. This chapter will present the physical and electrical characteristics of the patch antenna, along with the specific modifications in order to meet the radio link requirements as well. For the ease of reading, both the physical and radio link requirements are reminded in Table.

| | |
|---|---|
| **Physical requirements** | |
| Area (L x W x H) | 140 x 80 x 3 mm |
| **Radio link requirements** | |
| Operating Frequency | Uplink: 1525 - 1559<br>Downlink: 1626 - 1660 |
| Polarization | RHCP |
| Axial Ratio | $\approx$ 6 dB |
| Gain | has to meet the link budget calculations |

**Table 3.1:** Ground requirements for the proposed antenna

Eventually, a conclusion is drawn on how to the final design and the array implementation.

## 3.1 Design and radiation mechanism

**Design guidelines**

The patch antenna is a low profile antenna, light-weighted and inexpensive. Its basic design consists of a very thing metallic plate over a ground plane separated by a dielectric, the substrate as described in Figure 3.1. The dielectric material plays an important role in the antenna characteristics, influencing mainly the resonance frequency, bandwidth and the efficiency of the antenna. A thick substrate with a low permittivity, which for the common substrates is in the range of $2.2 \leq \epsilon_r \leq 12$, will provide a good efficiency and bandwidth but with a larger patch dimension. On the other hand, a thin substrate with high permittivity will decrease the patch

dimensions, having as drawback less efficiency and narrow bandwidths. The patch antenna has a directional beam pattern in the broadside direction [31].

The design procedure of the patch can be approximated by simplified formulations which take into account the dielectric permittivity, the resonant frequency and the substrate height [31]:

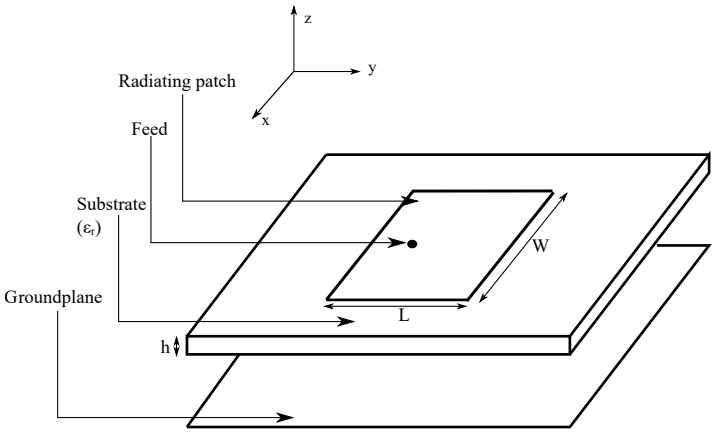


**Figure 3.1:** Main elements for a patch antenna

$$W = \frac{c}{2f_r}\sqrt{\frac{2}{\epsilon_r + 1}} \tag{3.1}$$

$$L = \frac{c}{2f_r\sqrt{\epsilon_{reff}}} - 2\Delta L \tag{3.2}$$

Where $c$ is the speed of light, $\epsilon_r$ is the relative permittivitty of the substrate, and $\epsilon_{reff}$ and $\Delta L$ are defined as:

$$\epsilon_{reff} = \frac{\epsilon_r + 1}{2} + \frac{\epsilon_r - 1}{2}\left(1 + 12\frac{h}{W}\right)^{-\frac{1}{2}} \tag{3.3}$$

$$\frac{\Delta L}{h} = 0.412\frac{(e_{reff} + 0.3)(\frac{W}{h} + 0.264)}{(e_{reff} - 0.258)(\frac{W}{h} + 0.8)} \tag{3.4}$$

Following the results from literature and the results of the simulations, the method applied in this project for reducing the slot dimensions is the high permittivity dielectric method.

**Radiation mechanism**

The radiation mechanism is depicted in Figure 3.2 with the voltage, current and impedance distribution on the patch surface. As it can observed in the picture, the electric field does not stop at the patches' edges, but it continues to extend beyond the periphery. This is the so called fringing effect [32]. As it can be seen from the figure, most of the electric field lines lie in the substrate and parts of some field lines exist also in air. As the substrate height and permittity increase, the field line will concentrate mostly in the substrate [31].

For all patch antennas with h « L and h « W, the mode with the lowest resonant frequency (dominant mode) has

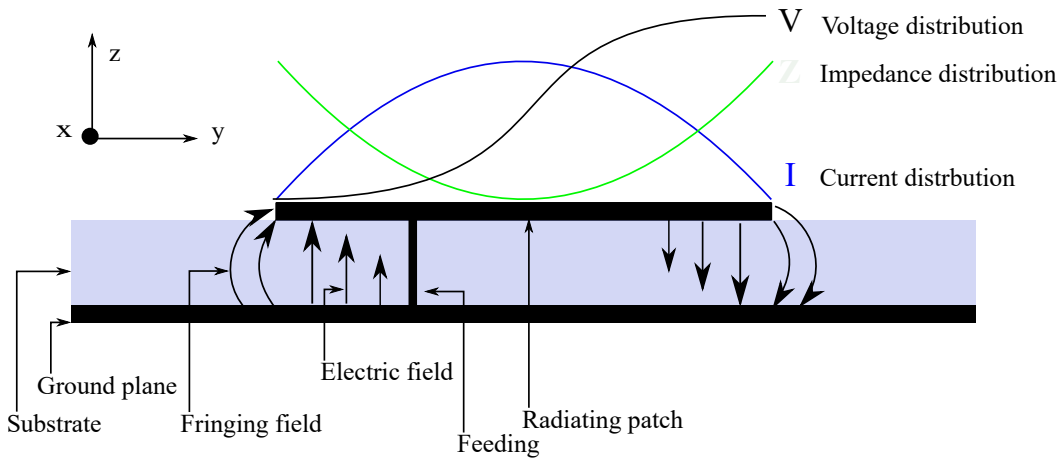


**Figure 3.2:** Radiation mechanism of a patch antenna

a resonant frequency given by [31]:

$$f_r = \frac{c}{2L\sqrt{\epsilon_r}} \tag{3.5}$$

The dimension that defines the resonant frequency is the length of the patch as seen from Equation 3.5 is $L$, which has a value of approximately $\frac{\lambda}{2}$. At a frequency of 1.6 GHz, this translates into 95 mm. Keeping in mind that the available area for the implementation is restrained to 140 x 80 x 3 mm, the implementation of a single antenna cannot be realized and not an antenna array as intended. Therefore, the size of the antenna will have to be reduced.

There are different ways to reduce the size of a patch antenna while keeping a certain resonant frequency. The ones tested in this paper were slot loading and high permittivity substrate (See appendix B.1 ). From Formula 3.2 it can be seen that when increasing the substrate permittivity, the length of the patch will decrease, as the dependence is inversely proportional. A study on the miniaturization of the patch for GPS application [33] shows that this method has as drawback a narrow bandwidth. However, for values for the permittivity kept in the range of 9 – 30, the results in term of bandwidth were satisfactory.

The slot loading method is also studied in [33] and it implies cutting slots in the patch surface as shown in appendix, Figures B.5 and B.6. This diverts the currents to a longer path resulting in an higher wavelength and implicitly a lower frequency. According to the sutdy mentioned earlier, the length of the slot controls the frequency dependency, their results showing a decrease of 500 MHz in frequency with a slot pf 11 mm length, while still using a high permittivity substrate with a value of 9.2. Another study performed in [34] shows a decrease in gain, efficiency and bandwidth as the slot length is increased.

## 3.2 Feeding techniques

### 3.2.1 Coaxial feeding

In this type of feeding the antenna is fed from underneath through a coaxial feed probe, as shown in Figure 3.3 A. The inner conductor extends through substrate and is soldered to the radiating patch while the outer conductor is connected to the ground plane. The disadvantages of this type of feeding are: *narrow bandwidth* and *difficulty in modelling* since the feeding presumes a hole through substrate [35].

### 3.2.2 Microstrip feeding

Microstrip feeding implies a conducting strip with a smaller width than the radiating patch, hence the name, connected directly to the patch, as shown in Figure 3.3 B. The disadvantages of this type of feeding are: *spurious radiation* and *undesired cross polarized radiation* [35].

### 3.2.3 Aperture feeding

This feeding technique is similar to the microstrip feeding, with the difference that the microstrip and the radiating patch are separated by the ground plane, as shown in Figure 3.3 C. The coupling between the two is made through a slot in the ground plane. The variations of the dimensions and position of the slot which reflect in the matching and the performance of the patch [35].

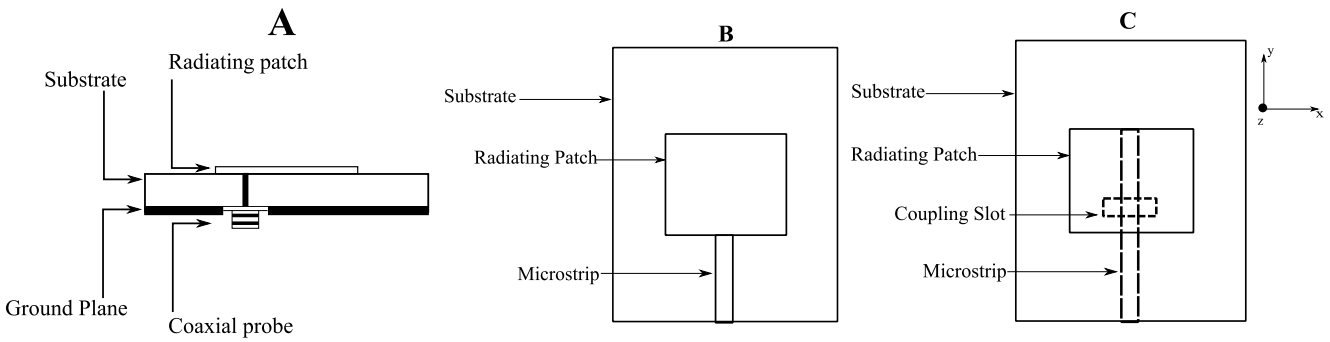


**Figure 3.3:** From left to right: coaxial, microstrip and aperture feeding for a patch antenna

This last type of feeding is preferred and used in this project due to advantages as: no physical connection between the feeding strip and the patch and better isolation between antenna element and feed network. Also, it allows independent optimization of the feed network from the antenna, which represent an advantage for this project, as the array elements locations are varied to obtain the desired isolation between them [35]. According to the study performed in [35], the aperture coupled feeding has the best results in term of bandwidth and matching.

## 3.3 Antenna polarization

The patch antenna is primarily linearly polarized. Circular polarization can be obtained by using different feed layouts or by making modification to the patch itself. A wave is circular polarized when the tip of electric field traces a circular contour in space. The electric field intensity had the same amplitude at any instance of time [31].

*Right hand circular polarization* occurs when the electric field had clockwise rotation when viewed along the propagation axis (the wave must travel away from the observer). Contrarily, *left hand circular polarization* occurs when the electric field has a counterclockwise rotation when viewed along the propagation axis (the wave must travel away from the observer) [36].

One technique of achieving circular polarization is by exciting the antenna in two orthogonal points in space as described in Figure 3.4, one with a 90° phase shift. The shape of the patch in this case has to be square, that is both dimension will be equal to $L$. In this way, two orthogonal electric field vector of the same magnitude are produced [31].

Circular polarization can also be obtained by feeding the antenna on the diagonal, as shown in Figure 3.5.

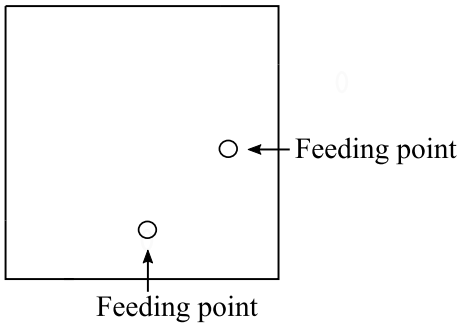


**Figure 3.4:** Orthogonal feeding points for a patch antenna for circular polarization

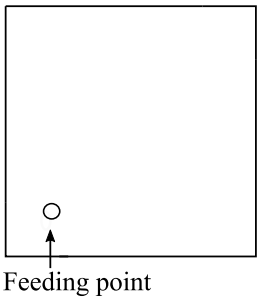


**Figure 3.5:** Diagonal feeding of a patch antenna for circular polarization

This method has a drawback that the circular polarization is maintained only over a very narrow band [31].

Another method of obtaining circular polarization is to truncate two opposite corners, or by cutting thin slots in the patch, as shown in Figure 3.6 and 3.7 respectively.

### 3.3.1 Axial Ratio

In practice, the amplitudes of the electric field may vary in difference time instances and therefore the wave does not have a perfect circular movement. The *axial ratio* can be used as a measure of the circular polarization quality and it is the ratio between the magnitudes of the electric field components, defined as [31]:

$$AR = \frac{|E_{majoraxis}|}{|E_{minoraxis}|} \tag{3.6}$$

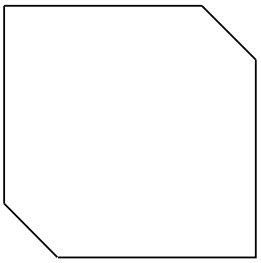

**Figure 3.6:** Truncated corners of a patch antenna for circular polarization

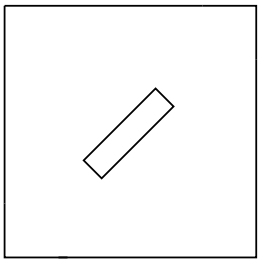

**Figure 3.7:** Slot in a patch antenna for circular polarization

The axial ratio is then converted into polarization loss as described in Figure 3.8.

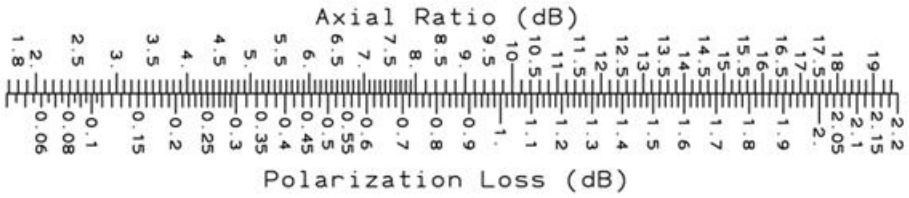


**Figure 3.8:** Axial ratio conversion to polarization losses (source: [37])

From the presented techniques which can be applied for obtaining a circular polarized patch, the ones applied in the project were the dual feeding, truncated corners and the cutting a slot in the center of the patch (See appendix B.1). The technique with the feed placed on the diagonal was not implemented as according to literature, the circular polarization is only maintained across a very narrow band. The one that gave the best results in terms of axial ratio was the first one, while the other two presented poor axial ratio across the second bandwidth. Also, other literature shows the same conclusion in [33] when the antenna has dual resonance, which is also the case in this project. Another study in [38] shows the bandwidth over which the axial ratio is maintained under 3 dB when circular polarization is obtained by truncating corners or cutting slots of different shapes. The results show values of the bandwidth in the range of 5 to 8 MHz, values which represent less than a quarter of the required bandwidth in this project.

## 3.4 Antenna matching

Matching circuits represent a useful technique when designing antennas, but they come with a degree of loss which comes from the parasitic nature of the components [39].

The purpose of matching is converting the antenna impedance to a new one which is close to the system's characteristic. In case of mobile communications, the target is 50 Ω. Other standards imply 70 Ω and 100 Ω, but in this project the 50 Ω value is used [39].

In order to establish the quality of matching, Γ, the voltage reflection coefficient is used, which is the ratio between the reflected wave and the incidence wave [39]. The reflection coefficient is the ratio between the amplitude of reflected voltage wave and the amplitude of the incident voltage wave, which is written as [40]:

$$\Gamma = \frac{V_o^-}{V_o^+} = \frac{Z_L - Z_0}{Z_L + Z_0} \tag{3.7}$$

where $V_o^-$ is the amplitude of the reflected voltage wave, $V_o^-$ is the amplitude of the incident voltage wave, $Z_L$ is the load impedance and $Z_0$ is the characteristic impedance of the transmission line, here considered 50 Ω as mentioned before. It can be seen from equation 3.7 that Γ can take any value between 0 and 1, 0 being perfect matched and 1 being complete reflection.

**Scattering Matrix**

A more practical representation of the incident and reflected waves is given by the scattering matrix. considering an N ports network, the scattering matrix defined in relation with the amplitudes of the voltage waves incident and the voltage waves reflected is [40]:

$$[V^-] = [S][V^+] \tag{3.8}$$

where the $[V^-]$ is the matrix of the amplitudes of the reflected waves, $[V^+]$ is the matrix of the amplitudes of the incident waves and $[S]$ is the scattering matrix, further written as [40]:

$$[S] = \begin{bmatrix} S_{11} & S_{12} & \cdots & S_{1N} \\ S_{21} & S_{22} & \cdots & S_{2N} \\ \vdots & \vdots & \ddots & \vdots \\ S_{N1} & S_{N2} & \cdots & S_{NN} \end{bmatrix} \tag{3.9}$$

A single element of the scattering matrix is defined as [40]:

$$S_{ij} = \left.\frac{V_i^-}{V_j^+}\right|_{V_k^+=0, k\neq j} \tag{3.10}$$

Formula 3.10 states that $S_{ij}$ is the ratio between the reflected wave $V_i^-$ coming out of port $i$, when an incident wave $V_j^+$ is applied at port $j$. Thus, $S_{ii}$ is the reflection coefficient of port $i$ when all other $N-1$ ports of the network are terminated in matched loads and $S_{ij}$ is the transmission coefficient from port $j$ to port $i$ when all other ports are terminated in matched loads [40].

**The Smith Chart**

When dealing with transmission lines impedance matching, the mathematical computation can become very difficult and time consuming. Therefore, a graphical representation is a simpler and more convenient approach, which is given by the Smith chart [41].

The Smith chart, illustrated in Figure 3.9, is the polar representation of the complex reflection coefficient, earlier defined as $S_{ii}$ and further referred to as $S_{11}$. The reflection are from the a normalized impedance $z = r + jx$, that

is the results of normalizing the complex load impedance $Z_L$ to the characteristic impedance, $Z_0$ [41].

The complete guide of using the Smith chart can be found in detail in [40], [41], [39] and other microwave literature, but in this project only the fundamental working principles of the impedance Smith chart are presented. The main components of the Smith chart are [41]:

- *The horizontal line* that is passing through in the center of the Smith chart is the line where the component is completely resistive. The resistance $r$ has the value zero in the left end of the line, infinite at the right end of the line and the center of the line represents the normalized value of 1.
- *The constant resistance circles* are the circles tangent to the right side of the Smith chart.
- *The lines of constant reactance* are line along which there is a constant value of the reactance $x$ and start from the outer side of the chart and end in the right side.

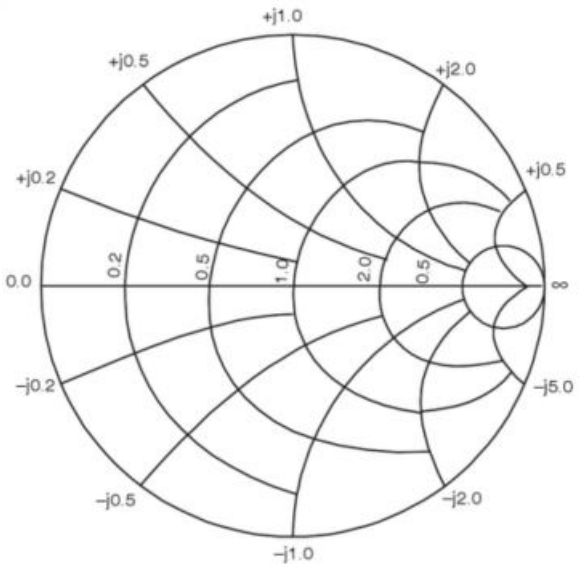


**Figure 3.9:** Impedance Smith Chart. Simplified figure, showing only the elements described in this section (source: [41])

As mentioned previously, the Smith chart is a very useful tool for designing a matching circuit. For any complex load there is an unique point on the Smith chart, the center of the diagram representing the best matching where there are no reflection (the reactance is zero and the $Z_L = Z_0$), that is the reflection coefficient is zero [39]. The location of a point on the Smith chart can be changed as described in Figure **??**

**Bode - Fano criteria**

Even if the components are lossless, which in reality is impossible to achieve, matching comes with another cost regarding bandwidth. This behavior is explained through Bode - Fano constraint which shows that a trade-off has to be made between bandwidth and matching, and it is written as [40]:

$$\int_0^\infty ln\frac{1}{\Gamma(\omega)}\,d\omega \leq \frac{\pi}{RC} \tag{3.11}$$

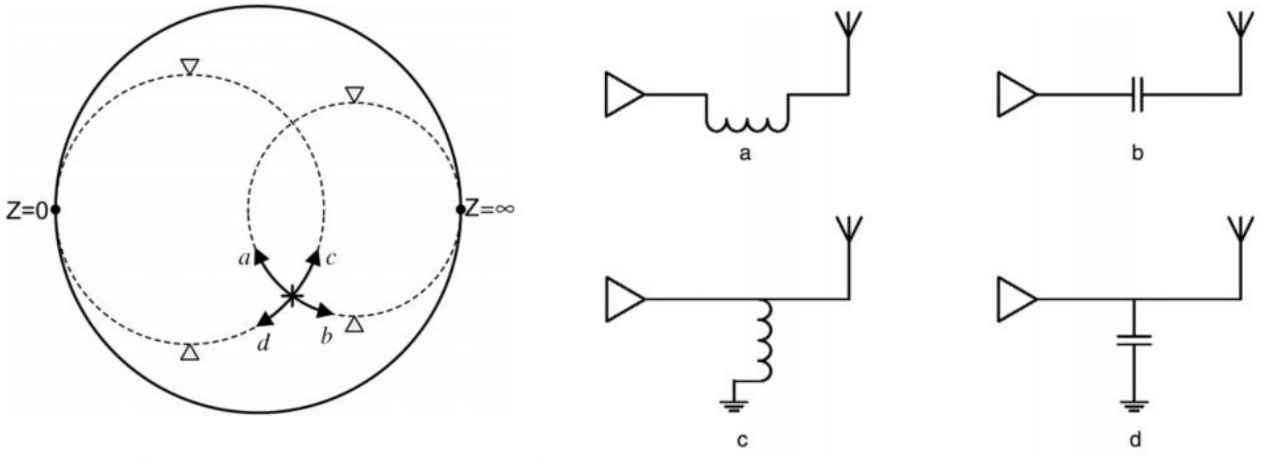


**Figure 3.10:** Impedance Smith Chart. Simplified figure, showing how the location of a point on the diagram can be moved (source: [39])

where $\Gamma(\omega)$ is the reflection coefficient obtained when looking into a lossless matching network. This can be synthesized as follows [40]:

$$\int_0^\infty ln\frac{1}{\Gamma(\omega)}\,d\omega = \int_{\Delta\omega} ln\frac{1}{\Gamma_m}\,d\omega = \Delta\omega ln\frac{1}{\Gamma_m} \leq \frac{\pi}{RC} \tag{3.12}$$

The above derivation shows that for a fixed matching circuit (R and C are constant), a higher bandwidth can be achieved if the reflection coefficient is also increased. Another observation would be that once the values of R and C are increased, either the bandwidth or the matching is worsened.

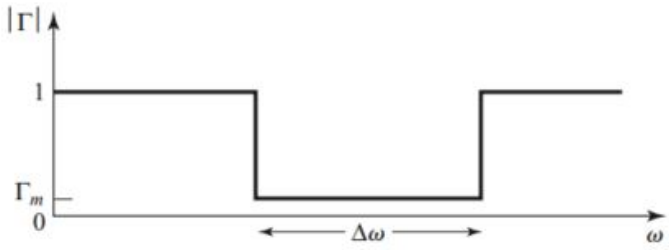


**Figure 3.11:** Illustration of Bode - Fano criterion, reflection coefficient over the available bandwidth (source: [40])

### Dual resonance

Dual resonance of a patch antenna can be obtained in different ways. [42] presents a stacked patch array for mobile satellite communication, with a total height of 15 cm, which is not in agreement with the targeted height in this project. Another method that is widely used in literature ([43] [44]) and has been tried in this project as well (See appendix B.1) is cutting slots of various forms in the patch. This solution showed poor results for axial

ratio along one of the bandwidths.

The matching network can also represent o solution for this issue. The drawback of this method is the loss introduced by the components. In [39] different circuits for matching the impedance across certain bandwidths are given, several being implemented in this project as well (See appendix B.1 and B.1.1). A matching circuit that showed good results in terms of dual band operation and low losses was the $\pi - circuit$ as illustrated in Figure 3.13. The main factor that influenced this choice was the small number of components, only series inductors (which in previous simulations proved to be very lossy when connected in shunt) and the small spacing between the obtained frequency bands. The $\pi - circuit$ not only serves for obtaining a dual resonance but it is also used for matching the antenna to a 50 $\Omega$ load [39].

As presented previously in 3.12, $\Gamma(\omega)$ is preferably a constant over the available bandwidth, as shown in

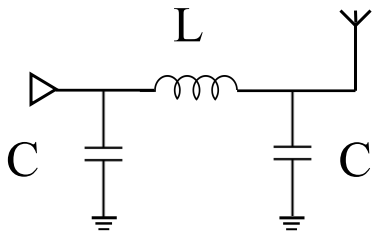


**Figure 3.12:** $\pi - circuit$ for matching with two shunt capacitors and one series inductor

Figure 3.11. When $\Gamma(\omega)$ is a Chebyshev polynomial, a ripple appears in the bandwidth. Depending on the type of Chebyshev polynomial, the ripple can appear in the passband of the filter (Type I) or in the stopband (Type II) [40]. Figure **??**hows the plot of the first four Chebyshev polynomials and it can be observed that the one which has two ripples is the fourth order polynomial. The formula formula for the Chebyshev fourth polynomial is [40]:

$$T_n(x) = 2xT_{n-1}(x) - T_{n-2}(x) \tag{3.13}$$

where $|x| \leq 1$ represents a ripple inside the passband and $|x| > 1$ represents a ripple in the stopband. Considering $x = \cos\theta$ for $|x| < 1$, the the formula for the Chebyshev fourth polynomial becomes [40]:

$$T_4(sec\theta_m \cos\theta) = sec^4\theta_m(\cos 4\theta_m + 4\cos 2\theta_m + 3) - 4sec^2(cos2\theta + 1) + 1 \tag{3.14}$$

The formula presented above are valid for prototype designs with up to four sections [40]. For synthesis, $\Gamma(\theta)$ is considered to be proportional to $T_N(sec\theta_m \cos\theta)$, where N is the number of sections, which results in [40]:

$$\Gamma(\theta) = Ae^{-jN\theta}T_N(sec\theta_m \cos\theta) \tag{3.15}$$

For $\theta = 0$ [40]:

$$\Gamma(0) = AT_N(sec\theta) = \frac{Z_L - Z_0}{Z_L + Z_0} \tag{3.16}$$

which results in [40]

$$A = \frac{Z_L - Z_0}{Z_L + Z_0}\frac{1}{T_N(sec\theta_m)} \tag{3.17}$$

If the maximum desired reflection coefficient is $\Gamma_m$, then $\Gamma_m = |A|$ because the maximum value of the Chebyshev polynomial in passband is one [40]. Therefore [40]:

$$T_N(sec\theta_m) = \frac{1}{\Gamma_m}\left|\frac{Z_L - Z_0}{Z_L + Z_0}\right| \tag{3.18}$$

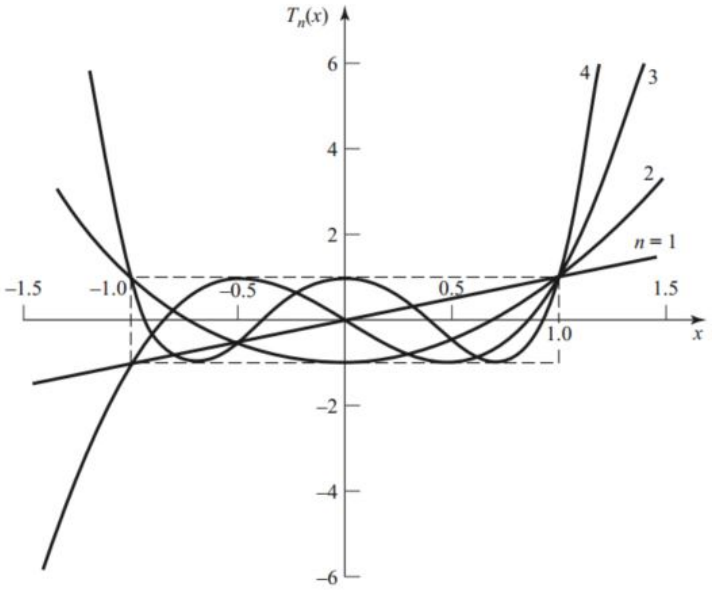


**Figure 3.13:** The first four Chebyshev polynomials (source: [40])

## 3.5 Antenna Array fundamentals

Prior to this section, the term of "array" was mentioned a couple of times. Also, the aim of designing an antenna array was specified from the very beginning. Only two types of array will be briefly discussed in this section, the planar and the linear array, as only these two types are intended to be applied in this project.

An antenna array is essentially an antenna comprised of multiple elements. Most of the times the elements of the array are identical and placed in such a way that the field from the elements add constructively in the desired direction. The type of the elements may be of any form, but in this project only the patch antenna array is presented [31].

In such an array of elements, the variables that affect the overall pattern of the antenna are: *the configuration of the array (geometrical design), the spacing between elements, the amplitude of the input signal, the phase of the input signal* and *the individual pattern of a single element* [31].

The geometry of the array affects not only the radiation pattern, but also the beam steering as it will be described further in this section and in the simulations' results. The elements can be placed in a line (1D),in a planar layout (2D) or in a 3D shape. Once again, only the first two case are presented and applied in this project. The linear array is formed by placing the elements along a line, as shown in Figure 3.14. This types of array are defined in this project $1xN$ array, $N$ being the number of elements in the array, and 1 defining the single dimension the elements are placed along. The planar array on the other hand has the elements placed

along two dimensions, as shown in Figure 3.15. This types of array are defined in this project $MxN$ array, $M$ being the number of elements along one dimension and $N$ the number of elements along the second dimension [31].

The spacing between elements is also an important parameter when designing the array. High distances can

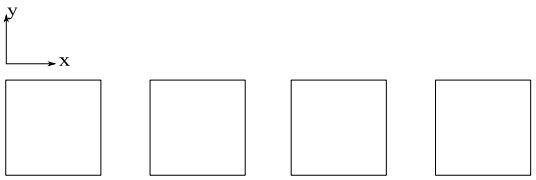


**Figure 3.14:** Linear array of patch antennas

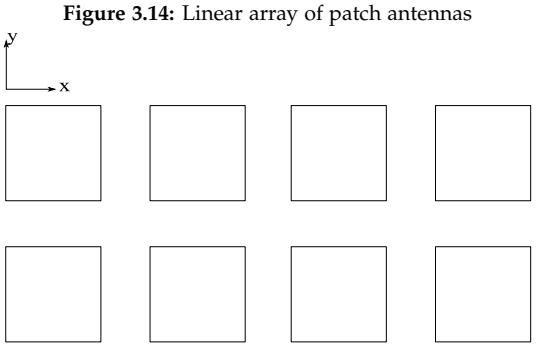


**Figure 3.15:** Planar array of patch antennas

result in increased directivity and high grating lobes, while small distances can have as an effect mutual coupling. Mutual coupling is an interchange of energy between antennas placed close to each other and in many cases it complicates the design and analysis of the array. It is attibuted to space waves, higher order waves surface waves and leaky waves [31].

For patch antennas, the coupling is a function of alignment and the edge to edge separation. The two patches can be placed collinearly along the E plane 3.16, or along the H plane 3.17 [31].

A parameter than can show the mutual coupling variations is $S21$(in the case of 2 ports), which is the transmission coefficient between the two ports. From Figure 3.18, it can be observed that in most of the cases, the patches in E-plane position exhibits a higher coupling than the ones in H plane. This is because in the lowest order, the fields along the E-plane are TM and the surface wave excitation is stronger. In the case of the patched positioned along the H-plane, the fields are TE and there is not a strong surface wave excitation. However, it can also be observed that for very small spacing and different dielectric characteristics, the curve representing H-plane overtakes the one of the E- plane [31].

### 3.5.1 Beamforming and beam steering

*Beam forming* is the technique of combining signal coming from multiple antenna elements into a single pattern. The new constructed beam can be fixed or can be steered in the directions desired. The *beam steering* can be accomplished by different techniques, such as: *phased arrays*, *Butler matrix*, *Rotman lenses*, *Monopulse antennas*[45]. The technique applied in this project for obtaining different beam directions is *phase shifting*.

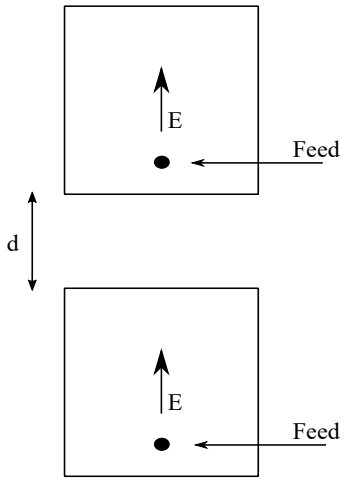


**Figure 3.16:** Patches collinearly in E-plane

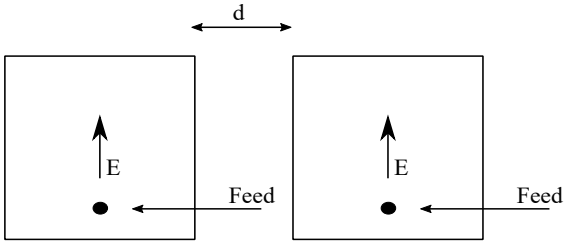


**Figure 3.17:** Patches collinearly in H-plane

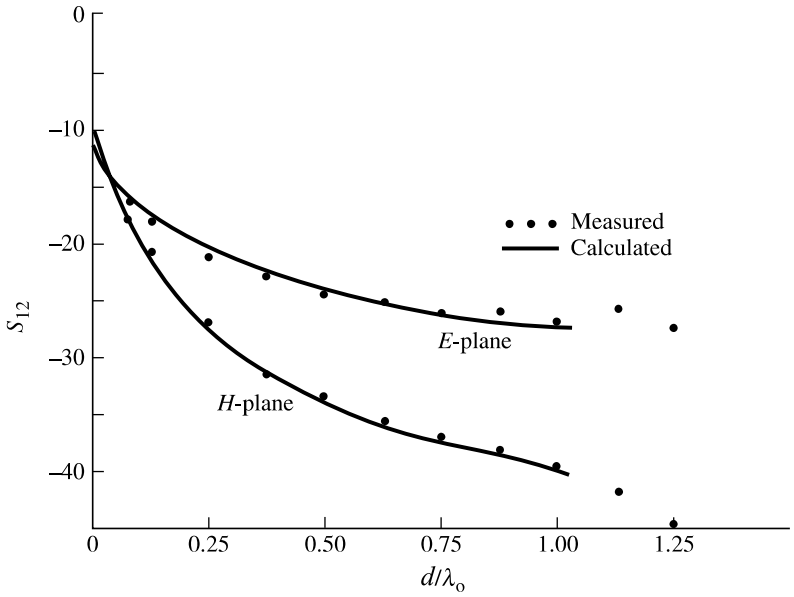


**Figure 3.18:** E plane vs H plane mutual coupling (source: [31])

# Chapter 4

# Array Implementation

This chapter will describe the antenna design and operation, starting from a single element, which is further implemented into a linear and a planar array. For the planar array, which was a primary target of the project, different layouts have been designed resulting in two most relevant designs that are presented in the end of this chapter.

Beside the gain and circular polarization, another major interest when implementing the array is the beam steering capabilities. While the linear array is capable of steering in only one direction, the planar array adds a second direction. Hence the project is more focused on the latter, although the gain and circular polarization requirements may be achieved with a linear array as well.

All simulations were performed in the electromagnetic simulation software CST Microwave Studio using the FDTD solver. For circuit implementation was used CST Studio Design, while data and image processing were performed in Matlab.

## 4.1 Single patch antenna

The design of a single element is included in the report in order to make an overall comparison with the array structure. However, every array design and simulation in this project started from defining and optimizing a single element. When implemented in the array form, because of the effects of the mutual coupling, some parameters like the input impedance were changed and resulted in different matching and different layouts. As a brief reminder of the conclusions from the previous theory chapter, the main design outlines are presented shorted in Table 4.1 and discussed in detail afterwards.

The first step in the single element design was choosing the antenna materials, especially the dielectric material used for the substrate. In this project *Preperm 900 LHF* has been used for the substrate, which has a permittivity of $\epsilon_r = 9$ and a loss tangent of $\delta = 0.0004$ [46]. Once again, the choice of using a high permittivity material has as purpose shrinking the patch dimensions. Consequently, the length of the patch is reduced from the initial required value of a $\frac{\lambda}{2} = 9.5cm$, to approximately $\frac{\lambda}{6} = 2.95cm$. The position of the patch is in the center of the board, as shown in Figures 4.1 and 4.2.

The second and one of the most challenging part is implementing and optimizing the feeding. As mentioned

| | |
|---|---|
| **Physical requirements** | |
| Available area for implementation (L x W x H) | 140 x 80 x 3 mm |
| **Radio link requirements** | |
| Operating Frequency | Uplink 1525 - 1559 Downlink 1626 - 1660 |
| Polarization | RHCP |
| Axial Ratio | $\approx$ 6 dB |
| Gain | has to meet the link budget calculations |
| **Implementation** | |
| Antenna type | Rectangular patch antenna |
| Miniaturization | High permittivity substrate |
| Circular polarization | Orthogonal feeding |
| Feeding | Aperture coupled microstrip |
| Dual resonance | $\pi$ - circuit |

**Table 4.1:** Guidelines for the antenna implementation and simulation

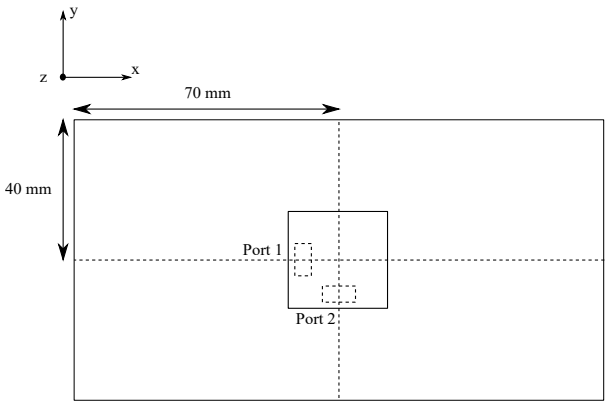


**Figure 4.1:** Position of the patch (top view)

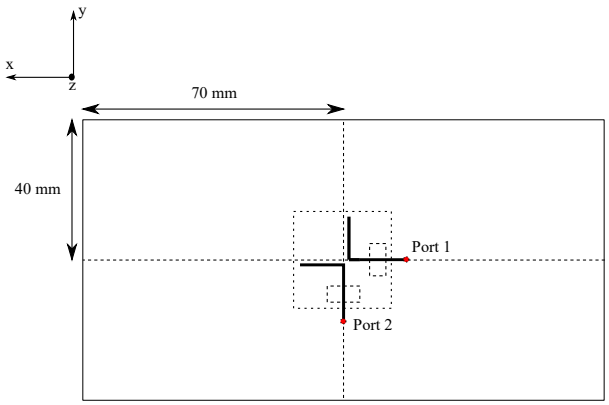


**Figure 4.2:** Position of the patch (bottom view)

| | $W_{fs}$ | $L_{fs}$ | $d_{fs}$ | $W_{fl}$ | $L_{fl}$ | $L_d$ | $L_s$ | $L_c$ | $d_f$ |
|---|---|---|---|---|---|---|---|---|---|
| Value [mm] | 4 | 8 | 9.5 | 0.8 | 15 | 2 | 7.5 | 12 | 2 |

**Table 4.2:** Feeding parameters using Rogers RO3006 as a feeding substrate ($h_{fs} = 0.25mm$)

before, the patch is fed by a microstrip line, through an aperture. The literature provides no basic formulas for the aperture, but just indications that all parameters involved should be optimized until a good coupling and matching is obtained [47]. Having both the aperture and the microstrip line on other planes and substrate than the patch, the feeding can be optimized and changed independently from the patch antenna.

The feeding substrate used in the simulation is *Rogers RO3006*, which has a permittivity $\epsilon_r$ equal to 6.15 and a loss tangent $\delta$ equal to 0.002 [48]. The height of the feeding substrate, $h_s$ is 0.25 mm and is chosen following the available standard heights of the substrate and also taking into consideration the low profile design of the antenna. Afterwards, the microstrip line and the aperture are adjusted to match the antenna at 50 Ω for a center frequency of 1.6 GHz. The main parameters that are varied and adjusted are presented in Figure 4.3 with their final value given in Table 4.2. The only indications in [47] regarding this feeding technique, are about the length of the stub, here given by $L_s + L_c$, that should be around $\frac{\lambda}{4}$. The reason for bending the line, was the limited space of the structure, in this way avoiding intersecting the two orthogonal microstrip lines.

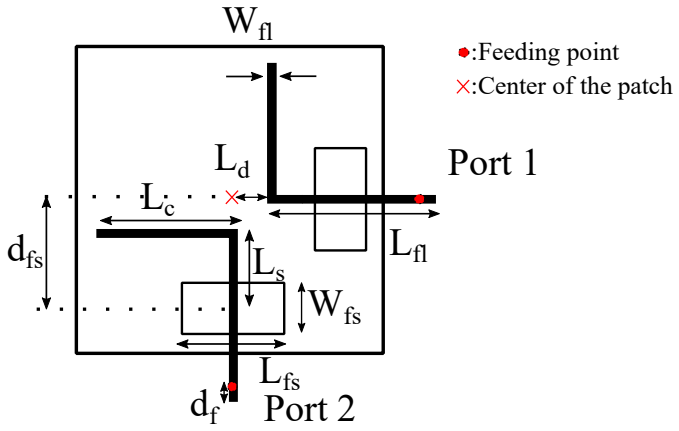


**Figure 4.3:** Feed modeling and parameters

### 4.1.1 Dual band matching

For obtainging dual resonance the $pi - circuit$, illustrated in Figure 4.4 and presented in Section 3.4, is used for both matching and obtaining dual resonance. The values of the components are given in Table 4.3. As an observation, the values of the components have been optimized aiming to obtain a good matching and a good isolation between the two bands. The values of the parasitic resistance, ESR and Q have been chosen from different components from manufacturers like *Murata*, $CoilCraft$ and *Vishay* [49] [50] [51] [52]. The characteristics of the components used in the simulations were among the best that were found among the components from the three vendors, while also taking into account the tolerances and frequency variations. The tolerances of the components are ±1%, but they cannot be input directly in the simulator. However, a brief yield analysis was

performed for the planar array in appendix B.6 where the tolerance of the components is also investigated. A more detailed discussion about the circuit modeling and components behavior is made in the appendix B.5.

In the frequency band of 1525-1559 MHz, a part of the bandwidth of 25 MHz of the total 34 MHz is cov-

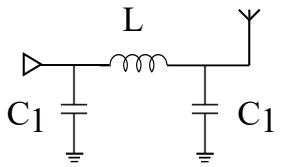


**Figure 4.4:** $\pi - circuit$ for matching and dual resonance

| C1 | | L | | C2 | |
|---|---|---|---|---|---|
| Value [pF] | ESR [Ω] | Value [nH] | Parasitic Resistance [Ω] | Value [pF] | ESR [Ω] |
| 2.9 | 0.1 | 11.7 | 0.5 | 2.4 | 0.1 |

**Table 4.3:** Components values for 1 element antenna

ered with a VSWR 3:1 (Voltage Standing Wave Ratio). The rest of the bandwidth, 9 MHz, it covered with a VSWR 6:1. In the frequency band of 1626 - 1660 MHz, a part of the bandwidth of 22 MHz of the total 34 MHz is covered with a VSWR 3:1. The rest of the bandwidth, 12 MHz, it covered with a VSWR 6:1. This can be further noticed in the total efficiency of the antenna, where the matching losses are included and the efficiency drops to a minimum of -6 dB.

The results for the single patch antenna show a realized gain above 0 dBi across both bandwidths, and aside the

| Frequency [GHz] | 1.525 | 1.544 | 1.559 | 1.626 | 1.644 | 1.660 |
|---|---|---|---|---|---|---|
| Realized Gain [dBi] | 2 | 4.53 | 2.81 | 2.66 | 5.1 | 0.525 |
| Radiation Efficiency [dB] | -2.4 | -1.3 | -1.43 | -1.08 | -1.23 | -2.9 |
| Total Efficiency [dB] | -4.56 | -2.12 | -3 .7 | -3.82 | -1.45 | -5.9 |
| Axial Ratio [dB] | 10 | 7 | 5 | 5 | 6 | 3 |

**Table 4.4:** Results for single patch antenna

upper limit of the high band, a realized gain over 2 dBi. The axial ratio maintains the target value $\leq$ 6 dB for the entire high band and only towards the upper part of the low band.

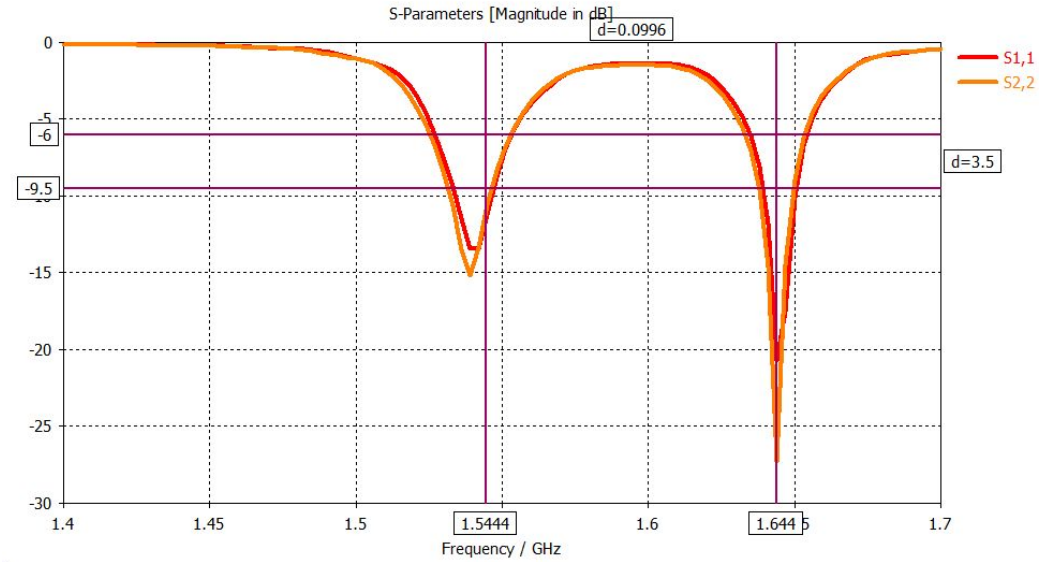


**Figure 4.5:** Reflection coefficient at both ports of the single patch antenna[dB]

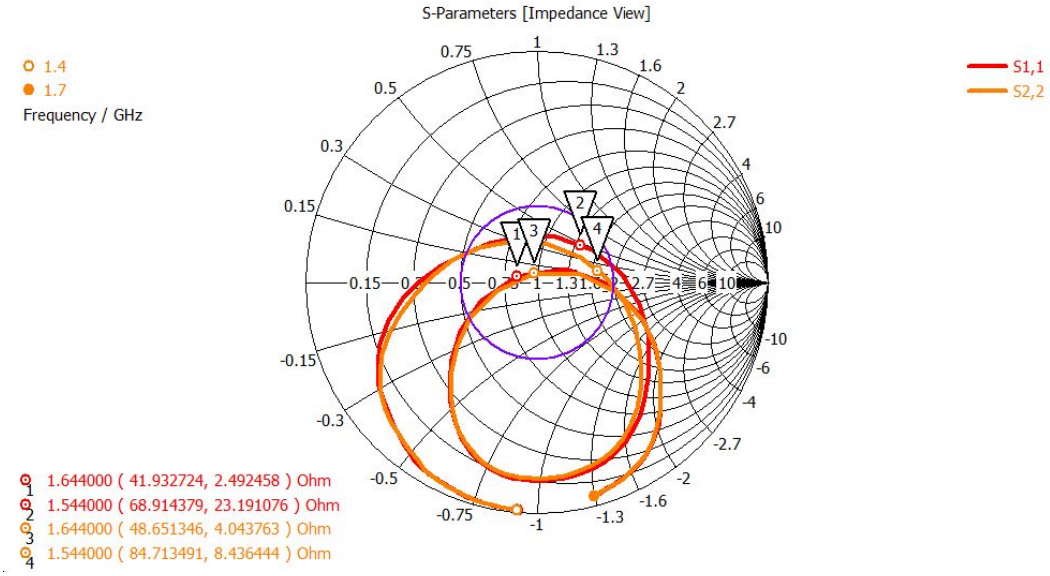


**Figure 4.6:** Reflection coefficient at both ports of the single patch antenna, (Impedance Smith chart - VSWR 2:1 circle)

## 4.2 1x2 Array

This section present the implementation of linear array, aiming to increase the gain of the antenna and simultaneously add the advantage of beam steering. The benefits and the costs of this solution are concluded in the end of the section.

For the 1 x 2 antenna array, the elements are placed as shown in Figure 4.7 and Figure 4.8, each patch being placed in the center of a half of the board. The design of the patch together with the feeding is the same as for the single element presented in the previous section. The edge to edge distance between elements In this layout, the distance between elements in terms of $\frac{d}{\lambda_0}$ is approximately 0.2. From figure 3.18 it can be seen that for this value in both E-plane and H-plane the transmission coefficient has values below $-10$ dB. Also in the simulation the transmission coefficient between ports 1 and 3 and 2 and 4 respectively has values below $-10$ dB.

For dual band matching of the antenna, the same pi circuit is used, the components having the values given in

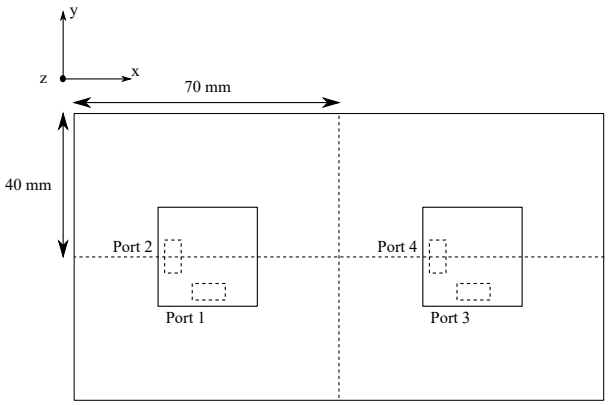


**Figure 4.7:** Position of the patches in 1x2 array(top view)

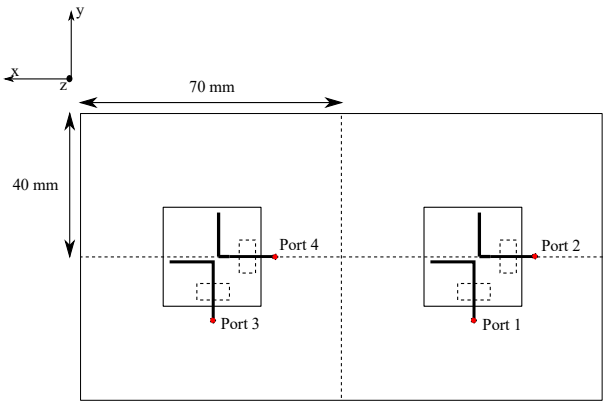


**Figure 4.8:** Position of patches in 1x2 array (bottom view)

Table 4.5.

| C1 | | L | | C2 | |
|---|---|---|---|---|---|
| Value [pF] | ESR [Ω] | Value [nH] | Parasitic Resistance [Ω] | Value [pF] | ESR [Ω] |
| 2.9 | 0.1 | 11.7 | 0.5 | 2.4 | 0.1 |

**Table 4.5:** Components values for in 1x2 array

| Frequency [GHz] | 1.525 | 1.544 | 1.559 | 1.626 | 1.644 | 1.660 |
|---|---|---|---|---|---|---|
| Realized Gain [dBi] | 4.07 | 5.48 | 4.68 | 4.93 | 6.1 | 2.88 |
| Radiation Efficiency [dB] | -1.59 | -1.4 | -0.99 | -0.49 | -1.16 | -1.7 |
| Total Efficiency [dB] | -3.13 | -1.81 | -2.6 | -2.63 | -1.5 | -4.7 |
| Axial Ratio [dB] | 9 | 8 | 5 | 4 | 4 | 2 |

**Table 4.6:** Results for 1 x 2 array

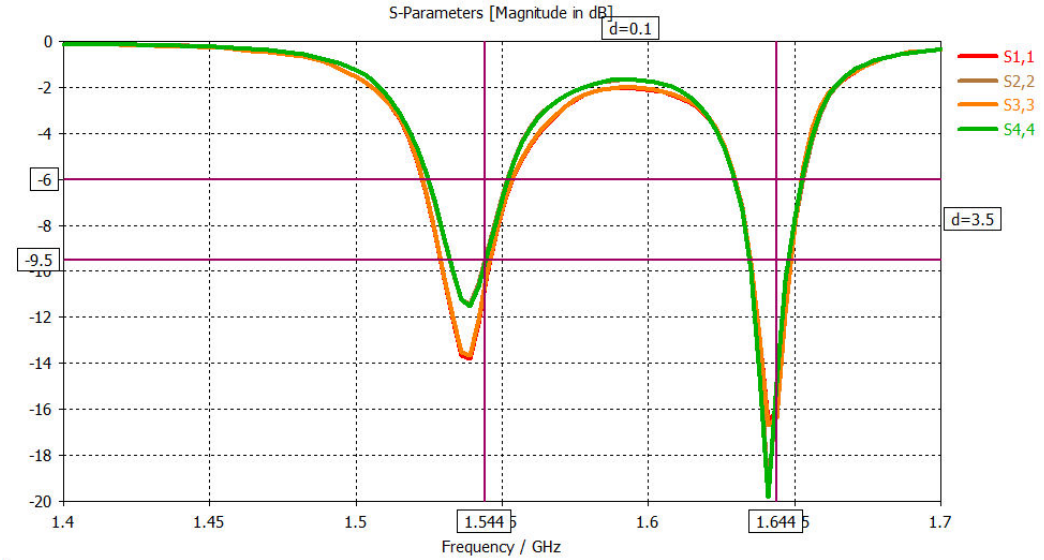


**Figure 4.9:** Reflection coefficient for all ports in 1x2 array [dB])

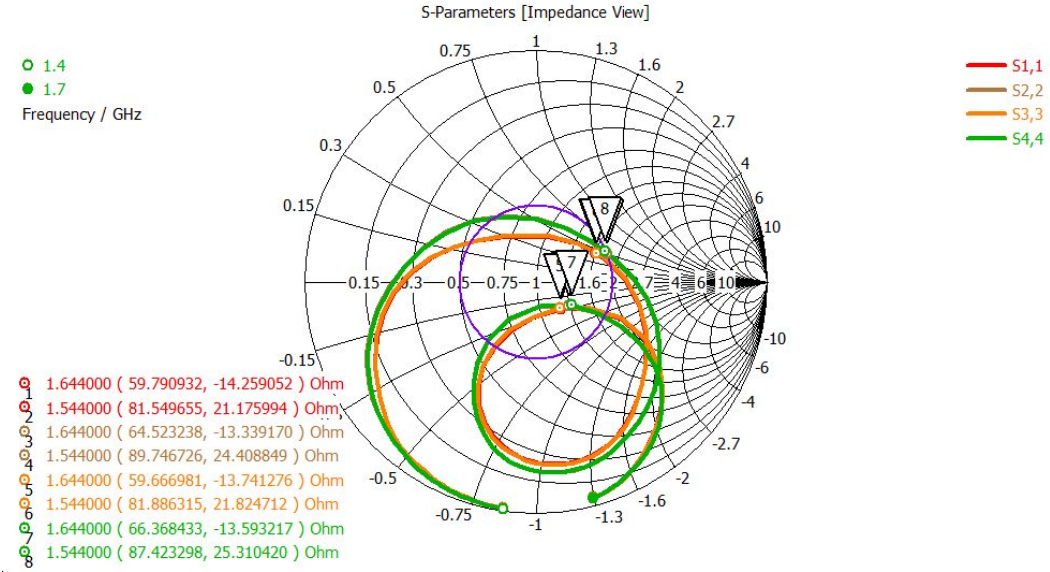


**Figure 4.10:** Reflection coefficient for all ports in 1x2 array (Impedance Smith Chart - VSWR 2:1 circle)

**Beam steering capabilities**

For a linear array, if the desired direction of the beam has the coordinate $\theta = \theta_0$, then the progressive phase shift along $x - axis$ must be equal to [31]:

$$\beta_x = -\frac{2\pi}{\lambda} d_x \sin\theta_0 \cos\phi_0 \tag{4.1}$$

where $d_x$ is the distance between the center of the patch elements on $x - axis$ (here equal to 70 mm).
For steering the beam at a $\theta_0 = 90°$ and $\phi = 0°$ and $\phi = 180°$, according to the Formula 4.2 the progressive phase shift along $x - axis$ should be 135°. By applying a 135° phase shift to each element at once, in both of the cases the beam has its maximum radiation direction at $\theta_0 = 36°$, where the realized gain varies for the two bandwidths. Due to the wide -3dB beam of 60°, the realized gain is higher than 0 dBi for at least $17° \leq \theta \leq 58°$ (the case of the narrower beam).

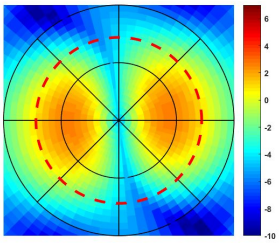

**Figure 4.11:** Sphere coverage in the top plane $0° \leq \theta \leq 90°$ at 1.525 GHz

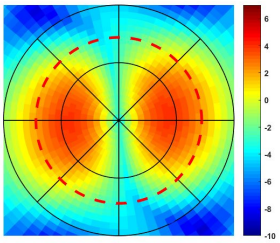

**Figure 4.12:** Sphere coverage in the top plane $0° \leq \theta \leq 90°$ at 1.544 GHz

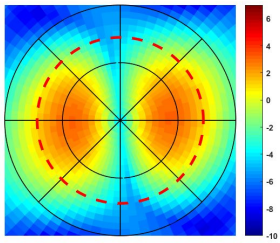

**Figure 4.13:** Sphere coverage in the top plane $0° \leq \theta \leq 90°$ at 1.559 GHz

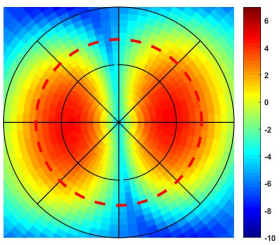

**Figure 4.14:** Sphere coverage in the top plane $0° \leq \theta \leq 90°$ at 1.626 GHz

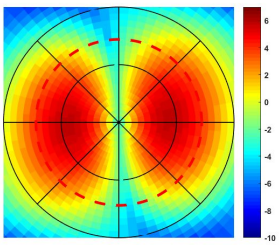

**Figure 4.15:** Sphere coverage in the top plane $0° \leq \theta \leq 90°$ at 1.644 GHz

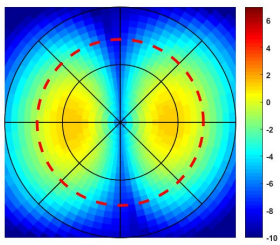

**Figure 4.16:** Sphere coverage in the top plane $0° \leq \theta \leq 90°$ at 1.660 GHz

Figures 4.21 to 4.26 represent 3D polar plots, three for the uplink frequency and three for the downlink frequency band. The construction of the 3D polar plot is described in Figure B.1 [53]. Each plot comprises 4 beams to show the coverage of the sphere in the upper plane of $0° \leq \theta \leq 90°$. The plotted beams on each polar plot are as follows:

- First beam: element 1 has a phase shift of 135° and the direction of radiation is at $\phi = 0°$.
- Second beam: element 2 has a phase shift of 135° and the direction of radiation is at $\phi = 180°$.

The results of the 1 x 2 array show a realized gain over 2 dBi across both frequency bands and axial ratio $\leq$ 6 dB across the high band and the upper part of the low band. The 1 x 2 array has a wide beam, which compensates to a degree the limitation of one direction steering.

## 4.3 2x2 Array

The reasons for implementing a planar array are obtaining higher gain values and improving the beam steering. This section presents the challenging design of the planar array, marking the advantages and disadvantages of this solution. Throughout the project, many arrangements of the elements have been investigated (See appendix B), with only two of them being presented here due to their overall performance. For both designs the link budget is calculated in order to see the usability of the solution for the initial purpose of mobile satellite communication.

In all layouts examples, the following assumptions are made:

- Port 1 and 2 correspond to element 1
- Port 3 and 4 correspond to element 2
- Port 5 and 6 correspond to element 3
- Port 7 and 8 correspond to element 4

### 4.3.1 First design

The first design of the array places the elements by geometrical considerations. The board is split in four equal areas and each patch has its center in the center of an area, as shown is Figures 4.17 and 4.18.

In this geometrical layout, high mutual coupling occurs between closely placed elements, that is element 1

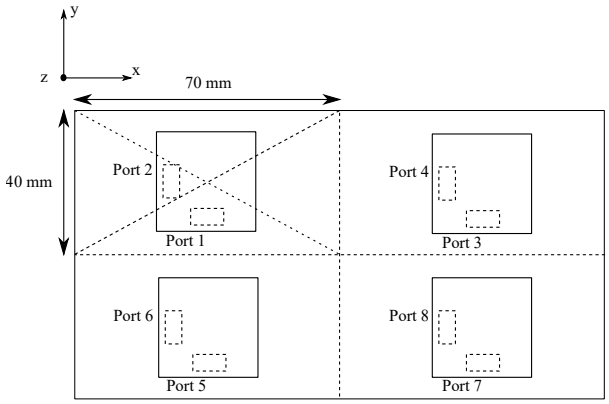


**Figure 4.17:** Position of the 2x2 array (top view)

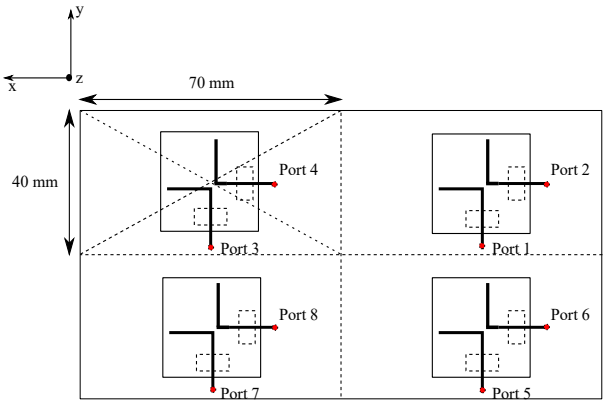


**Figure 4.18:** Position of the 2x2 array (bottom view)

and 3 and 2 and 4 respectively. Although the E-plane mutual coupling usually has higher values than H-plane mutual coupling, in this case higher values occur for ports aligned in H-plane. These cases occur for very small separations between elements and high dielectric constants of the substrate, which is also the case for this design (See appendix B.4). The separation between element 1 and element 3 in terms of $\frac{d}{\lambda_0}$ is approximately 0.05. Therefore, while port 1 and port 5 have a transmission coefficient of $S_{15}$ = -7.31 dB, port 2 and port 6 have a

transmission coefficient of $S26$ = -6.24 dB. The same happens in the case of elements 2 and 4, with ports 3 and port 7 having a transmission coefficient of $S_{37}$= -7.31 dB, port 4 and port 8 have a transmission coefficient of $S48$ = -6.24 dB. Because of a higher coupling between ports in H- plane, two different sets of values have been used for the $\pi - circuit$, as it can be observed in Table 4.7.

After applying the $\pi - circuit$ for obtaining dual resonance, the values of the coupling coefficients change, which is to be expected as the properties of the antenna change. For the H-plane ports, the coupling becomes even worse going from -6.24 dB to -5.35 dB, while in the case of E-plane ports, the coupling decrease to values below -10 dB. Figures 4.19 and 4.20shows the return loss in dB and on the Smith chart for the 2 x 2 array, obtained in

| | C1 | | L | | C2 | |
|---|---|---|---|---|---|---|
| Odd | Value [pF] | ESR [Ω] | Value [nH] | Parasitic resistance [Ω] | Value [pF] | ESR [Ω] |
| Ports | 3 | 0.18 | 12.4 | 0.5 | 2.3 | 0.18 |
| Even | Value [pF] | ESR [Ω] | Value [nH] | Parasitic resistance [Ω] | Value [pF] | ESR [Ω] |
| ports | 1.5 | 0.18 | 13 | 0.5 | 2.2 | 0.18 |

**Table 4.7:** Components values for 2x2 array, SMD model

the simulation. The frequency markers are fixed on the center frequency of each band, 1.544 GHz and 1.644 GHz respectively. The return loss show a narrower band for the odd ports, that is for both low band and high band only 7 MHz bandwidth from 30 MHz is covered with a VSWR 2:1, 20 MHz of the bandwidth is covered with a VSWR 3:1, while the rest of the bandwidth is covered with a VSWR 6:1. For the even ports, the whole bandwidth is covered with a VSWR 2:1. This can be also noticed in the results, where the total efficiency decreases with up to 2 dB towards the limits of the bands and has show a low loss for the center of the band.

Figures 4.19 and 4.20shows the return loss in dB and on the Smith chart for the 2 x 2 array, obtained in the simulation. The frequency markers are fixed on the center frequency of each band, 1.544 GHz and 1.644 GHz respectively. The return loss show a narrower band for the odd ports, that is for both low band and high band only 10 MHz bandwidth from 30 MHz is covered with a VSWR 2:1, 20 MHz of the bandwidth is covered with a VSWR 3:1, while the rest of the bandwidth is covered with a VSWR 6:1. For the even ports, the whole bandwidth is covered with a VSWR 2:1. This can be also noticed in the results, where the total efficiency decreases with up to 2 dB towards the limits of the bands and has show a low loss for the center of the band.

| Frequency [GHz] | 1.525 | 1.544 | 1.559 | 1.626 | 1.644 | 1.660 |
|---|---|---|---|---|---|---|
| Realized Gain [dBi] | 4.58 | 6.4 | 6.16 | 6.18 | 6.41 | 3.97 |
| Radiation Efficiency [dB] | -1.2 | -0.9 | -0.6 | -0.6 | -1 | -1.7 |
| Total Efficiency [dB] | -2.6 | -1 | -1.2 | -1.4 | -1.3 | -3.8 |
| Axial Ratio [dB] | 6 | 4.5 | 3 | 2.5 | 3 | 3.5 |

**Table 4.8:** Results for 2 x 2 array, $1^{st}$ layout

### Beam steering capabilities

For a planar array, if the desired direction of the beam has the coordinates $\theta = \theta_0$ and $\phi = \phi_0$, then the progressive phase shift along $x - axis$ and $y - axis$ respectively must be equal to [31]:

$$\beta_x = -\frac{2\pi}{\lambda} d_x \sin\theta_0 \cos\phi_0 \tag{4.2}$$

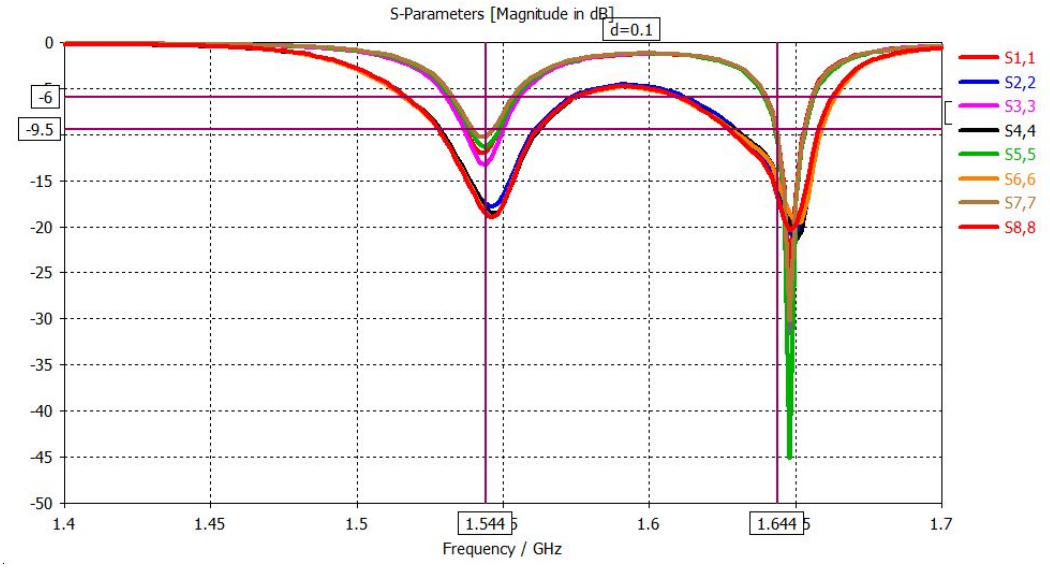


**Figure 4.19:** Reflection coefficient for all ports in 2 x 2 array, $1^{st}$ layout [dB]

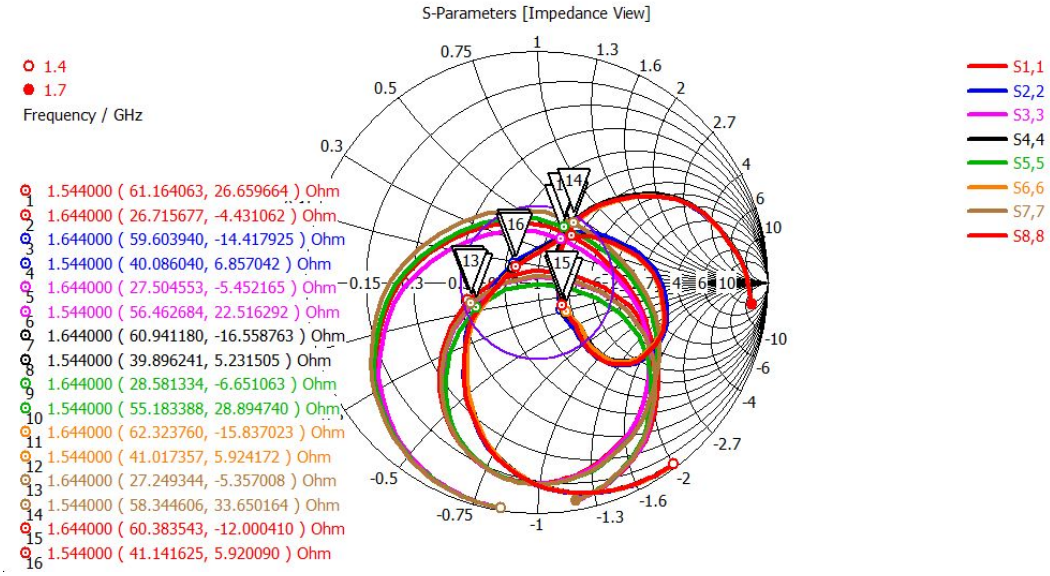


**Figure 4.20:** Reflection coefficient for all ports in 2 x 2 array, $1^{st}$ layout (Impedance Smith Chart - VSWR 2:1 circle) [dB]

$$\beta_y = -\frac{2\pi}{\lambda} d_y \sin\theta_0 \sin\phi_0 \tag{4.3}$$

where $d_x$ is the distance between the center of the patch elements on $x-axis$ (here equal to 70 mm) and $d_y$ is the distance between the center of the patch elements on $y-axis$ (here equal to 40 mm).

For steering the beam at a $\theta_0 = 90°$ and $\phi = 0°$,according to formula 4.2 the progressive phase shift along $x-axis$ should be 135°. By applying a 135° phase shift to elements 1 and 3, the beam has its maximum radiation direction at $\theta_0 = 36°$, where the realized gain varies for the two bandwidths. Due to the wide -3dB beam of 60°, the realized gain is higher than 0 dBi for $12° \leq \theta \leq 65°$.

For steering the beam at a $\theta_0 = 90°$ and $\phi = 90°$,according to formula 4.3 the progressive phase shift along $y-axis$ should be 77°. By applying a 77° phase shift to elements 3 and 4, the beam has its maximum radiation direction at $\theta_0 = 20°$, where the realized gain varies for the two bandwidths. Due to the wide -3dB beam of 90°, the realized gain is higher than 0 dBi for $0° \leq \theta \leq 65°$.

The value of $\theta_0 = 90°$ is not achievable for this array because of different factors like the geometry of the array, surface waves and mutual coupling [54]. This also can be observed in angle of the maximum radiation, which is lower for the $y-axis$ where the elements are closer to each other and the mutual coupling had higher level. The axial ratio is maintained under 6 dB along both frequency bands for values of $0° \leq \theta \leq 65°$.

Figures 4.21 to 4.26 represent 3D polar plots, three for the uplink frequency and three for the downlink frequency band. The construction of the 3D polar plot is described in Figure B.1 [53]. Each plot comprises 4 beams to show the coverage of the sphere in the upper plane $0° \leq \theta \leq 90°$. The plotted beams on each polar plot are as follows:

- First beam: elements 1 and 3 have a phase shift of 135° and the direction of radiation is at $\phi = 0°$.
- Second beam: elements 3 and 4 have a phase shift of 77° and the direction of radiation is at $\phi = 90°$.
- Third beam: elements 2 and 4 have a phase shift of 135° and the direction of radiation is at $\phi = 180°$.
- Fourth beam: elements 1 and 2 have a phase shift of 77° and the direction of radiation is at $\phi = 270°$.

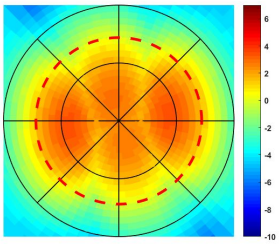


**Figure 4.21:** Sphere coverage in the top plane $0° \leq \theta \leq 90°$ at 1.525 GHz

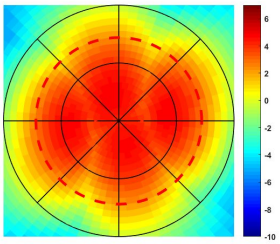


**Figure 4.22:** Sphere coverage in the top plane $0° \leq \theta \leq 90°$ at 1.544 GHz

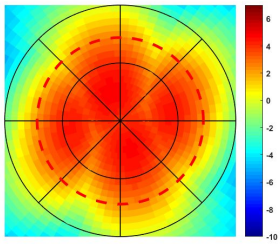


**Figure 4.23:** Sphere coverage in the top plane $0° \leq \theta \leq 90°$ at 1.559 GHz

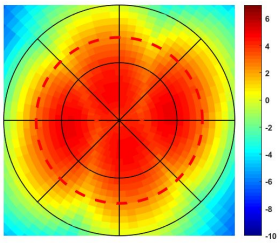

**Figure 4.24:** Sphere coverage in the top plane $0° \leq \theta \leq 90°$ at 1.626 GHz

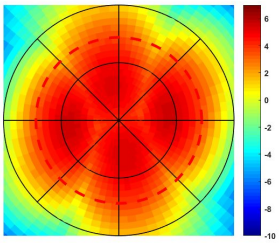

**Figure 4.25:** Sphere coverage in the top plane $0° \leq \theta \leq 90°$ at 1.544 GHz

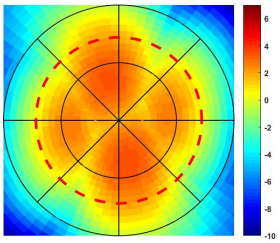

**Figure 4.26:** Sphere coverage in the top plane $0° \leq \theta \leq 90°$ at 1.660 GHz

| Frequency [GHz] | 1.525 | 1.544 | 1.559 | 1.626 | 1.644 | 1.660 |
|---|---|---|---|---|---|---|
| Axial Ratio [dB] | 6 | 5 | 3 | 3 | 5 | 8 |

**Table 4.9:** Axial ratio value when the beam is steered ($\theta \leq 65°$), $1^{st}$ layout

### Link budget calculation

The link budged follows the example of the one presents in 2.1.3. Two link budget calculations are shown, one for the lowest gain obtained in both bands and one for the highest gain obtained in both bands. This is not necessarily the case in reality but it shows the transmission performance in the worst and best case scenarios.

| | Unit | f |
|---|---|---|
| UPLINK | | |
| Frequency | GHz | 1.626-1.660 |
| MS EIRP | dBW | 6.97 |
| Path loss | dB | 187 |
| Atmospheric loss | dB | 0.1 |
| Polarization loss | dB | 0.17 |
| Satellite G/T | dB/K | 12.7 |
| Boltzmann constant | dBW/K/Hz | -228.6 |
| Bandwidth | dBHz | 52.76 |
| Up-path C/N_0 | dBHz | 59.75 |
| DOWNLINK | | |
| Frequency | GHz | 1.525 |
| Satellite EIRP | dBW | 50 |
| Path loss | dB | 187 |
| Atmospherics loss | dB | 0.1 |
| Polarization loss | dB | 0.45 |
| MS G/T | dB/K | -15.45 |
| Boltzmann constant | dBW/K/Hz | -228.6 |
| Bandwidth | | 52.76 |
| Down-path C/N_0 | dBHz | 76.2 |
| TOTAL | | |
| Mean overall C/N_0 | dBHz | 59.63 |
| Mean overall C/N | dB | 6.87 |

**Table 4.10:** Link budget calculation for lowest gain values on both Uplink and Downlink, $1^{st}$ layout

| | Unit | f |
|---|---|---|
| UPLINK | | |
| Frequency | GHz | 1.626-1.660 |
| MS EIRP | dBW | 9.41 |
| Path loss | dB | 187 |
| Atmospheric loss | dB | 0.1 |
| Polarization loss | dB | 0.12 |
| Satellite G/T | dB/K | 12.7 |
| Boltzmann constant | dBW/K/Hz | -228.6 |
| Bandwidth | dBHz | 52.76 |
| Up-path C/N_0 | dBHz | 62.24 |
| DOWNLINK | | |
| Frequency | GHz | 1.525 |
| Satellite EIRP | dBW | 50 |
| Path loss | dB | 187 |
| Atmospherics loss | dB | 0.1 |
| Polarization loss | dB | 0.27 |
| MS G/T | dB/K | -15.63 |
| Boltzmann constant | dBW/K/Hz | -228.6 |
| Bandwidth | | 52.76 |
| Down-path C/N_0 | dBHz | 77.28 |
| TOTAL | | |
| Mean overall C/N_0 | dBHz | 62.11 |
| Mean overall C/N | dB | 9.35 |

**Table 4.11:** Link budget calculation for highest gain values on both Uplink and Downlink, $1^{st}$ layout

The calculation of the link budget is made using the following values:

- 2 W transmission power of the user terminal
- 40 dBi gain of the spot team(minimum level)
- 50 dBW EIRP of the spot beam out of 70 dBW, maximum attainable [15]
- 100° K system noise temperature A.1.1.

From the link budgets calculations and , it can be seen that in the case of the minimum gain performance on both bands, the values of the $C/N$ undergoes the required values for voice and data services shown in Table 2.5. Also, when steering the beam of the array, due to the large width, not many directions of the beam are needed which can reduce the complexity of the beam steering network.

### 4.3.2 Second design

The first design showed high values for the transmission coefficient between elements placed above each other due to narrow width of the board, which is already 1 cm larger than the phone width so no further enlargement is considered. In the second design, the elements are not placed one above the other, but with a shift of the same size as one element as shown in Figures 4.27 and 4.28.

With this placement of the elements, the transmission coefficient between the ports drops below $-10$ dB. A

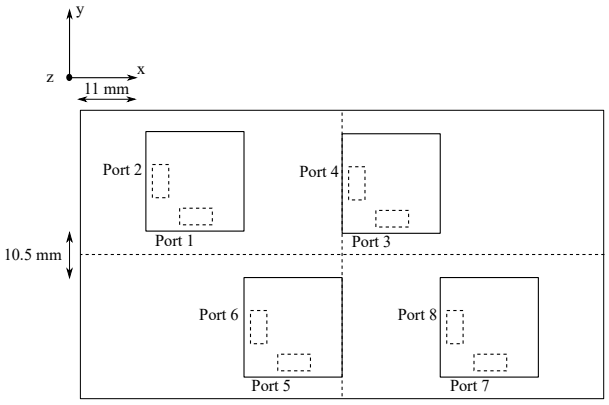


**Figure 4.27:** Spread placing of the 2x2 array (top view)

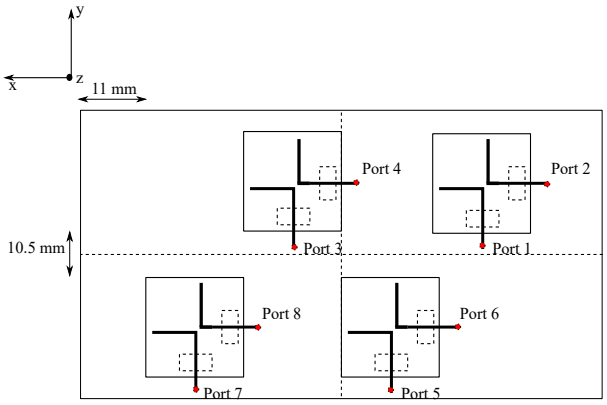


**Figure 4.28:** Spread placing of the 2x2 array (bottom view)

more rigorous study is made in [55], where a similar case is treated, when the patches are places in a similar way, with the conclusion that moving the patches further away from each other, in any direction, will result in a decrease of the coupling between them. In the same study, an investigation is made of rotating the patches at different angles relative to each other. This does not give considerable change in the coupling according to their results, the best option being still the first, moving the patches away from each other in any direction.

The same $\pi - network$ used in the previous layouts is applied for obtaining dual resonance, with the values of the components presented in Table 4.7.

Figures 4.29 and 4.30shows the return loss in dB and on the Smith chart for the 2 x 2 array. The frequency markers are fixed on the center frequency of each band, 1.544 GHz and 1.644 GHz respectively. The return loss show a narrower band for the odd ports, that is for the low band only 10 MHz bandwidth from 30 MHz is covered with a VSWR 2:1, 25 MHz of the bandwidth is covered with a VSWR 3:1, while the rest of the bandwidth is covered with a VSWR 6:1. In case of the high band, only 5 MHz bandwidth from 30 MHz is covered with a VSWR 2:1, 15 MHz of the bandwidth is covered with a VSWR 3:1, while the rest of the bandwidth is covered with a VSWR 6:1. This can be also noticed in the results, where the total efficiency decreases with up to 2 dB towards the limits of the bands and has show a low loss for the center of the band.

#### Beam steering capabilities

For steering the beam in 4 main directions, $\phi = 0°$, $\phi = 90°$, $\phi = 180°$, and $\phi = 270°$ ,the same phase shifts as in the case of the first design are applied. The main direction are slightly shifted from the ones mentioned above, resulting in $\phi = 20°$, $\phi = 120°$, $\phi = 200°$, and $\phi = 300°$ . This is a result of spreading the elements on

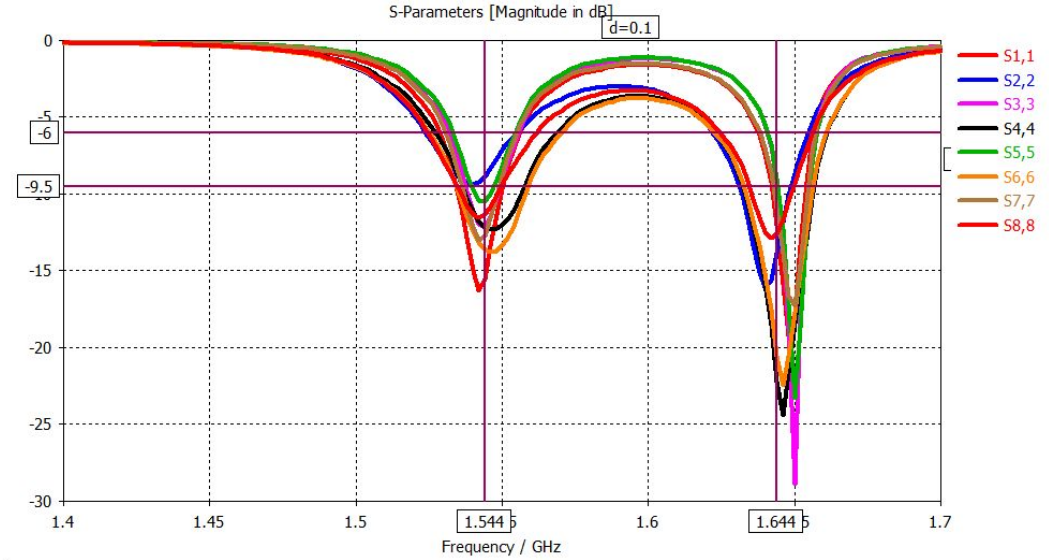


**Figure 4.29:** Reflection coefficient for all ports in 2 x 2 array, $2^{nd}$ layout [dB]

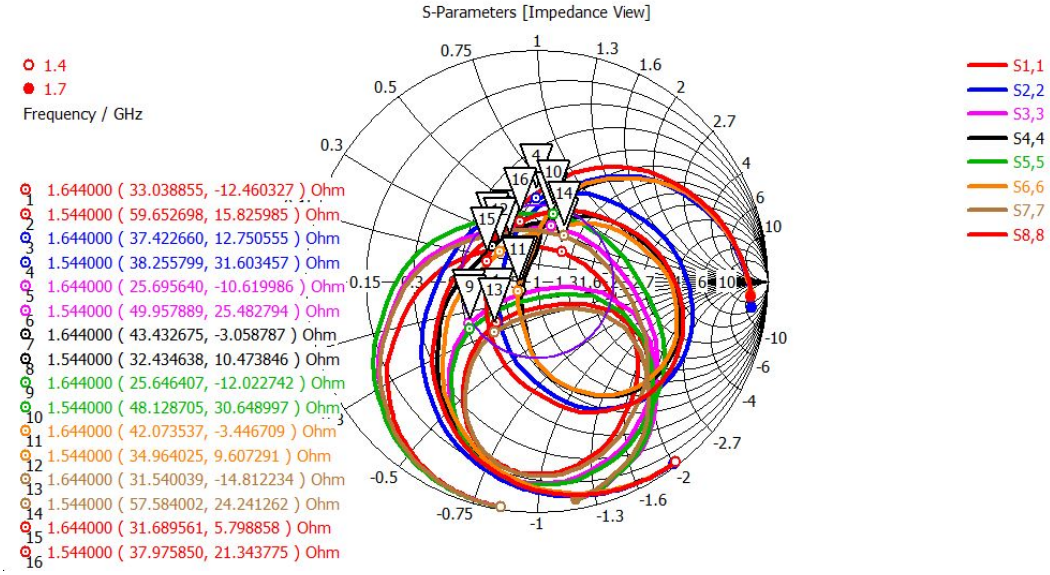


**Figure 4.30:** Reflection coefficient for all ports in 2 x 2 array, $2^{nd}$ layout (Impedance Smith Chart - VSWR 2:1 circle)

| Frequency [GHz] | 1.525 | 1.544 | 1.559 | 1.626 | 1.644 | 1.660 |
|---|---|---|---|---|---|---|
| Realized Gain [dBi] | 4.49 | 6.34 | 6.33 | 6.13 | 6.71 | 4.88 |
| Radiation Efficiency [dB] | -1.18 | -0.92 | -0.73 | -0.54 | -0.92 | -1.46 |
| Total Efficiency [dB] | -2.81 | -1.07 | -1.13 | -1.56 | -1.11 | -2.98 |
| Axial Ratio [dB] | 6.5 | 6 | 5 | 3 | 5 | 6 |

**Table 4.12:** Results for the 2x2 array, $2^{nd}$ layout

the board and not having them in the same position on $x - axis$ as in the first design. However, as the shift is approximately the same for all four beams, this does not affect the overall sphere coverage, resulting in a similar patter as for the one in the first design.

The phase shifts are calculated and applied in order to steer the beam at $\theta_0 = 90°$ for all four values of $\phi$. This again cannot be achieved from reasons specified in the case of the first model. For the directions $\phi = 20°$, and $\phi = 200°$, the main lobe direction is at $\theta_0 = 36°$, where the realized gain varies for the two bandwidths. Due to the wide -3dB beam of 60°, the realized gain is higher than 0 dBi for at least $10° \leq \theta \leq 65°$.

For the directions $\phi = 120°$, and $\phi = 300°$, the main lobe direction is at $\theta_0 = 23°$, where the realized gain varies for the two bandwidths. Due to the wide -3dB beam of 76°, the realized gain is higher than 0 dBi for at least $0° \leq \theta \leq 62°$.

The axial ratio for $0° \leq \theta \leq 65°$ has values less than 7 dB, with an exception in the case of the the end of the high band, f = 1.660 GHz, where for $\phi = 20°$ and $\phi = 200°$ the axial ratio reaches 11 dB.

Figures 4.31 to 4.36 represent 3D polar plots, three for the uplink frequency and three for the downlink frequency band. Each plot comprises 4 beams to show the coverage of the sphere in the upper plane $0° \leq \theta \leq 90°$. The plotted beams on each polar plot are as follows:

- First beam: elements 1 and 3 have a phase shift of 135° and the direction of radiation is at $\phi = 20°$.
- Second beam: elements 3 and 4 have a phase shift of 77° and the direction of radiation is at $\phi = 120°$.
- Third beam: elements 2 and 4 have a phase shift of 135° and the direction of radiation is at $\phi = 200°$.
- Fourth beam: elements 1 and 2 have a phase shift of 77° and the direction of radiation is at $\phi = 300°$.

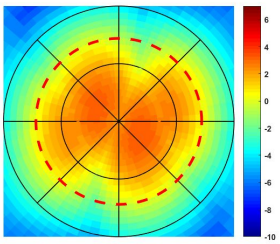

**Figure 4.31:** Sphere coverage in the top plane $0° \leq \theta \leq 90°$ at 1.525 GHz

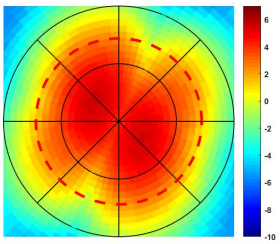

**Figure 4.32:** Sphere coverage in the top plane $0° \leq \theta \leq 90°$ at 1.544 GHz

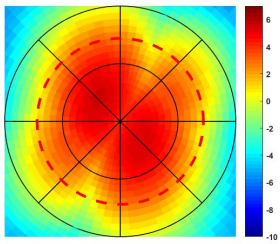

**Figure 4.33:** Sphere coverage in the top plane $0° \leq \theta \leq 90°$ at 1.559 GHz

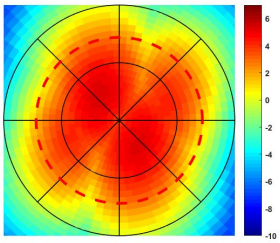

**Figure 4.34:** Sphere coverage in the top plane $0° \leq \theta \leq 90°$ at 1.626 GHz

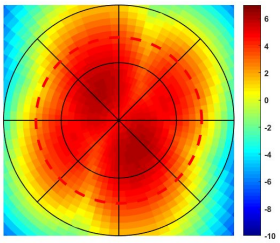

**Figure 4.35:** Sphere coverage in the top plane $0° \leq \theta \leq 90°$ at 1.644 GHz

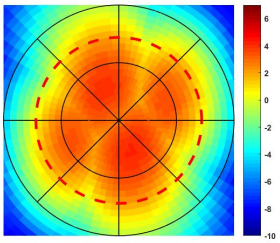

**Figure 4.36:** Sphere coverage in the top plane $0° \leq \theta \leq 90°$ at 1.660 GHz

| Frequency [GHz] | 1.525 | 1.544 | 1.559 | 1.626 | 1.644 | 1.660 |
|---|---|---|---|---|---|---|
| Axial Ratio [dB] | 7 | 6 | 7 | 3 | 5 | 11 |

**Table 4.13:** Axial ratio value when the beam is steered ($\theta \leq 65°$), $1^{st}$ layout

### Link budget calculation

As in the case of the first design, two link budget calculations are shown, one for the lowest gain obtained in both bands and one for the highest gain obtained in both bands.

| | Unit | f |
|---|---|---|
| UPLINK | | |
| Frequency | GHz | 1.626-1.660 |
| MS EIRP | dBW | 7.88 |
| Path loss | dB | 187 |
| Atmospheric loss | dB | 0.1 |
| Polarization loss | dB | 0.45 |
| Satellite G/T | dB/K | 12.7 |
| Boltzmann constant | dBW/K/Hz | -228.6 |
| Bandwidth | dBHz | 52.76 |
| Up-path C/N_0 | dBHz | 60.38 |
| DOWNLINK | | |
| Frequency | GHz | 1.525 |
| Satellite EIRP | dBW | 50 |
| Path loss | dB | 187 |
| Atmospherics loss | dB | 0.1 |
| Polarization loss | dB | 0.52 |
| MS G/T | dB/K | -15.54 |
| Boltzmann constant | dBW/K/Hz | -228.6 |
| Bandwidth | | 52.76 |
| Down-path C/N_0 | dBHz | 75.12 |
| TOTAL | | |
| Mean overall C/N_0 | dBHz | 60.24 |
| Mean overall C/N | dB | 7.48 |

**Table 4.14:** Link budget calculation for lowest gain values on both Uplink and Downlink, $2^{nd}$ layout

| | Unit | f |
|---|---|---|
| UPLINK | | |
| Frequency | GHz | 1.626-1.660 |
| MS EIRP | dBW | 9.71 |
| Path loss | dB | 187 |
| Atmospheric loss | dB | 0.1 |
| Polarization loss | dB | 0.34 |
| Satellite G/T | dB/K | 12.7 |
| Boltzmann constant | dBW/K/Hz | -228.6 |
| Bandwidth | dBHz | 52.76 |
| Up-path C/N_0 | dBHz | 62.3 |
| DOWNLINK | | |
| Frequency | GHz | 1.525 |
| Satellite EIRP | dBW | 50 |
| Path loss | dB | 187 |
| Atmospherics loss | dB | 0.1 |
| Polarization loss | dB | 0.45 |
| MS G/T | dB/K | -13.66 |
| Boltzmann constant | dBW/K/Hz | -228.6 |
| Bandwidth | | 52.76 |
| Down-path C/N_0 | dBHz | 77 |
| TOTAL | | |
| Mean overall C/N_0 | dBHz | 62.1 |
| Mean overall C/N | dB | 9.42 |

**Table 4.15:** Link budget calculation for highest gain values on both Uplink and Downlink, $2^{nd}$ layout

From the link budgets calculations in Table 4.14 and 4.15, it can be seen that in the case of the minimum gain performance on both bands, the values of the $C/N$ meets the required values for voice and data services shown in Table 2.5. The same as in the case of the first planar array, the wide beam represents an advantage for the beam steering.

### 4.3.3 Comparison between arrays

This section briefly summarizes the results from the simulation based on the results that have been shown throughout this chapter. This discussion will contribute to the final conclusion that will be drawn in Chapter 6.

Starting by comparing the results of the liniar array with the results of the planar arrays, the ones of a liniar array have lower values for the realized gain.For the ease of reading, the values of the gain for the 3 arrays are given in Table 4.16. As expected, doubling the number of elements would also reflect as an increase in the gain. The axial ratio respects the expected values in the case of the planar array.

A significant difference between the arrays appears at beam steering, where as known from the theory, the linear array can only scan in one direction, while the planar arrays can scan at any point in space. All three array can only scan up to an angle of $\theta_0 = 36^\circ$, but due to the wide beam, the sphere coverage can extend up to $\theta_0 = 60^\circ$.

From comparing only the two planar arrays it can be seen that both 2 x 2 arrays have similar performance

| Frequency [GHz] | | 1.525 | 1.544 | 1.559 | 1.626 | 1.644 | 1.660 |
|---|---|---|---|---|---|---|---|
| Realized Gain [dBi] | 1x2 array | 4.07 | 5.48 | 4.68 | 4.93 | 6.1 | 2.88 |
| | 2x2 array $1^{st}$ layout | 4.58 | 6.4 | 6.16 | 6.18 | 6.41 | 3.97 |
| | 2x2 array $2^{nd}$ layout | 4.49 | 6.34 | 6.33 | 6.13 | 6.71 | 4.88 |

**Table 4.16:** Realized gain for the three implemented arrays

in terms of gain and axial ratio. In the case of the second layout, the established value of 6 dB for the axial ratio is not met anymore in the lower frequency band.

When steering the beam, the coverage given by the two arrays is similar, both having the same scanning capabilities and wide beams. The axial ratio worsens for both arrays, for the second array exceeding the traget value of 6 dB in most of the cases.

# Chapter 5

# Implementation

This chapter presents the manufacturing of the first design of the planar array. Going from simulations to real implementation poses a variety of challenges and the results are not always as expected because of the factors like: imperfections of the materials, imperfection of the components, alignment of the feeding and many others which will be mentioned throughout this chapter.

## 5.1 Implementation

The manufacturing of the antenna prototype has been made with different materials and dimensions than the simulated version, using the available materials and components. The materials used for fabricating the prototype are:

- *Preperm 700HF* with a height of 3.2 mm for the antenna substrate
- *FR4* with a height of 0.5 mm for the feeding substrate.
- For the length and width of the board, the same dimensions have been kept, 140 x 80 mm.
- For the patch antenna, copper tape has been used.

The substrate used for the antenna, Preperm 700HF has a dielectric constant of $\epsilon_r$ =7 and a loss tanget of $\gamma$ =0.0006 [56]. Lowering the dielectric constant will result in an increase of the resonance frequency of the patch. This will impose an enlarging of the patch dimensions, to adjust the resonance frequency as in the previous simulated array. Therefore, the patch will have the dimensions 33 x 33 mm, in order to have a resonance at 1.6 GHz.

The substrate used for the feeding, FR4, has a dielectric constant of $\epsilon_r$ = 4.3 and a loss tangent of $\gamma$ = 0.25 as defined by the simulation program. By changing the feeding substrate with one with a lower dielectric constant, will result in a change of the feeding parameters, as presented in Table 5.1. The tangent loss of the FR4 is considerably larger than the tangent loss of Rogers (12 times larger), which will also affect the efficiency of the antenna.

For an easy manufacturing process, the feeding microstrip lines were extended to the rim of the feeding board. Keeping the initial lengths as in the simulations would require an embedded coaxial feeding, which due to the short time, it could not be realized. All the microstrip lines keep the same length, as not to introduce unwanted

| | $W_{fs}$ | $L_{fs}$ | $d_{fs}$ | $W_{fl}$ | $L_{fl}$ | $L_d$ | $L_s$ | $L_c$ | $d_f$ |
|---|---|---|---|---|---|---|---|---|---|
| Value [mm] | 3 | 13 | 10.5 | 1 | 15 | 2 | 7.5 | 12 | 2 |

**Table 5.1:** Feeding parameters for the prototype using FR4 as a feeding substrate ($h_{fs} = 0.5mm$)

phase shifts. The components were placed directly on the microstrip line and for grounding, a small pad was added. The grounding pad is then connected to the ground plane through a copper cable.

The first prototype with the above mentioned characteristics proved to be impractical because of the grounding

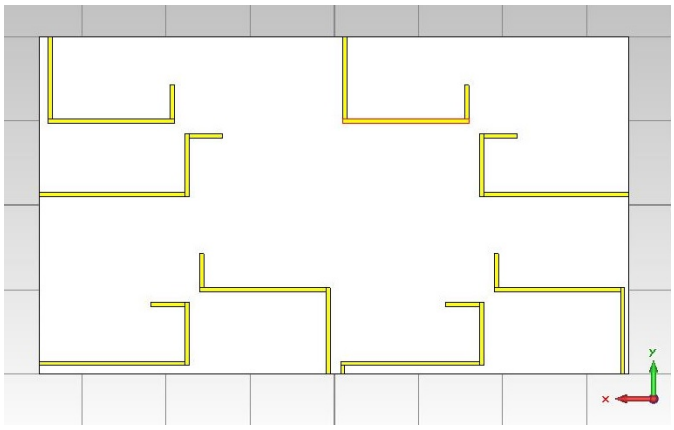

**Figure 5.1:** Microstrip lines adjusted for the prototype design

pads (See Figures C.1 and C.2 in appendix), where the soldering introduced a height which was considerable for the coupling between the slot and antenna. Tested in the simulation, an air gap of 0.5 mm would completely affect the coupling. Therefore, for the next prototype, the feeding board was enlarged with 2 mm in each direction, resulting in a 144 x 84 mm feeding board (see Figure in appendix). The antenna board was kept as initially mentioned.

In Figure 5.2 it can be noticed that ground pads have been enlarged as well. Initially, the copper cable was

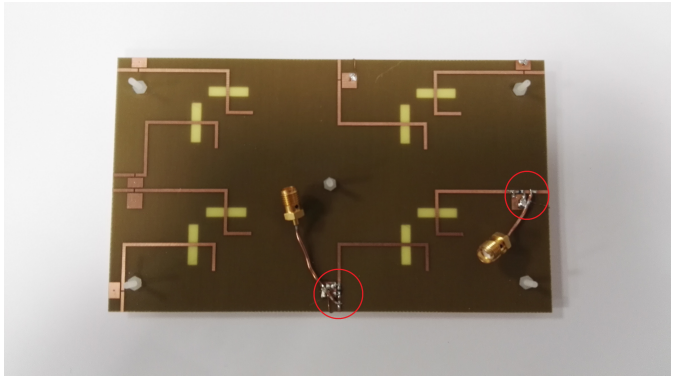

**Figure 5.2:** Prototype feeding board, FR4, 144 x 84 mm (top view)

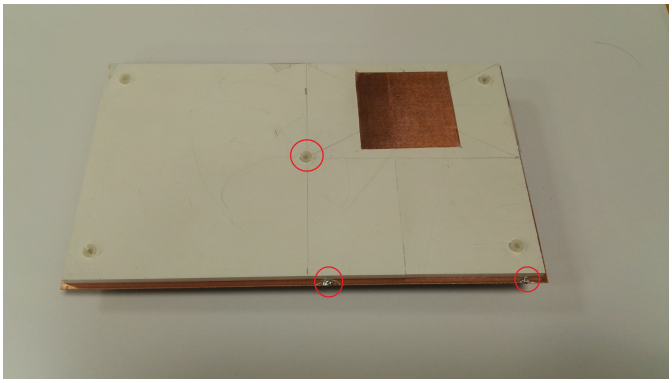

**Figure 5.3:** Prototype antenna, FR4, 144 x 84 mm (bottom view)

connected to the other side through a small hole. This resulted again into an air gap, because of the wire in between the ground plane and the substrate. Eventually the wire was grounded as shown in Figure 5.4.

For the new enlarged substrate, simulations were performed as well to investigate how the dual band matching

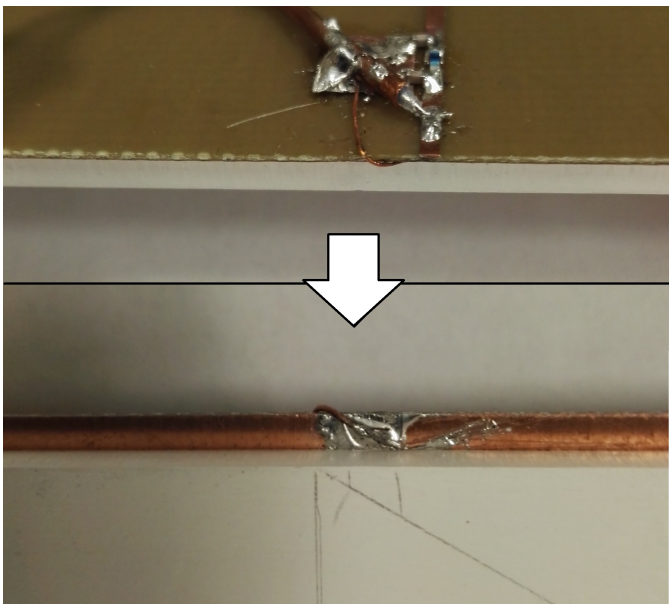

**Figure 5.4:** Grounding copper wire for the enlarged feeding board

will change for the new structure, as shown in Figures 5.5 and 5.7.

In the first simulation of the prototype, the matching is performed in CST Design as in the simulations in Chapter 4 and as described in the appendix B.5. The values of the components optimized in the simulation programs are given in Table 5.2 and the results of the array performance are given in Table 5.3.

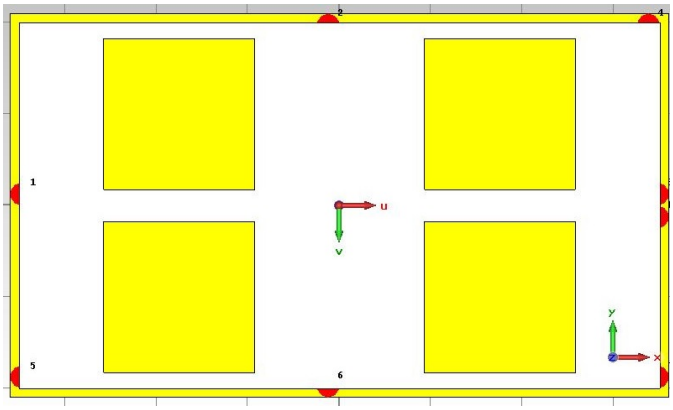


**Figure 5.5:** Prototype simulation with a feeding board of 144 x 84 mm (top view)

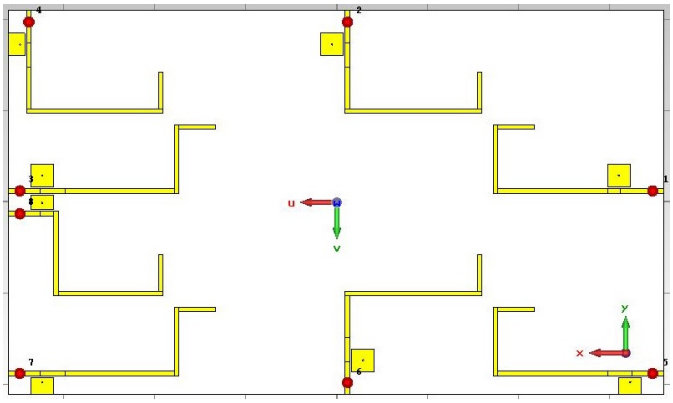


**Figure 5.6:** Prototype simulation with a feeding board of 144 x 84 mm (back view)

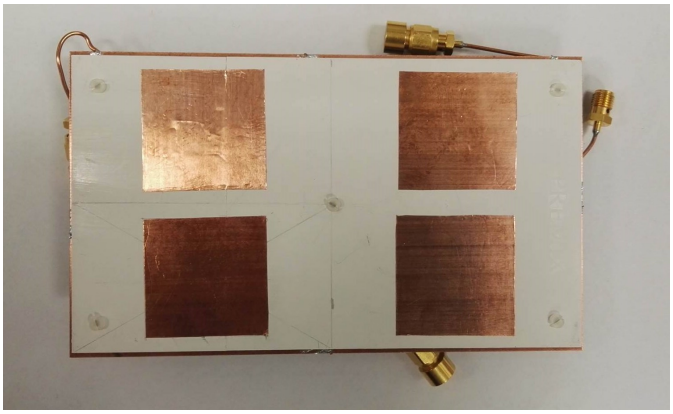

**Figure 5.7:** Prototype antenna array with a feeding board of 144 x 84 mm (top view)

| | C1 | | L | | C2 | |
|---|---|---|---|---|---|---|
| Odd Ports | Value [pF] | ESR [Ω] | Value [nH] | Parasitic resistance [Ω] | Value [pF] | ESR [Ω] |
| | 3.9 | 0.1 | 5.6 | 0.5 | 0.2 | 0.1 |
| Even ports | Value [pF] | ESR [Ω] | Value [nH] | Parasitic resistance [Ω] | Value [pF] | ESR [Ω] |
| | 3.3 | 0.1 | 5.5 | 0.5 | 0.2 | 0.1 |

**Table 5.2:** Components values for 2 x 2 array prototype, SMD model

| Frequency [GHz] | 1.525 | 1.544 | 1.559 | 1.626 | 1.644 | 1.660 |
|---|---|---|---|---|---|---|
| Realized Gain [dBi] | 4.18 | 4.88 | 5.13 | 6.05 | 5.55 | 4.27 |
| Radiation Efficiency [dB] | -2.9 | -2.12 | -1.54 | -1.5 | -2.17 | -2.9 |
| Total Efficiency [dB] | -3.2 | -2.61 | -2.42 | -1.7 | -2.36 | -3.7 |
| Axial Ratio [dB] | 7 | 5.5 | 4.5 | 5.5 | 6 | 5.5 |

**Table 5.3:** Simulated results for 2 x 2 array prototype

For a more practical approach, the program allows component implementation in the CST Microwave environment. This option only allows the input of the component value and parasitic resistance, as in the case of the SMD modeling from CST Design. The same values for the components are assigned to the components added in CST Microwave as shown in Figure 5.8.

Because of the high computation time, only two ports from one element have been simulated in this man-

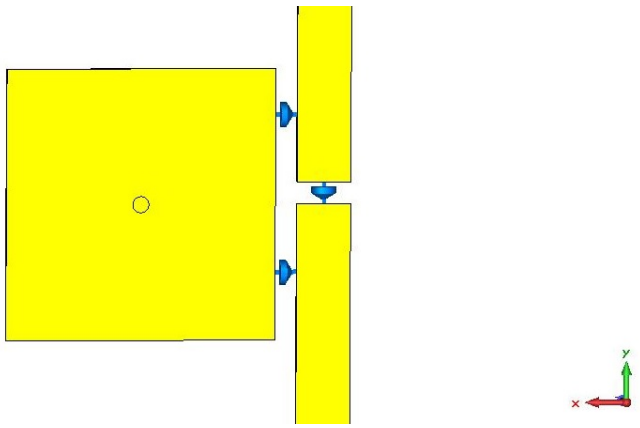


**Figure 5.8:** Adding components in CST Microwave environment

5

ner at the beginning. Figures 5.9 and 5.10 illustrates the reflection coefficient of the ports obtained from the two simulations. The difference between the two results, although the component are defined approximately the same, can appear from various implementation of the second design, like the following:

- the length of the components in CST Design is considered infinitesimal and the connections between them are considered lossless while in CST Microwave, each component has a length as the one specified in practice (0.4 mm)
- when placing the components in CST Microwave environment, an additional length of the microstrip line

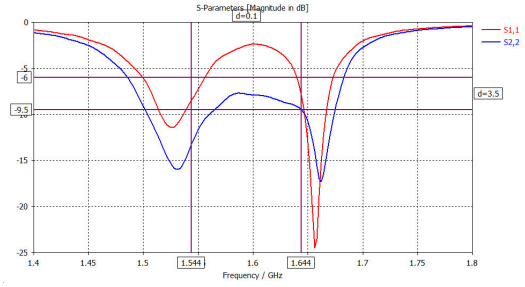


**Figure 5.9:** Reflection coefficient for the prototype simulation where components are added in CST Design environment

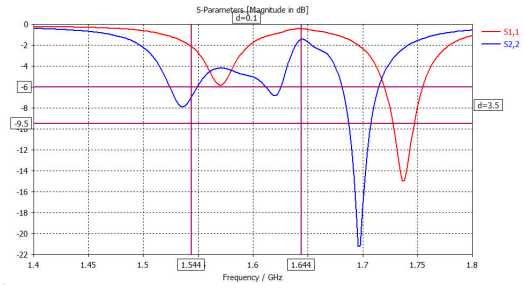


**Figure 5.10:** Reflection coefficient for the prototype simulation where components are added in CST Microwave environment

is added between the feeding point and the matching circuit

- the grounding in CST Design is made directly to each component, while in CST Microwave is made through a wire that is connected to the ground plane, which will introduce additional losses

Due to the short available time for the implementation and the long computation time of the electromagnetic solver, different sets of components' values close to the ones obtained in simulations, were tried directly on the prototype, the final values being given in Table 5.4. Because of the frail design, only one of the port was measured on the vector network analyzer, that is port 2 of element 1, shown in Figure 5.11. It can be observed that the resonances are in 1.466 GHz and 1.566 GHz. This shift can be caused by various implementation flaws like:

- the additional high inductance from the grounding wire in series with the ground plane
- the nonuniform patch element which is applied as a copper tape
- bad alignment of the patch with the feeding slots
- variance of the components

The total efficiency measured in the antenna test facility Starlab is shown in Figure 5.12, with a value of -4.8 dB in the low band an -4.77 dB in the high band. On the simulation, the total efficiency has a value of -3.1 dB in the low band and -2.7 dB in the high band. The differences may be caused by different factors: from the measurement devices imperfections to the placement of the antenna and prototype design flaws.

The manufactured prototype showed various implementation problems and as a consequence only one port was measured and presented. However, the reader should have in mind that the prototype was made with the

| C1 | L | C2 |
|---|---|---|
| Value [pF] | Value [nH] | Value [pF] |
| 4.3 | 4.3 | 1.6 |

**Table 5.4:** Components values for the prototype array

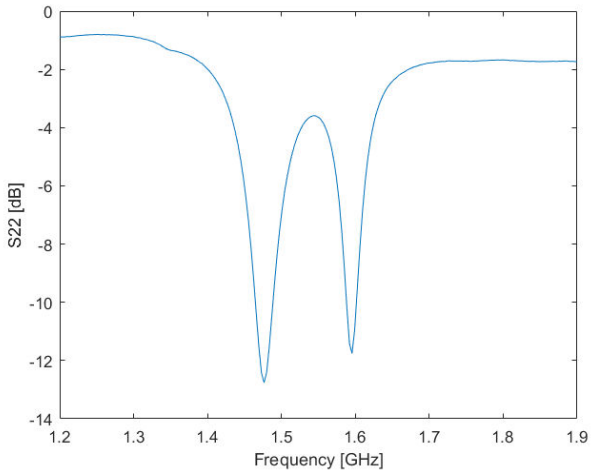


**Figure 5.11:** Reflection coefficient of a single port from the prototype

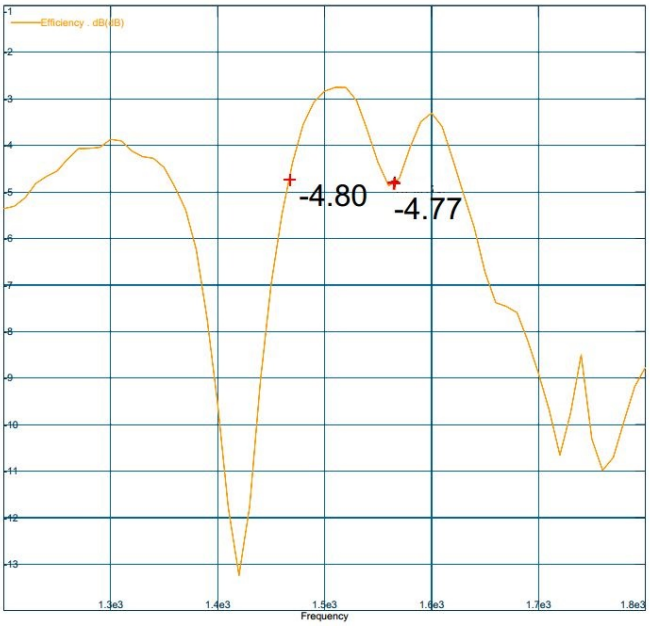


**Figure 5.12:** Total efficiency of a single port from the prototype

available materials and manufacturing techniques. The independent feeding modeling proved to be very useful and simplified the process. Therefore, whenever a problem appeared to the feeding board (grounding pads, components, etc), the antenna board did not need any modification, as it was attached with the help of nylon screws.

### 5.1.1 Phase shifter implementation and losses

The technique applied in this project for obtaining different beam directions is *phase shifting* the input signal of each antenna, through post processing. In practice this requires a phase shifter which introduces considerable losses. For example, a 4-bit digital phase shifter [57] in the frequency range 1.2 - 2.4 GHz introduces a 3.2 to 5 dB loss, while a 6-bit digital phase shifter [58] in the same frequency range introduces a 5 to 6 dB loss.

Applied to the proposed antenna array, the insertion loss of the phase shifter is significant high. An analog phase shifter, which has the same effect but a different implementation, also introduces considerable losses in the range of 3 dB [59]. In [60], different implementations of the phase shifter are presented. The ones that present advantages for the low Gigahertz frequencies, which is the case in this project are *local oscillator path beamforming*, *baseband beamforming* and *digital beamforming*.

Another solution would be using predefined beam patterns which can be achieved through a Butler matrix. In the case of the proposed antenna, it can be observed from the results, that by only 4 steered beam patterns, optimal results of the gain and axial ratio are obtained for $0^\circ \leq \theta \leq 65^\circ$.

By implementing the beam pattern with the fixed phase shifts specified in Chapter 4, this would require each port to have at least 2 phase shifters: one for 77 and one for 135 degrees. Using the phase shifters presented in [61], each with a loss of 0.5 dB and considering that only 2 antennas need to be connected at a times, will result in an overall $2dB$ loss for the realized gain, as each antenna has 2 individual ports. However, by using the second layout, if all the ports have the same matching network, the 2 ports can be connected to one matching network and therefore to a single phase shifter, through the use of T-junction and a microstrip line of length $\frac{\lambda}{4}$ for introducing the $90^\circ$. By using only two phase shifter for a beam direction, the loss is reduced to 1 dB.

# Chapter 6

# Conclusion and Further Development

## 6.1 Conclusion

The main purpose of the project was to design an beam steerable antenna array for a modular phone with application in mobile satellite communications. The design and simulations were created and performed in CST Microwave, an electromagnetic simulator. The design started from the design of a single element, followed by the implementation in the linear array form and finalizing with two designs for planar array.

In the beginning of the project an analysis of the link and modular phone was made in order to establish the main characteristics and performance requirements of the antenna. Based on the findings from the analysis, the selected antenna type to be implemented in the array was a patch antenna which operates in L-band, using the Inmarsat satellites. Another main aspect of the array implementation that resulted from the analysis, was that it cannot be deployed in the available area of the modular phone, given the small, individual tiles. This led to relocating the array to an external add-on, a cover that can be attached to the modular phone through the use of a tile and will have similar dimensions with the modular phone.

The main conflict was still the available space for the array structure because of the large dimensions of an antenna array operating in L-band. Consequently, a high dielectric was used for the antenna substrate which together with the small spacing between elements in the case of a planar array (2 x 2 array), resulted in high mutual coupling between patches. Because of this, different matching networks were used for the different ports of a single antenna, which in the implementation stage will introduce more losses. Therefore, another design of the planar array was proposed in the final of the project, but with a drawback in terms of axial ratio performance. The results of both designs were then input in the link budget, to see if they meet the requirements of the carrier to noise ratio. In the case of the linear array (1 x 2 array), the distance between elements is larger and the coupling does not pose a problem to the antenna performance but with the cost of a lower gain.

Beam steering was also implemented, paying close attention to the gain and axial ratio variations. The latter worsens considerably in the case of the second design, reaching a value of 11 dB or 1.2 dB when translated into polarization losses. The main goal was to follow the specifications of an Inmarsat product, which has an axial ratio of 6 dB. Another parameter of interest was the maximum steering angle, that in the case of both arrays was $36^\circ$ in the $x-axis$ and $23^\circ$ in the $y-axis$. This is compensated by the wide beam, which measures $60^\circ$ in the $x-axis$ and $90^\circ$ in the $y-axis$. In the case of the linear array, the beam can only be steered on the $x-axis$, where it showed similar characteristics with the planar array.

## 6.2 Future Development

As shown in the simulation, the main impediment for the overall performance was the available area. Enlarging the cover in such a way that would allow an uniform and larger spacing between the array elements could bring an improvement. In this way the antennas would not be so closely placed and there would not be mutual coupling between elements and it would not be necessary the use of a high dielectric substrate.

For the $1^{st}$ layout of 2 x 2 array, a further improvement would be reducing mutual coupling by other means than moving the antennas. According to the results in [55], rotating the antennas relative to each other does not reduce considerable the coupling between element. An attempt has been made to make cut in the dielectric between the patches, but no improvement has been obtained (See appendix B.3.2).

In the case of the $2^{nd}$ design of the 2 x 2 array, taking into consideration that the mutual coupling effect is not as strong as in the first design, the $\pi - network$ components can have the same value for all ports, but without significant effect on the realized gain and the axial ratio. However, this will simplify the physical implementation and further result in a lower losses when introducing the phase shifter.

By applying the $\pi - network$ with the components value from table 6.1, both frequency bands are covered with a maximum return loss of -4 dB, VSWR 4.4:1. The realized gain and the axial ratio are presented in Table 6.2.

Another further improvement of the matching network of the second layout would be to apply a higher or-

| | C1 | | L | | C2 | |
|---|---|---|---|---|---|---|
| All ports | Value [pF] | ESR [Ω] | Value [nH] | Parasitic resistance [Ω] | Value [pF] | ESR [Ω] |
| | 1.5 | 0.18 | 13 | 0.5 | 2.2 | 0.18 |

**Table 6.1:** Components values for 2x2 array, $2^{nd}$ layout, SMD model

| Frequency [GHz] | 1.525 | 1.544 | 1.559 | 1.626 | 1.644 | 1.660 |
|---|---|---|---|---|---|---|
| Realized Gain [dBi] | 4.81 | 6.24 | 6.38 | 6.66 | 6.69 | 4.83 |
| Radiation Efficiency [dB] | -1.11 | -0.83 | -0.64 | -0.52 | -0.88 | -1.38 |
| Total Efficiency [dB] | -2.48 | -1.16 | -1.07 | -1.03 | -1.09 | -2.94 |
| Axial Ratio [dB] | 8 | 6 | 5 | 4 | 4 | 3 |

**Table 6.2:** Results for the 2x2 array, $2^{nd}$ layout - same $\pi - network$ for all ports

der Chebyshev circuit. This could result in a wider bandwidth but considering that more components are added to each port higher losses may occur.

For future study and results validation, should be considered manufacturing a prototype with the materials used in the initial simulation. Also, better manufacturing techniques should be used to avoid the small imperfections that occur because of handling.

# Bibliography


[1] "Esa telecommunication satellites." http://www.esa.int/Our_Activities/Telecommunications_Integrated_Applications/Telecommunications_satellites.

[2] "Satellite phones." http://www.bluecosmo.com/satellite-phones.

[3] "Comparison between smartphones." http://www.gsmarena.com/compare.php3?idPhone1=7821&idPhone2=7242&idPhone3=7972.

[4] "Early 2015 smartphone comparison guide." http://www.gizmag.com/2015-smartphone-comparison-guide-1/36992/.

[5] "The difference between cellular phones and satellite phones." http://www.vizocomsat.com/blog/difference-cellular-phones-satellite-phones/.

[6] "Comparison between smartphones." https://atap.google.com/ara/.

[7] "Google ara phone." http://www.extremetech.com/extreme/185417-google-turns-on-the-worlds-first-modular-s

[8] A. Tatomirescu and G. F. Pedersen, "User body loss study for popular smartphones," *9th European Conference in Antennas and Propagation*, 2015.

[9] O. M. Bucci, "Active arrays for satellite communications," *Antennas and Propagation Conference (LAPC) Loughborough*, 2012.

[10] "Inmarsat website." http://www.inmarsat.com/services/.

[11] P. M. Tsai, "University of hawaii lecture notes link budget." https://www.csie.ntu.edu.tw/~hsinmu/courses/_media/wn_11fall/link_budget.pdf, September 2011.

[12] L. J. Ippolito, *Satellite Communications System Engineering*. Wiley, 2005.

[13] L. Ibbotson, *The Fundamentals of Signal Transmission: Optical Fibre, Waveguides and Free Space*. Elsevier Science, 1998.

[14] A. Goldsmith, *Wireless Communications*. Cambridge University Press, 2005.

[15] "Inmarsat 4f2 technical description," tech. rep.

[16] E. T. . . V6.19.0, "Universal mobile telecommunications system (umts); user equipment (ue) radio transmission and reception (fdd) 3gpp ts 25.101 version 6.19.0 release 6)," tech. rep., 3GPP.

[17] ITU-R, "Recommendation itu-r m.1181," tech. rep., 1995.

[18] *IsatPhonePro Brochure*, 2015.

[19] Inmarsat, "Notification of implementation of gmpcs-mou arrangements," tech. rep.

[20] TECOM, "T-4000 inmarsat high gain antenna," tech. rep.

[21] A. Ray, "15 questions and answers about project ara,"

[22] "Modular phone." `https://upload.wikimedia.org/wikipedia/commons/6/6a/Phonebloks_open.jpg`.

[23] "Project ara." `https://en.wikipedia.org/wiki/Project_Ara`, August 2015.

[24] S. Ilcev, *Global Mobile Satellite Communications: For Maritime Land and Aeronautical Applications*. Springer US, 2005.

[25] S. Fu, Y. Cao, Y. Zhou, and S. Fang, "Improved low-profile helical antenna design for inmarsat applications," *International Journal of Antennas and Propagation*, vol. 2012, May 2012.

[26] L. Wang, H. C. Yang, and Y. Li, "A novel printed dipole antenna using in high latitudes for inmarsat," *Progress In Electromagnetics Research Letters*, vol. 20, pp. 37–44, 2011.

[27] S. Ta, I. Park, and R. Ziolkowski, "Dual-band wide-beam crossed asymmetric dipole antenna for gps applications," *Electronic Letters*, vol. 48, no. 25, 2012.

[28] R.Lelaratne and R.J.Langley, "Dual-band patch antenna for mobile satellite systems," *IEE Proceedings Microwave Antennas and Propagation*, 2000.

[29] "GPS antennas." `http://www.digikey.dk/en/product-highlight/y/yageo/$`.

[30] "Flip covers." `http://www.snapdeal.com/products/mobiles-flip-cases-covers`.

[31] C. A. Balanis, *Antenna Theory Analysis and Design*. Wiley, third edition ed., 2005.

[32] D. Orban and G. Moernaut, "The basics of patch antennas." RF Globalnet newsletter, September 2009.

[33] S. S. Holland, "Miniaturization of microstrip patch antennas for gps applications," Master's thesis, University of Massachusetts, 2008.

[34] J. P. S. Raj Kumar and M. D. Uplane, "Effect of slots in ground plane and patch on microstrip antenna performance," *International Journal of Recent Trends in Engineering*, 2009.

[35] A. Kumar, J. Kaur, and R. Singh, "Performance analysis of different feeding techniques," *International Journal of Emerging Technology and Advanced Engineering*, 2013.

[36] C. Balanis, *Advanced Engineering Electromagnetics, 2nd Edition*. Wiley, 2012.

[37] "Axial ratio [db] to polarization loss [db]." `http://antennadesigner.org/polarization_loss_given_a-r.html`.

[38] N. Z. N. Chen and X. Qing, "Slotted microstrip antennas for circular polarization with compact size," *IEEE Antennas and Propagation Magazine*, vol. 55, April 2013.

[39] Z. Zhang, *Antenna Design for Mobile Devices*. Wiley, first edition ed., 2011.

[40] D. Pozar, *Microwave Engineering*. Wiley, 2012.

[41] K. Sharma, *Fundamental of Microwave & Radar Engineering*. S Chand & Company Limited, 2011.

[42] R. M. Siva Chebolu, Supriyo Dey and M. Itoh, "A dual-band stacked microstrip antenna array for mobile satellite applications," *IEEE Antennas and Propagation Magazine*, vol. 1, 1995.

[43] Chandrabhan, V. Singh, B. Mishra, and A. Kumar, "Second international conference on advances in computing and communication engineering," *IEEE TRANSACTIONS ON ANTENNAS AND PROPAGATION*, 2015.

[44] Chandrabhan, V. Singh, B. Mishra, and A. Kumar, "Formulation of resonance frequencies for dual-band slotted rectangular microstrip antennas," *IEEE Antennas and Propagation Magazine*, vol. 54, August 2012.

[45] "Beam forming networks." `http://www.microwaves101.com/encyclopedias/beam-forming-networks`.

[46] PREMIX, "Preperm 900hf," tech. rep., PREMIX, 2013.

[47] P. D. M. Pozar, "A review of aperture coupled microstrip antennas: History, operation, development, and applications," May 1996.

[48] *RO3000® Series Circuit MaterialsmRO3003 $^{TM}$ , RO3006$^{TM}$, RO3010$^{TM}$ and RO3035$^{TM}$ High Frequency Laminates*.

[49] *Murata Inductor LQW2BAN13NG00*.

[50] *Murata Capacitor GJM0223C1E2R3WB01*.

[51] *Coilcraft 0806SQ, 0807SQ, 0908SQ Air Core Inductors*.

[52] *Vishay capcitors VJ....W1BC Basic Commodity Series*.

[53] "3d polar plot." `http://www.mathworks.com/matlabcentral/fileexchange/13200-3d-polar-plotcomments`.

[54] D. M. P. M. IEEE and D. H. S. S. M. IEEE, "Scan blindness in infinite phased arrays of printed dipoles," *IEEE Transactions on Antennas and Propagation*, vol. AP-32, June 1984.

[55] S. Thomas, "A study on the mutual coupling effects between 2 rectangular patch antennas as a function of their separation and angles of elevation," Master's thesis, National University of Singapore.

[56] PREMIX, "Preperm 700hf," tech. rep., PREMIX, 2013.

[57] *Digital Phase Shifter MAPS-010143*.

[58] *Digital Phase Shifter MAPS-010163*.

[59] *Analog Phase Shifter HMC934LP5E*.

[60] A. S. Y. P. S. M. IEEE, M. Taghiv, and S. M. IEEE, "Supporting and enabling circuits for antenna arrays in wireless communications," *Proceedings of the IEEE*, vol. 100, July 2012.

[61] *Murata Phase Shifter for ISM2.4GHz*.

[62] "Atmospheric attenuation." `http://www.propagation.gatech.edu/ECE6390/project/Fall2012/Team09/Team9GeoSatTech_website_FINAL/SatCom%20website/atmosphericAttenuation.html`.

[63] "GPS GNSS low noise amplifier." MAX2659.

[64] T. Milligan, *Modern Antenna Design*. Wiley, 2005.

[65] J. Hautcoeur, F. Colombel, X. Castel, M. Himdi, and E. M. Cruz, "Performances of transparent monopole antenna versus meshed silver layer (AgGL)," *Progress In Electromagnetics Research C*, vol. 22, pp. 259–271, 2011.

[66] R. Gordon, "Criteria for choosing transparent conductors," *MRS Bulletin*, August 2000.

[67] G. A. Mavridis, D. E. Anagnostou, and M. T. Chryssomallis, "Evaluation of the quality factor, q, of electrically small microstrip·patch antennas," *IEEE Antennas and Propagation Magazine*, vol. 53, August 2011.

[68] *CST Studio Suite Help*.

# Appendix A

# Additional theoretical background

In this section additional information and pictures are added which are mentioned in the Prestudy.

## A.1 Chapter 2

**L-band Antennas in mobile satellite communication**

In [24], a classification of the mobile satellite antennas is made in terms of gain and radiation pattern.

| Type of antenna | Gain class | Typical Gain [dBi] | Typical G/T [dBK] | Typical Antenna (Dimension) | Typical GMSC Services |
|---|---|---|---|---|---|
| Omnidirectional | Low | 0-4 | -27 to -23 | Quadrifilar Drooping - Dipole Patch | LSD (Messages) Ship (Inmarsat - C) Vehicles & Aircraft |
| Semidirectional (Only in Azimuth) | Medium | 4-8 | -23 to -18 | Array (2-4 elements) Helical, Patch | Voice/HSD Ship (Inmarsat-M) Vehicles |
| | | 8-16 | -18 to -10 | Phased array (20 elements) | |
| Directional | High | 17-20 | -8 to -6 | Dish (0.8 m Φ) | Voice/HSD Ship(Inmarsat-A, B) |
| | | 20-24 | -4 | Dish (1 m Φ) | |

**Table A.1:** Classification of L-Band Antenna Systems in GMSC [24]

Figure A.1 and A.2 show the measurement of a smartphone cover, similar to the one that is proposed for the antenna implementation.

The atmospheric losses that can occur in satellite communications are illustrated in Figure A.3.


**Figure A.1:** Width of top of the cover


**Figure A.2:** Width of bottom of the cover

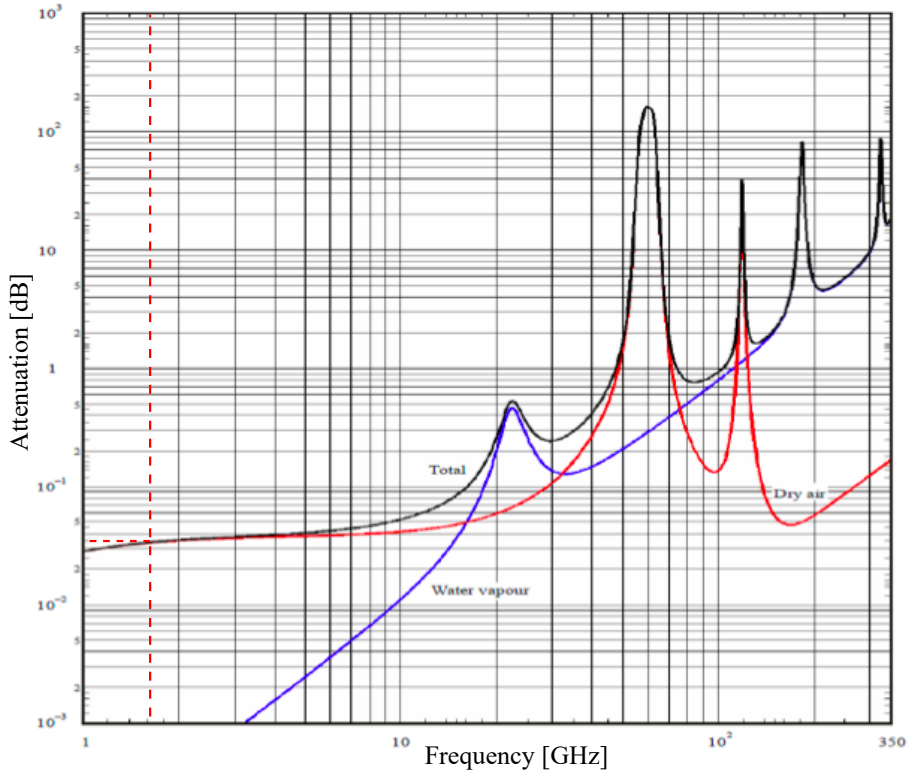


**Figure A.3:** Atmospheric losses (source: [62] )

### A.1.1 System noise temperature calculation

As described in **??**, the figure of merit is the difference between the antenna gain and the system noise temperature. The system noise temperature combines all noise contribution on the signal path. The major contribution come from the antenna and the low noise amplifier (LNA), which are the only terms considered in this project for the calculation of the system noise temperature [12] . Therefore, the formula used for computing the system temperature is:

$$T_S = T_A + T_{LNA} \tag{A.1}$$

where $T_S$ is the total system noise temperature, $T_A$ is the antenna noise temperature and $T_LNA$ is the low noise amplifier noise temperature. The noise at the antenna from the radio path is called **radio noise** or sky noise. According to Figure A.4, the antenna "sees" a noise temperature of 12 K when pointed toward the sky ($\theta = 90°$), 100 K when pointed toward the horizon ($\theta = 0°$) and 300 K when pointed toward the ground ($\theta = 180°$). Knowing the gain of the antenna in all directions and making an interpolation between the points in which the sky noise temperature is defined, the following formula is applied to compute the antenna temperature [31]:

$$T_A = \frac{\int_0^{2\pi}\int_0^{\pi} G(\theta,\phi)T_B(\theta,\phi)\sin\theta\, d\theta\, d\phi}{\int_0^{2\pi}\int_0^{\pi} G(\theta,\phi)\sin\theta\, d\theta\, d\phi} \tag{A.2}$$

where $G(\theta,\phi)$ is the antenna gain pattern and $T_B(\theta,\phi)$ is the noise temperature of the environment. By using the radiation pattern of first design, $f = 1.525$, for computing A.2, the antenna temperature has a value of 43 K, while if using the radiation pattern of the first design when the beam is steered, the antenna noise temperature has a value of 38 K. For further calculations, the mean value of 40 K will be considered.

The LNA noise temperature is computed following the specifications of [63], with a noise figure of 0.8 dB. The noise figure has the following formula [12]

$$NF = 10log(1 + \frac{T_{LNA}}{T_0}) \tag{A.3}$$

where $T_0$ is the reference temperature, which in the datasheet of the example LNA is stated to be 25° C or 298° K. In this case, the $T_{LNA}$ will have a noise temperature of approximately 60 K. Given these values the total system noise temperature is:

$$T_S = T_A + T_{LNA} \rightarrow T_S = 40K + 60K = 100K \tag{A.4}$$

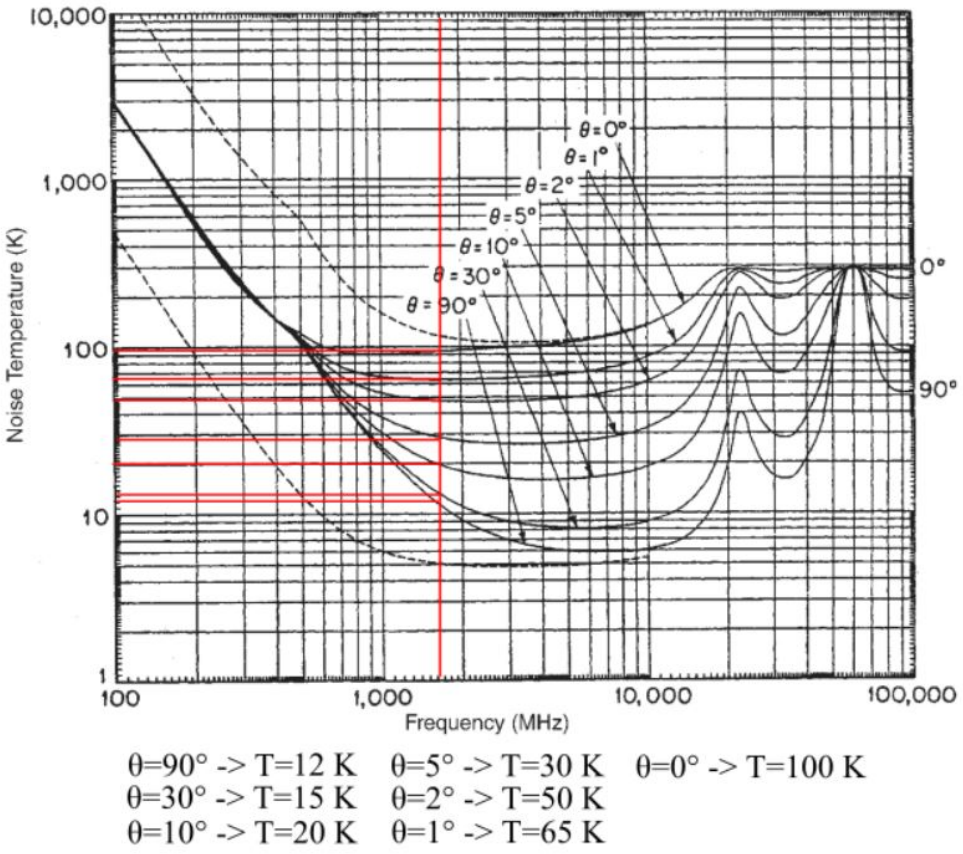


**Figure A.4:** Antenna sky temperature [64]

# Appendix B

# Additional simulations

During the development of the antenna array, other solutions and designs have been tried out. These either did not present the optimum results, either the model did not suffice all the necessary parameters. However, they were an important step in the learning curve and helped to design the final model, therefore some of them are presented in this section.

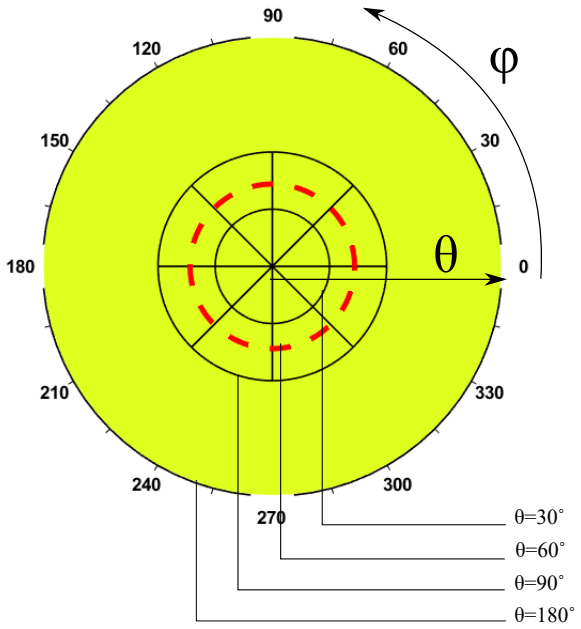


**Figure B.1:** 3D Polar Plot explanation (source: [53])

## B.1 Design of the patch

During the project many design of the patch antenna were tested for testing their performance in circular polarization, miniaturization and dual resonance.

### Glass antenna

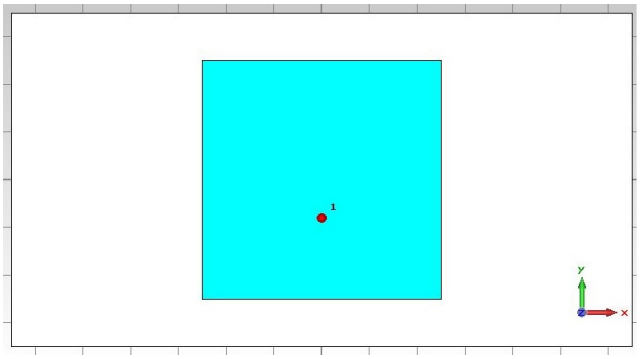


**Figure B.2:** Transparent conductor patch for screen antenna

The transparent conductor for the patch presented in B.2, was simulated in two different ways. The first was assuming a silver mesh as in [65]. With the given sheet resistance from the paper, the conductivity was computed and them implemented in the program. The second implementation was following the study in [66], where a comparison of the transparent conductors in made. The trade off in choosing a good conductor will be regarding the transparency. Even by choosing the best conductor, with the lowest transparency, the conductivity was still low compared to the one of copper, which resulted in a low radiation efficiency.

### Circular polarization

The following designs have been tried out for obtaining circular polarization. Results shown an axial ratio withing the desired values (up to 6 dB) only over a narrow band width. In the case of dual resonance, one of the frequency bands has has higher values of axial ratio, with up to 12 dB.

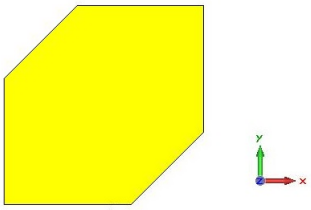


**Figure B.3:** Patch antenna with truncated corners for circular polarization

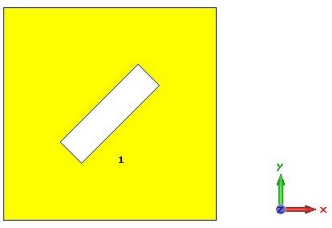


**Figure B.4:** Patch antenna with cut slot for circular polarization

### Antenna miniaturization

The following designs have been tried out for reducing the dimensions of the patch antenna. The study in [33] shown that for a 500 MHz reduction in frequency two slots of 11 mm were needed. Here the reduction in frequency is of approximately 2.5 GHz, which translates into more and longer slots. Also, because of the dual feeding, the slots have to be added on both patch dimensions. According to [67], the radiation efficiency decreases considerably with the the increase of the slot length.

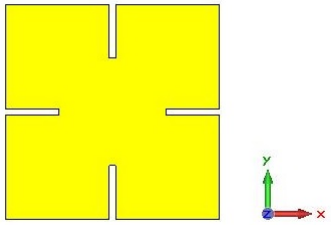

**Figure B.5:** Patch antenna loaded with slots for miniaturization

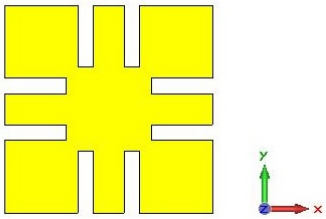

**Figure B.6:** Patch antenna loaded with slots for miniaturization

### Dual resonance

Using slots for obtaining dual resonance has shown similar problems with maintaining the axial ratio under 6 dB over both bandwidths. Also, as mentioned earlier, according to [67], the radiation efficiency tends to decrease when slots are made on the patch surface.

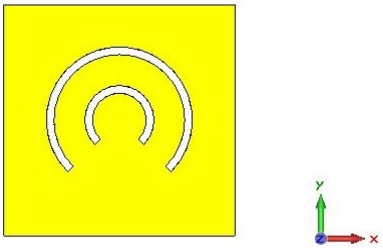

**Figure B.7:** Patch antenna loaded with slots for dual resonance, two slots in a circular form

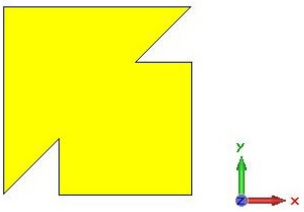

**Figure B.8:** Patch antenna loaded with slots for dual resonance, two V slots

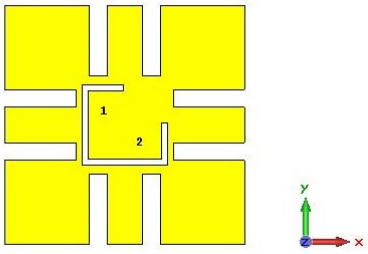


**Figure B.9:** Patch antenna loaded with slots for dual resonance, C shaped slot

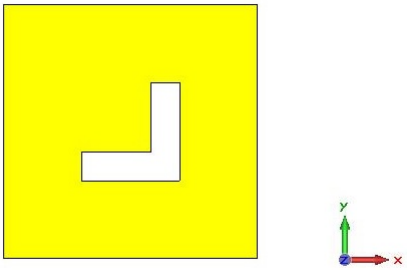


**Figure B.10:** Patch antenna loaded with slots for dual resonance, L shaped slot

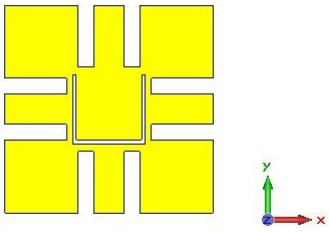


**Figure B.11:** Patch antenna loaded with slots for dual resonance, U shaped slot

Other circuits for obtaining dual resonance were used as well, but they either implemented high losses or did not give the right separations between the frequency band. For example, the circuit in Figure B.12 introduced a 5 dB loss when assuming the same parasitic for the components as in 4.7, while the circuit in Figure B.13 could not achieve a performance of VSWR 2:1 along the two frequency bands.

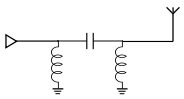

**Figure B.12:** $\pi - circuit$ for obtaining dual resonance using two inductors in shunt and one capacitor in series

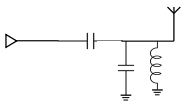

**Figure B.13:** Matching circuit for obtaining dual resonance using 2 capacitors and one inductor

### B.1.1 Previous array simulations

All the simulations have the layout presented in Figures B.14, B.15, B.16 and B.17 and the following parameters(alphabetical order):

- **dfs**: distance from center of the patch to the feeding slot
- **dy**: distance from end of the feeding line and port location
- **fed**: distance from the center of the patch and beginning of the feeding line
- **ha**: height of the copper trace **= 0.05 mm**
- **hs**: height of the antenna substrate **= 5 mm**
- **hs2**: height of the feeding substrate **= 0.2 mm**. The material of the feeding substrate is Rogers RO3006, with a permitivity of $\epsilon = 6.15$ and a loss tangent of $\epsilon = 0.002$.
- **lfl**:length of the feeding line **= 15 mm**
- **lfs**: length of the feeding slot **= 4 mm**
- **lp**:length of the patch **= 28 mm**
- **ps1**:phase shift for patch 1 **= 0**
- **ps2**:phase shift for patch 2 **= 0**
- **ps3**:phase shift for patch 3 **= 0**
- **ps4**:phase shift for patch 4 **= 0**
- **wfl**:width of the feeding line **= 3.375 mm**
- **wfs**:width of the feeding slot **= 8 mm**
- **wp**:width of the patch **= 28 mm**
- **xp1**:center of the first patch on x axis **= -42 mm**
- **xp2**:center of the second patch on x axis **= 14 mm**

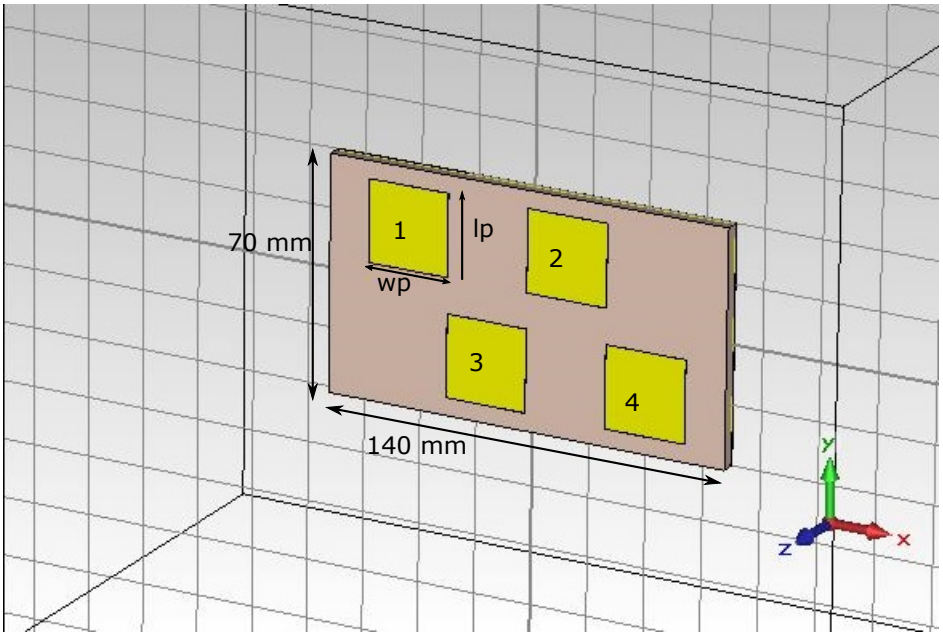


**Figure B.14:** Front view of the array

- **xp3**:center of the third patch on x axis **= -14 mm**
- **xp4**:center of the fourth patch on x axis **= 42 mm**
- **yp1**:center of the first patch on y axis **= 20 mm**
- **yp2**:center of the second patch on y axis **= 20 mm**
- **yp3**:center of the third patch on y axis **= -20 mm**
- **yp4**:center of the fourth patch on yaxis **= -20 mm**

**Any variations from the indicated values will be stated for each simulation**

**TEST582 vs TEST588**

The main difference between these 2 simulations is the antenna substrate height and the patch dimensions, as following:

- TEST582
  - wp=lp=28 mm
  - hs=5 mm
- TEST588
  - wp=lp=29 mm
  - hs=3 mm

Also, another difference is made in schematics, in the matching network as presented in Figures B.18 and B.19.

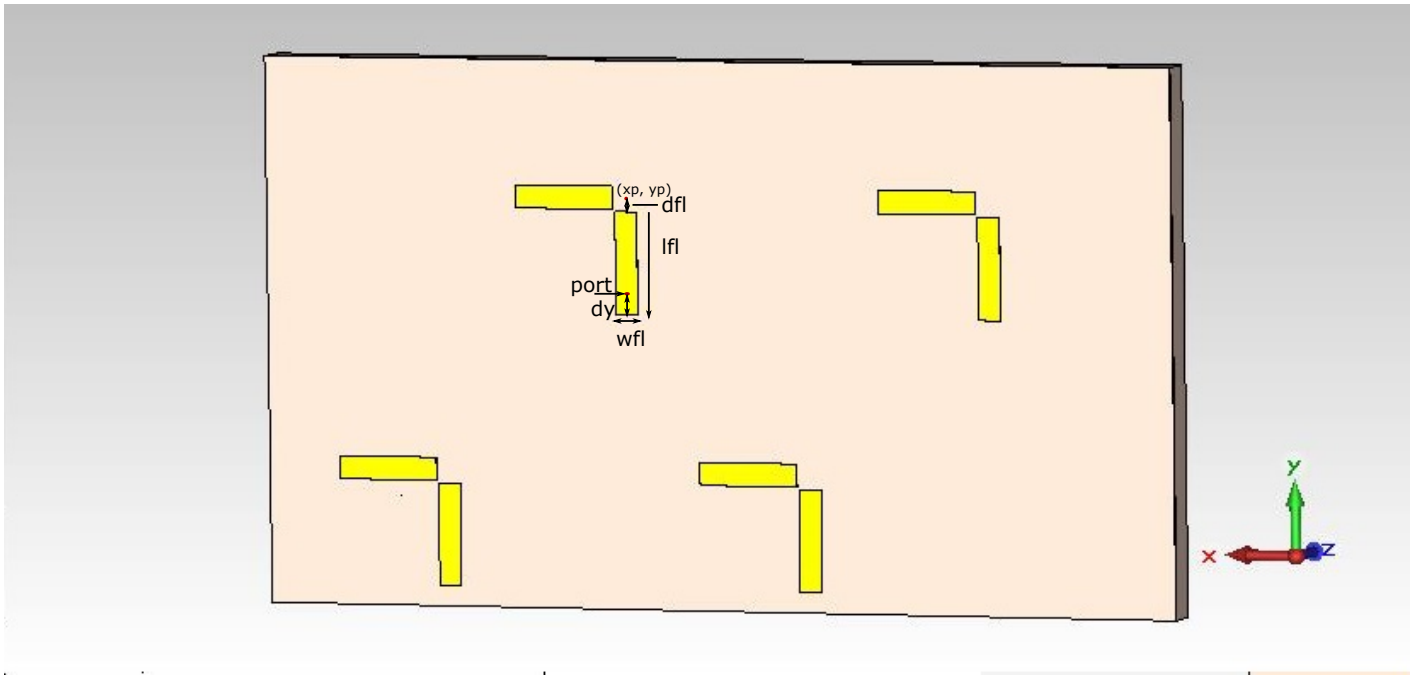


**Figure B.15:** Back view of the array

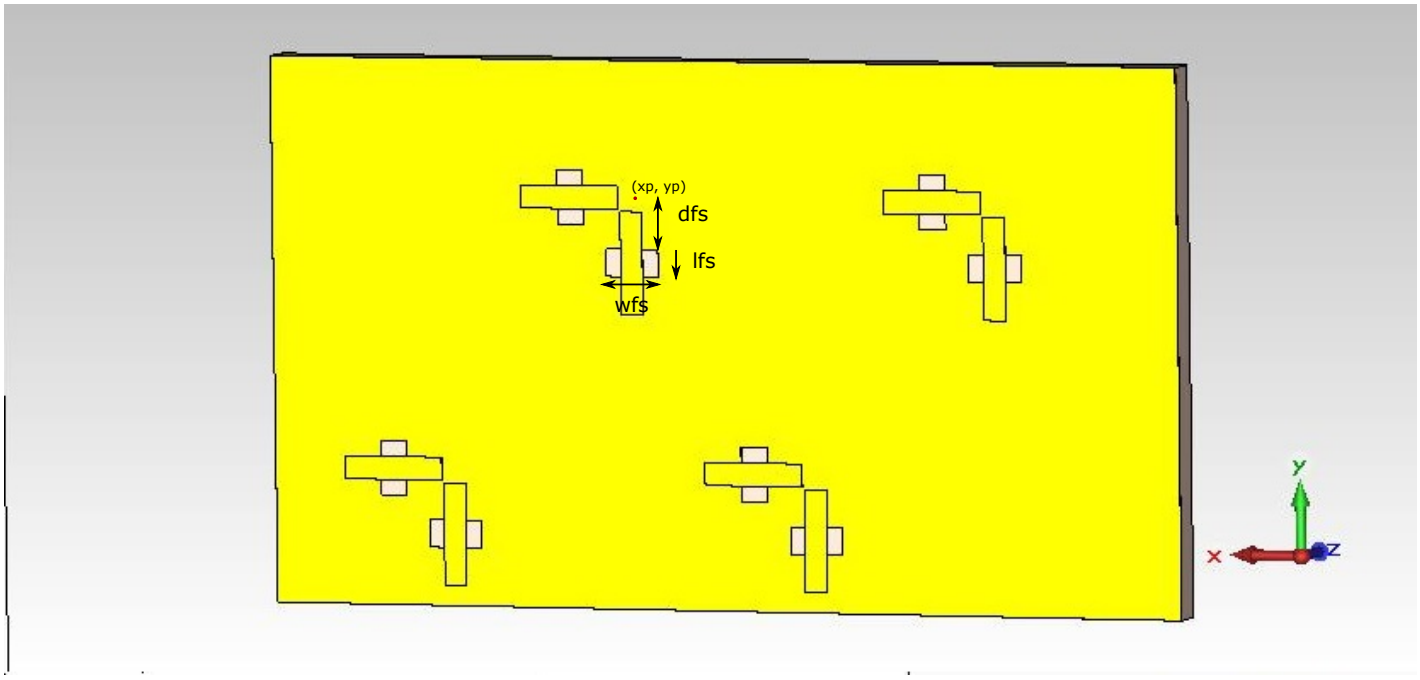


**Figure B.16:** Back view of the array, feeding substrate hidden


**Figure B.17:** Side view of the array

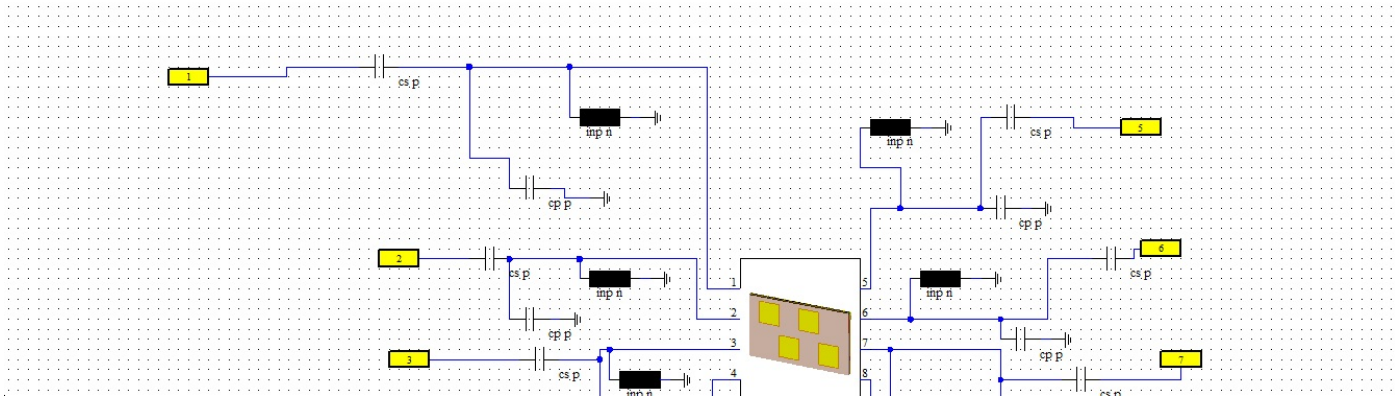


**Figure B.18:** Schematics test582

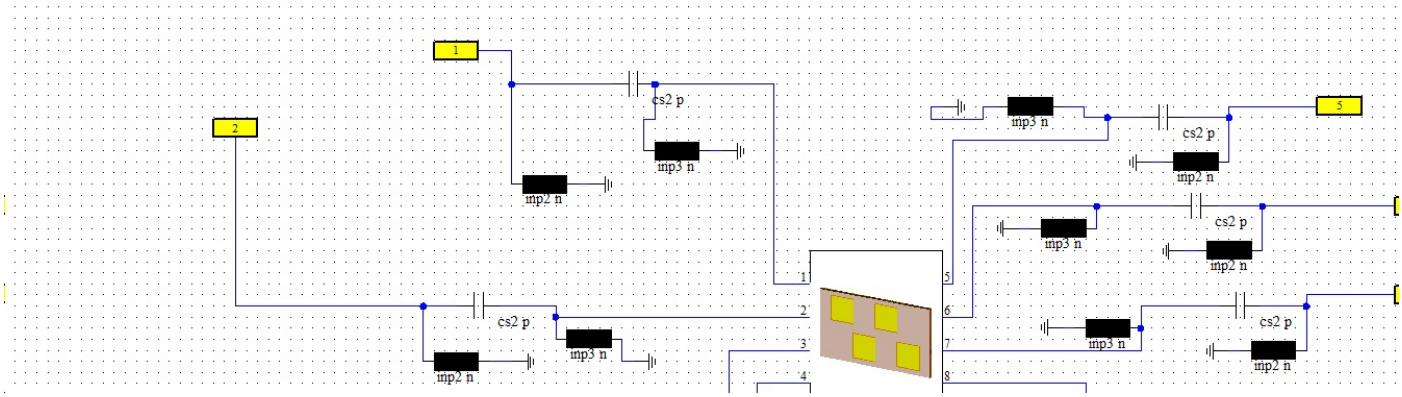


**Figure B.19:** Schematics test588

**TEST582**

The material of the antenna substrate is Preperm 960, with a permitivity of $\epsilon = 9.6$ and a loss tangent of $\epsilon = 0.0008$.

**Table B.1:** Results for TEST582

| Freq[GHz] | R. Gain[dBi] | T. Eff[dB] | Freq[GHz] | R. Gain[dBi] | T. Eff[dB] | Freq[GHz] | R. Gain[dBi] | T. Eff[dB] |
|---|---|---|---|---|---|---|---|---|
| 1.525 | 5.84 | -1.13 | 1.544 | 5.65 | -1.38 | 1.559 | 5.38 | -1.7 |
| 1.626 | 6.08 | -1.22 | 1.644 | 6.15 | -1.2 | 1.660 | 5.24 | -2 |

**TEST588**

The material of the antenna substrate is Preperm 960, with a permitivity of $\epsilon = 9.6$ and a loss tangent of $\epsilon = 0.0008$.

**Table B.2:** Results for TEST588

| Freq[GHz] | R. Gain[dBi] | T. Eff[dB] | Freq[GHz] | R. Gain[dBi] | T. Eff[dB] | Freq[GHz] | R. Gain[dBi] | T. Eff[dB] |
|---|---|---|---|---|---|---|---|---|
| 1.525 | 0.755 | -6.22 | 1.544 | 2.72 | -4.3 | 1.559 | 3.62 | -3.7 |
| 1.626 | 3 | -4.3 | 1.644 | 1.49 | -5.9 | 1.660 | -0.6 | -8 |

**TEST589**

The material of the antenna substrate is Preperm 900, with a permitivity of $\epsilon = 9$ and a loss tangent of $\epsilon = 0.0004$.

- wp=lp=28 mm
- hs=5 mm

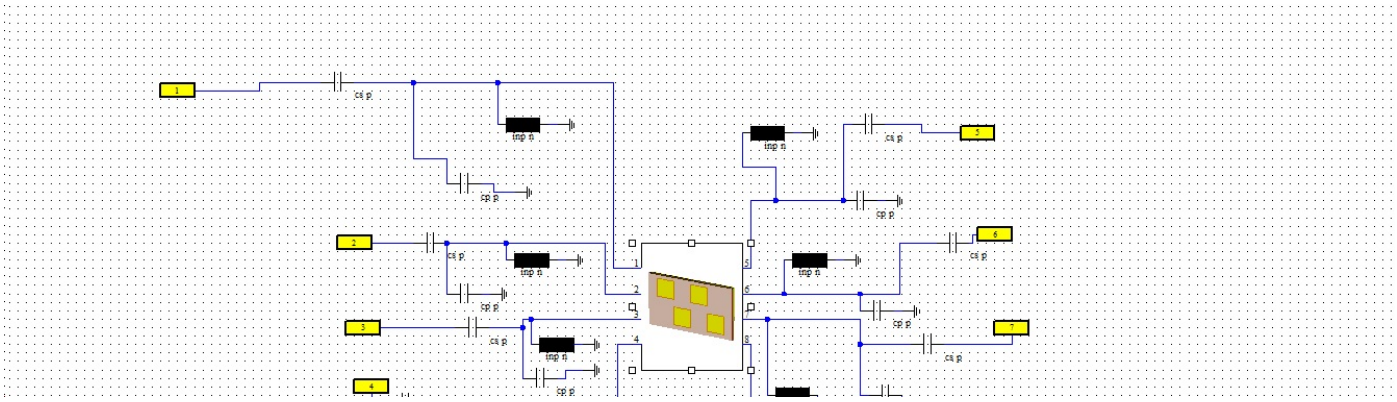

**Figure B.20:** Schematics test589

**Table B.3:** Results for TEST589

| Freq[GHz] | R. Gain[dBi] | T. Eff[dB] | Freq[GHz] | R. Gain[dBi] | T. Eff[dB] | Freq[GHz] | R. Gain[dBi] | T. Eff[dB] |
|---|---|---|---|---|---|---|---|---|
| 1.525 | 5.67 | -1.27 | 1.544 | 5.93 | -1.06 | 1.559 | 5.89 | -1.15 |
| 1.626 | 6.1 | -1.07 | 1.644 | 6.17 | -1.1 | 1.660 | 5.9 | -1.5 |

**TEST5891 vs TEST5892**

The main difference between these 2 simulations is the antenna substrate height and the patch dimensions, as following:

- TEST5891
  - wp=lp=29 mm
  - hs=5 mm
- TEST5892
  - wp=lp=30 mm
  - hs=5 mm

**TEST5891**

The material of the antenna substrate is Preperm 900, with a permitivity of $\epsilon = 9$ and a loss tangent of $\epsilon = 0.0004$.

- wp=lp=29 mm
- hs=3 mm

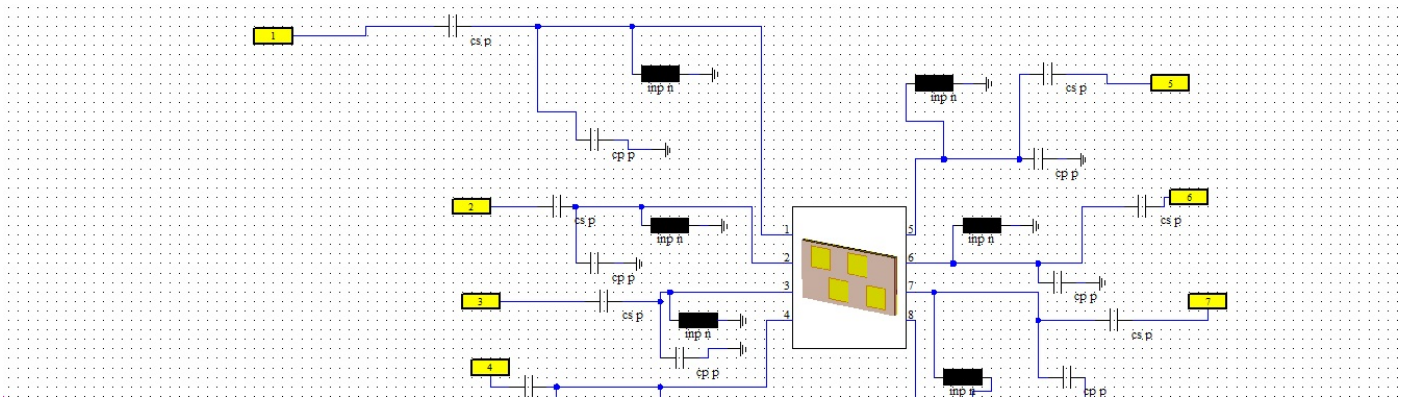

**Figure B.21:** Schematics test5891

**Table B.4:** Results for TEST5891

| Freq[GHz] | R. Gain[dBi] | T. Eff[dB] | Freq[GHz] | R. Gain[dBi] | T. Eff[dB] | Freq[GHz] | R. Gain[dBi] | T. Eff[dB] |
|---|---|---|---|---|---|---|---|---|
| 1.525 | 5.7 | 1.2 | 1.544 | 5.5 | -1.5 | 1.559 | 5.3 | -1.8 |
| 1.626 | 6 | -1.2 | 1.644 | 6.126 | -1.2 | 1.660 | 5.2 | -2.15 |

**TEST5892**

The material of the antenna substrate is Preperm 900, with a permitivity of $\epsilon = 9$ and a loss tangent of $\epsilon = 0.0004$.

- wp=lp=30 mm
- hs=3 mm

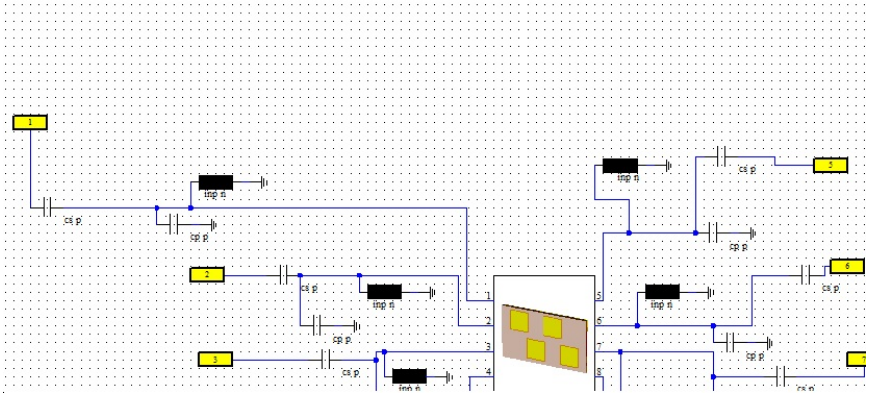

**Figure B.22:** Schematics test5892

**Table B.5:** Results for TEST5892

| Freq[GHz] | R. Gain[dBi] | T. Eff[dB] | Freq[GHz] | R. Gain[dBi] | T. Eff[dB] | Freq[GHz] | R. Gain[dBi] | T. Eff[dB] |
|---|---|---|---|---|---|---|---|---|
| 1.525 | 5.98 | -1 | 1.544 | 5.35 | -1.75 | 1.559 | 4.93 | -2.2 |
| 1.626 | 5.48 | -1.9 | 1.644 | 5.86 | -1.5 | 1.660 | 5.59 | -1.8 |

**TEST5894**

The material of the antenna substrate is Preperm 900, with a permitivity of $\epsilon = 9$ and a loss tangent of $\epsilon = 0.0004$.

- wp=lp=29.5 mm
- hs=3 mm

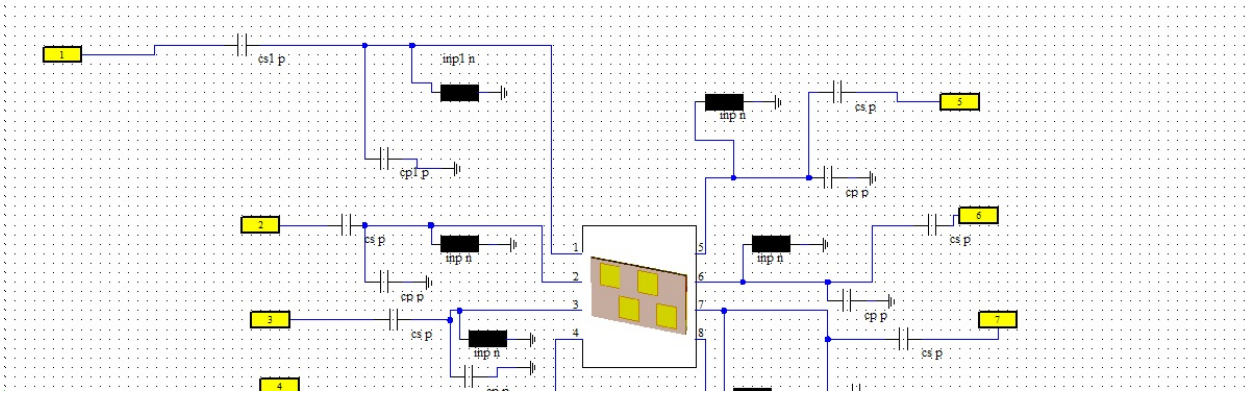


**Figure B.23:** Schematics test5894

**Table B.6:** Results for TEST5894

| Freq[GHz] | R. Gain[dBi] | T. Eff[dB] | Freq[GHz] | R. Gain[dBi] | T. Eff[dB] | Freq[GHz] | R. Gain[dBi] | T. Eff[dB] |
|---|---|---|---|---|---|---|---|---|
| 1.525 | 5.25 | -1.9 | 1.544 | 5 | -2.15 | 1.559 | 4.72 | 2.5 |
| 1.626 | 5.21 | -2.3 | 1.644 | 5.95 | -1.75 | 1.660 | 6.37 | -1.4 |

**TEST58982 vs TEST58983**

The main difference between these two simulation is the positions of the patches.

**TEST58982** The material of the antenna substrate is Preperm 900, with a permitivity of $\epsilon = 9$ and a loss tangent of $\epsilon = 0.0004$.

- wp=lp=29.5 mm
- hs=3 mm
- xp1=-xp4=-50.85 ; xp2=-xp3= 16.95

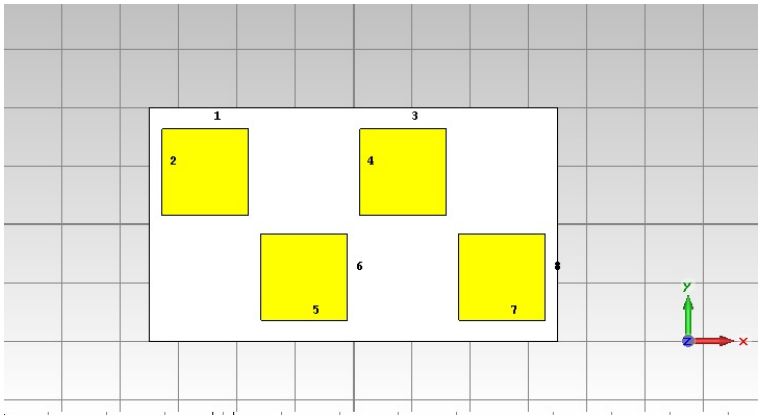


**Figure B.24:** Layout test58982

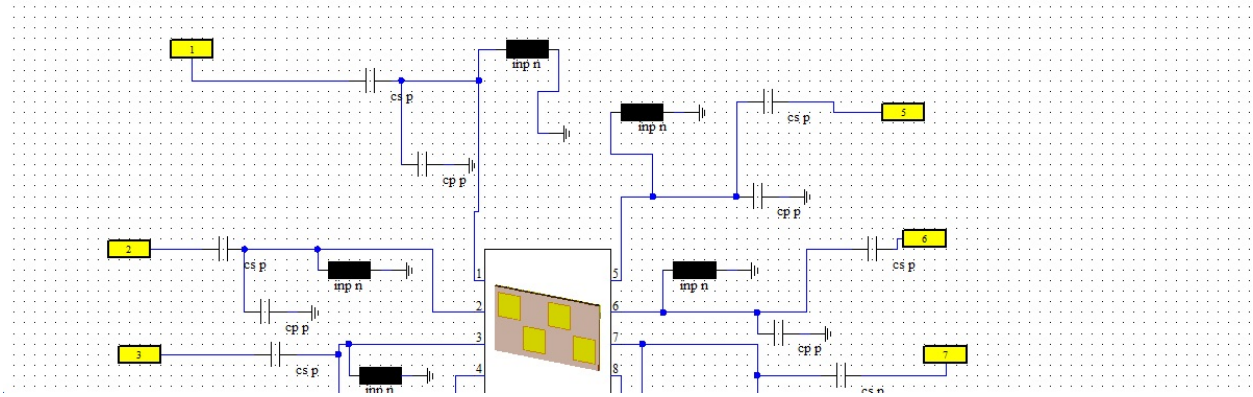


**Figure B.25:** Schematics test58982

**Table B.7:** Results for TEST58982

| Freq[GHz] | R. Gain[dBi] | T. Eff[dB] | Freq[GHz] | R. Gain[dBi] | T. Eff[dB] | Freq[GHz] | R. Gain[dBi] | T. Eff[dB] |
|---|---|---|---|---|---|---|---|---|
| 1.525 | 5.7 | -1.54 | 1.544 | 5.62 | -1.6 | 1.559 | 5.26 | -2 |
| 1.626 | 5.58 | -2 | 1.644 | 6.28 | -1.43 | 1.660 | 6.56 | -1.2 |

**TEST58983** The material of the antenna substrate is Preperm 900, with a permitivity of $\epsilon = 9$ and a loss tangent of $\epsilon = 0.0004$.

- wp=lp=29.5 mm
- hs=3 mm
- xp1=-xp4=-xp2=xp3= 35

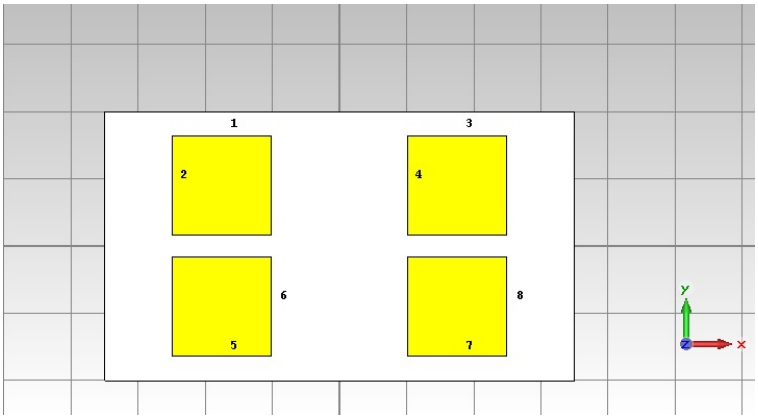


**Figure B.26:** Layout test58983

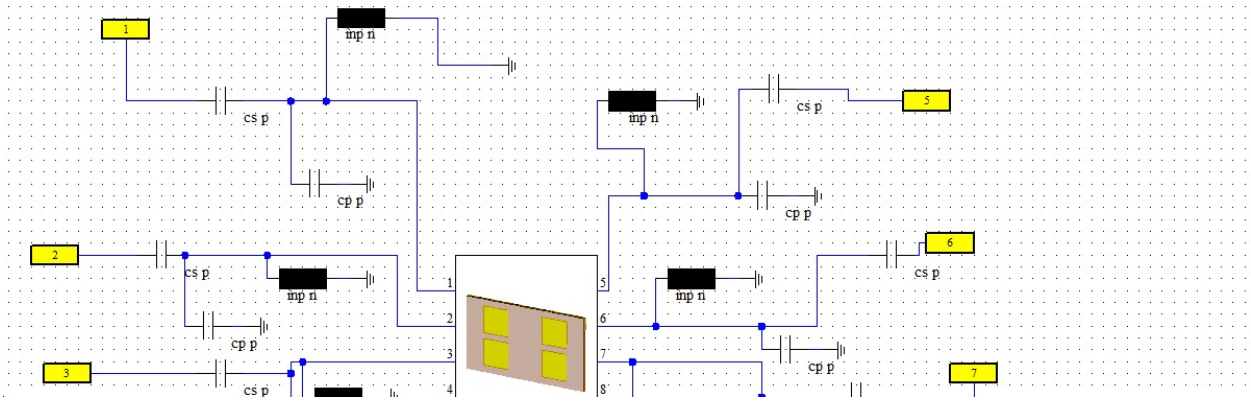


**Figure B.27:** Schematics test58983

**Table B.8:** Results for TEST58983

| Freq[GHz] | R. Gain[dBi] | T. Eff[dB] | Freq[GHz] | R. Gain[dBi] | T. Eff[dB] | Freq[GHz] | R. Gain[dBi] | T. Eff[dB] |
|---|---|---|---|---|---|---|---|---|
| 1.525 | 5.7 | -1.5 | 1.544 | 5.62 | -1.7 | 1.559 | 5.3 | -2.1 |
| 1.626 | 5.8 | -1.8 | 1.644 | 6.36 | -1.3 | 1.660 | 6.37 | -1.3 |

**TEST59**

**This array has 6 elements.**
The material of the antenna substrate is Preperm 900, with a permitivity of $\epsilon = 9$ and a loss tangent of $\epsilon = 0.0004$.

- wp=lp=29.5 mm
- hs=3 mm
- xp1=-xp4=-xp2=xp3= 35, xp5=xp6=0

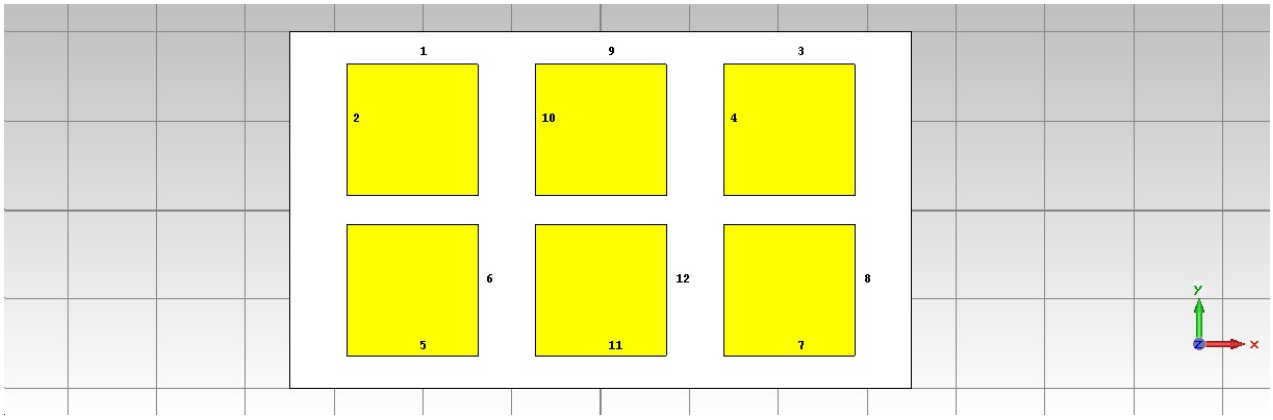


**Figure B.28:** Layout test59

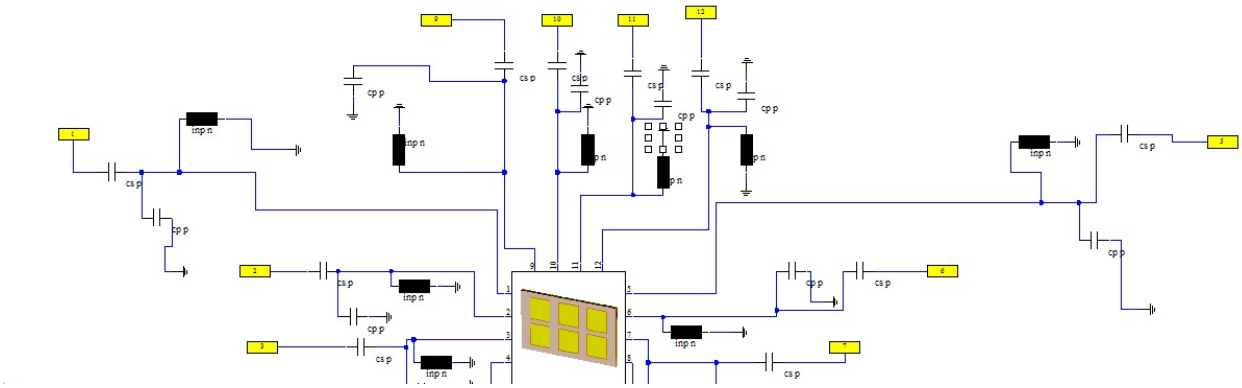

**Figure B.29:** Schematics test59

**Table B.9:** Results for TEST59

| Freq[GHz] | R. Gain[dBi] | T. Eff[dB] | Freq[GHz] | R. Gain[dBi] | T. Eff[dB] | Freq[GHz] | R. Gain[dBi] | T. Eff[dB] |
|---|---|---|---|---|---|---|---|---|
| 1.525 | 6.48 | -0.7 | 1.544 | 6.14 | -1.1 | 1.559 | 5.8 | -1.5 |
| 1.626 | 6.18 | -1.3 | 1.644 | 6.36 | -1.2 | 1.660 | 5.96 | -1.7 |

## Phaseshifting

**Table B.10:** Realized gain in the direction $\phi = 180°$, f= 1.626

| | test582 | test588 | test589 | tst5891 | test5892 | test5894 | test58982 | test58983 | test59 |
|---|---|---|---|---|---|---|---|---|---|
| R.Gain[dBi] | 2.33 | -3.46 | 2.29 | 1.28 | 1.35 | 1.18 | 1.49 | 1.23 | |

**Phase shift** 60°

## B.2 Additional 2 x 2 array simulations

### B.2.1 2x2 array, $3^{rd}$ layout

Another design also by geometrical consideration would be to equally separate the antennas on length and on height as shown in Figure **??**.

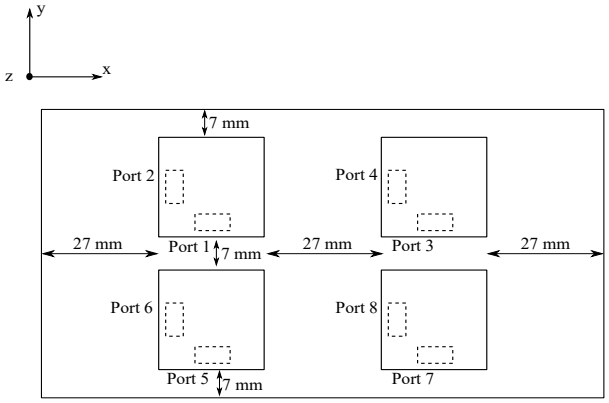


**Figure B.30:** Equidistant placing of the 2x2 array (top view)

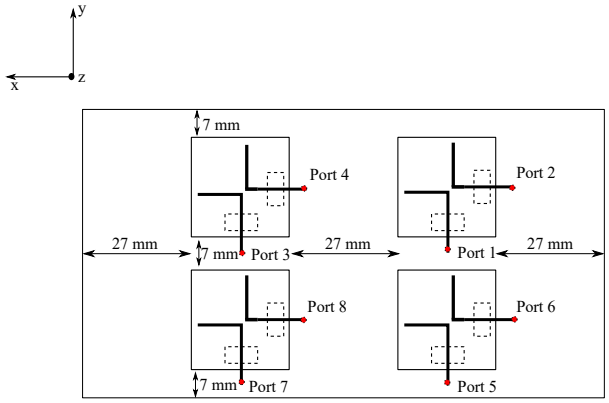


**Figure B.31:** Equidistant placing of the 2x2 array (bottom view)

This design bring the elements even closer, the distance between elements 1 and 3 and 2 and 4 measuring only 7 mm, where in the case of the 1st design was 10.5 mm. The coupling coefficients have similar values as in the case of the first layout. The same values of the components are used for the $\pi - circuit$ as in the case of the first layout. After applying the $\pi - circuit$, the values of the coupling coefficients change. For the H-plane ports, the coupling becomes even worse going from $-6.24$ dB to $-4$ dB, while in the case of E-plane ports, the coupling decrease to values below $-10$ dB.

| | C1 | | L | | C2 | |
|---|---|---|---|---|---|---|
| Odd | Value [pF] | ESR [Ω] | Value [nH] | Parasitic resistance [Ω] | Value [pF] | ESR [Ω] |
| Ports | 3 | 0.1 | 12.4 | 0.5 | 2.3 | 0.1 |
| Even | Value [pF] | ESR [Ω] | Value [nH] | Parasitic resistance [Ω] | Value [pF] | ESR [Ω] |
| ports | 1.5 | 0.1 | 13 | 0.5 | 2.2 | 0.1 |

**Table B.11:** Components values for 2x2 array, SMD model

| Frequency [GHz] | 1.525 | 1.544 | 1.559 | 1.626 | 1.644 | 1.660 |
|---|---|---|---|---|---|---|
| Realized Gain [dBi] | 5.12 | 6.31 | 5.84 | 6.16 | 5.58 | 2.56 |
| Radiation Efficiency [dB] | -0.94 | -0.68 | -0.52 | -0.6 | -1.2 | -1.9 |
| Total Efficiency [dB] | -1.89 | -0.79 | -1.27 | -1.12 | -1.73 | -4.72 |
| Axial Ratio [dB] | < 5.5 | < 4 | < 2 | < 2.5 | < 3.5 | < 3.5 |

**Table B.12:** Results for four 2x2 array(FDTD simulation), $3^{rd}$ layout

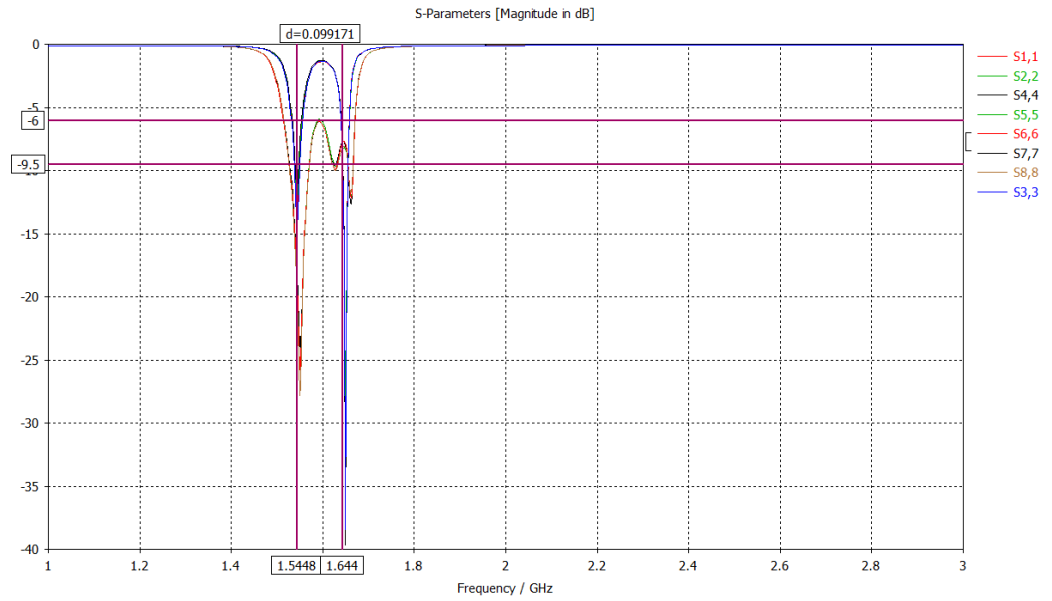


**Figure B.32:** Return loss for 2x2 array, $3^{rd}$ layout [dB], (FDTD simulation)

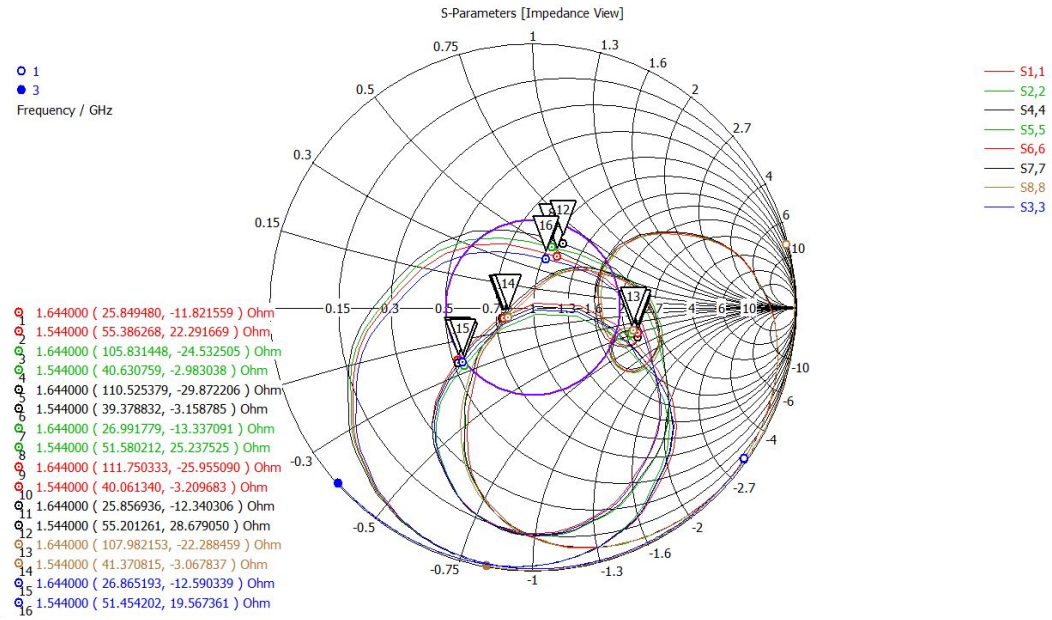


**Figure B.33:** Return loss for 2x2 array, $3^{rd}$ layout (Impedance Smith Chart), (FDTD simulation)

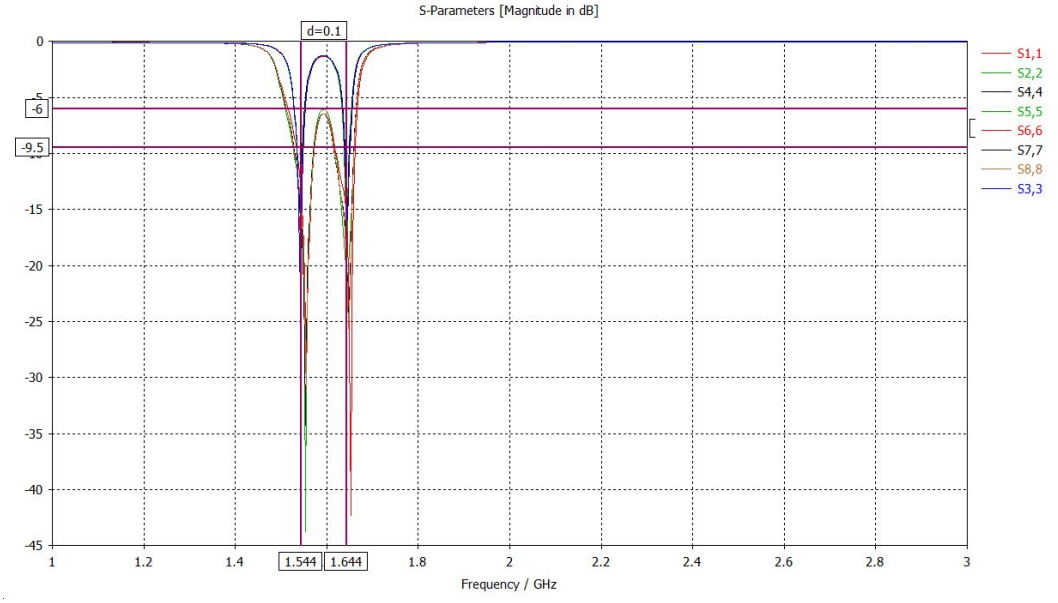


**Figure B.34:** Return loss for 2x2 array, $3^{rd}$ layout [dB], (Method of moments simulation)

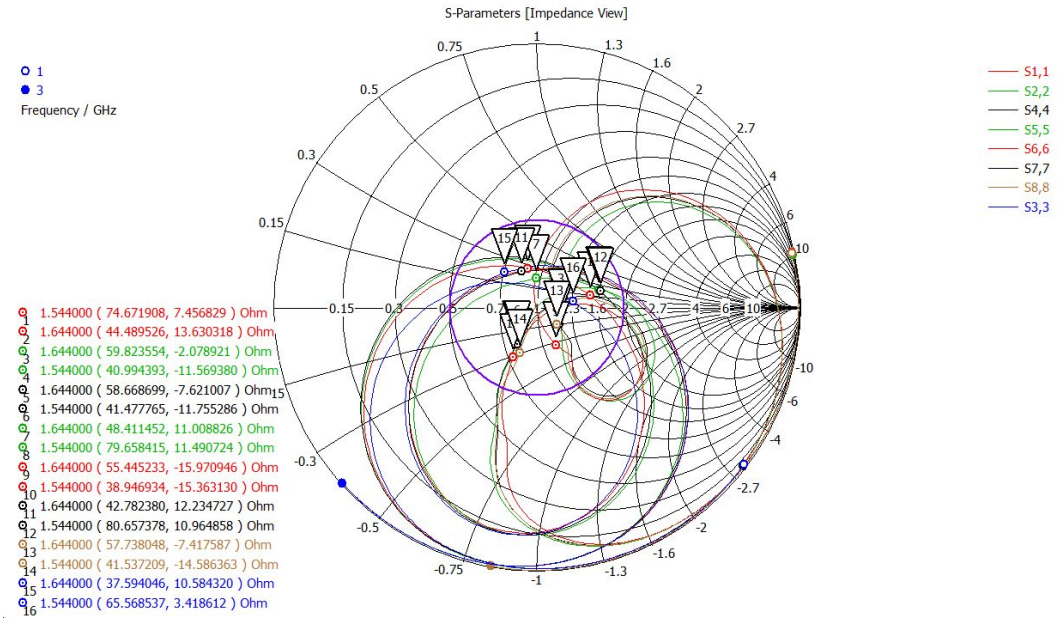


**Figure B.35:** Return loss for 2x2 array, $3^{rd}$ layout (Impedance Smith Chart), (Method of moments simulation)

| Frequency [GHz] | 1.525 | 1.544 | 1.559 | 1.626 | 1.644 | 1.660 |
|---|---|---|---|---|---|---|
| Realized Gain [dBi] | 5.68 | 6.03 | 5.3 | 5.81 | 4.93 | 1.94 |
| Radiation Efficiency [dB] | -0.7 | -0.46 | -0.36 | -1.16 | -1.8 | -2.56 |
| Total Efficiency [dB] | -1.31 | -1.02 | -1.77 | -1.48 | -2.35 | -5.32 |
| Axial Ratio [dB] | < 5 | < 3 | < 2 | < 4 | < 4.5 | < 4 |

**Table B.13:** Results for the 2x2 array (Method of Moments simulation), $3^{rd}$ layout

### B.2.2 2x2 array $4^{th}$ layout

The fourth design is similar to the third one, but it slightly overlaps the antennas, enlarging the distance from the side of the patch to the side of the board in length. The position of the elements on the board is represented in Figure **??**.

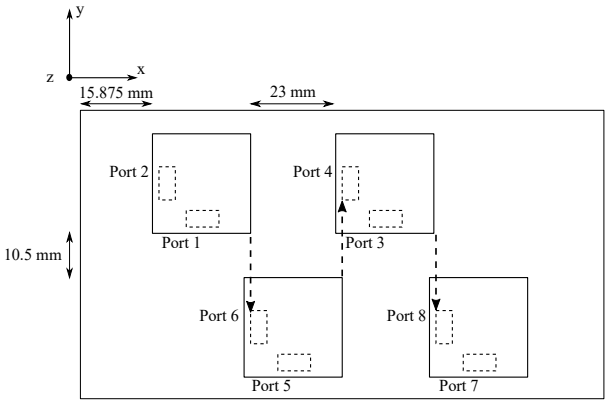


**Figure B.36:** Spread placing of the 2x2 array (top view)

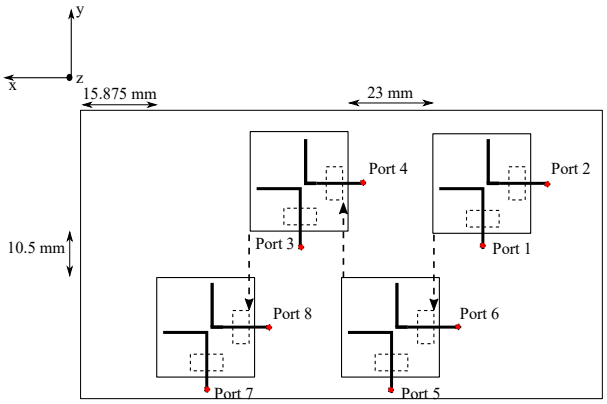


**Figure B.37:** Spread placing of the 2x2 array (bottom view)

The results in terms of return loss and coupling coefficients are similar to the one in the third design, with value of the coupling coefficients under $-10$ dB.

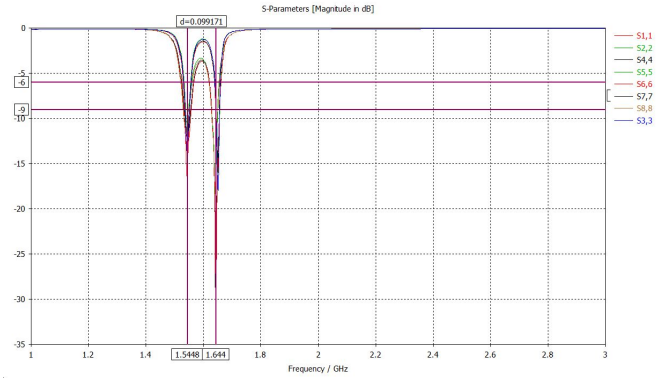


**Figure B.38:** Return loss for 4x4 array, $1^{st}$ layout [dB], (FDTD simulation)

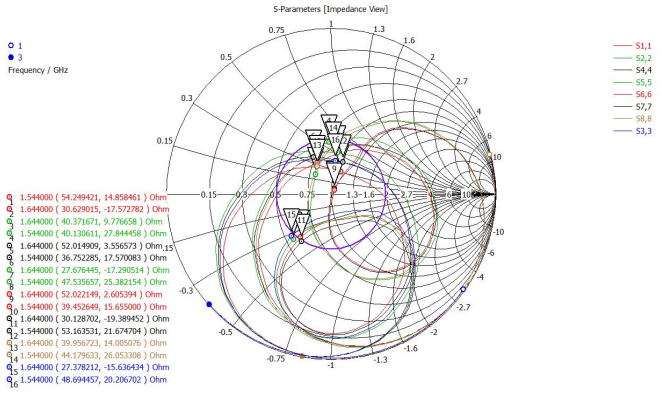


**Figure B.39:** Return loss for 4x4 array, $4^{th}$ layout (Impedance Smith Chart), (FDTD simulation)

Figures 4.29 and 4.30shows the return loss in dB and on the Smith chart for the 2 x 2 array, obtained in the FDTD simulation. The frequency markers are fixed on the center frequency of each band, 1544 MHz and 1644 MHz respectively. The return loss show a narrower band for the odd ports, that is for the low band only 10 MHz bandwidth from 30 MHz is covered with a VSWR 2:1, 25 MHz of the bandwidth is covered with a VSWR 3:1, while the rest of the bandwidth is covered with a VSWR 6:1. In case of the high band, only 5 MHz bandwidth from 30 MHz is covered with a VSWR 2:1, 15 MHz of the bandwidth is covered with a VSWR 3:1, while the rest of the bandwidth is covered with a VSWR 6:1. This can be also noticed in the results, where the total efficiency

decreases with up 2$dB$ towards the limits of the bands and has show a low loss for the center of the band.

Figures B.38 and B.39shows the return loss in dB and on the Smith chart for the 2 x 2 array, obtained in the Method of moments simulation. The frequency markers are fixed on the center frequency of each band, 1544 MHz and 1644 MHz respectively. The return loss show a narrower band for the odd ports, that is for the low band only 20 MHz bandwidth from 34 MHz is covered with a VSWR 2:1, 25 MHz of the bandwidth is covered with a VSWR 3:1, while the rest of the bandwidth is covered with a VSWR 6:1. In case of the high band 20 MHz of the bandwidth is covered with a VSWR 3:1, while the rest of the bandwidth is covered with a VSWR 6:1. This can be also noticed in the results, where the total efficiency decreases with up 2$dB$ towards the limits of the bands and has show a low loss for the center of the band.

| Frequency [GHz] | 1.525 | 1.544 | 1.559 | 1.626 | 1.644 | 1.660 |
|---|---|---|---|---|---|---|
| Realized Gain [dBi] | 4.71 | 6.29 | 6.17 | 6.11 | 6.42 | 4.38 |
| Radiation Efficiency [dB] | -1.11 | -0.86 | -0.69 | -0.56 | -0.96 | -1.5 |
| Total Efficiency [dB] | -2.5 | -0.99 | -1.16 | -1.4 | -1.22 | -3.3 |
| Axial Ratio [dB] | < 6.5 | < 5.5 | < 4 | < 3 | < 5 | < 6 |

**Table B.14:** Results for the 2x2 array (FDTD simulation), $4^{th}$ layout

| Frequency [GHz] | 1.525 | 1.544 | 1.559 | 1.626 | 1.644 | 1.660 |
|---|---|---|---|---|---|---|
| Realized Gain [dBi] | 5.19 | 6.25 | 6.01 | 6 | 5.87 | 3.62 |
| Radiation Efficiency [dB] | -0.87 | -0.64 | -0.47 | -0.91 | -1.51 | -2.17 |
| Total Efficiency [dB] | -1.95 | -0.99 | -1.3 | -1.5 | -1.73 | -4.02 |
| Axial Ratio [dB] | < 5.5 | < 4 | < 3 | < 3 | < 5 | < 6 |

**Table B.15:** Results for the 2x2 array (Method of Moments simulation),$4^{th}$ layout

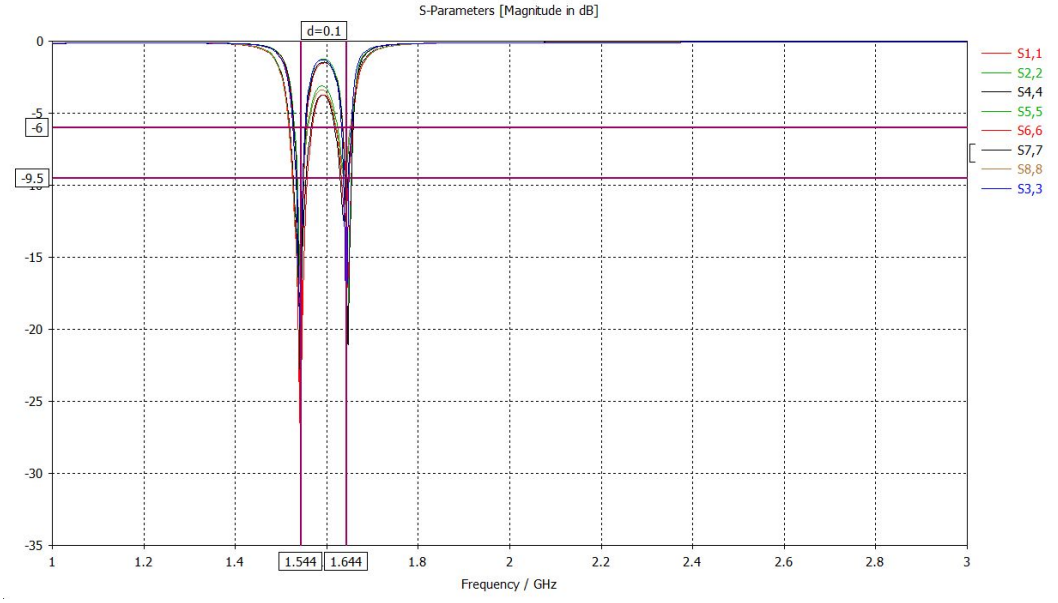


**Figure B.40:** Return loss for 4x4 array, $1^{st}$ layout [dB], (Method of Moments simulation)

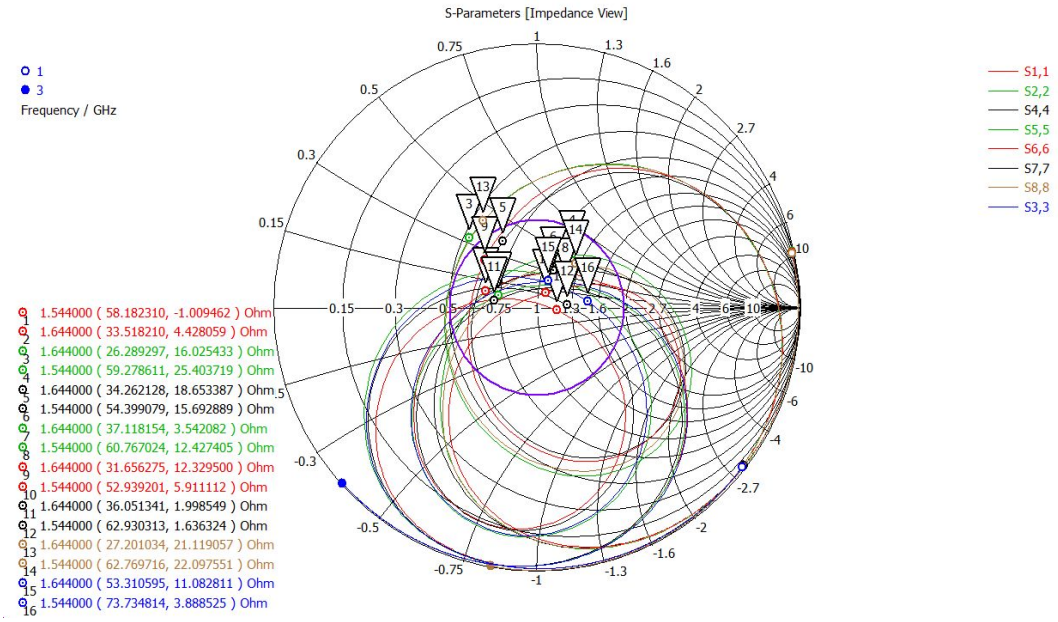


**Figure B.41:** Return loss for 4x4 array, $4^{th}$ layout (Impedance Smith Chart), (Method of Moments simulation)

## B.3 Further development

### B.3.1 1 x 2 array

The linear array has been simulated on a lower permittivity substrate (see Figure B.42), $\epsilon_r = 4.4$, and the obtained results are shown in

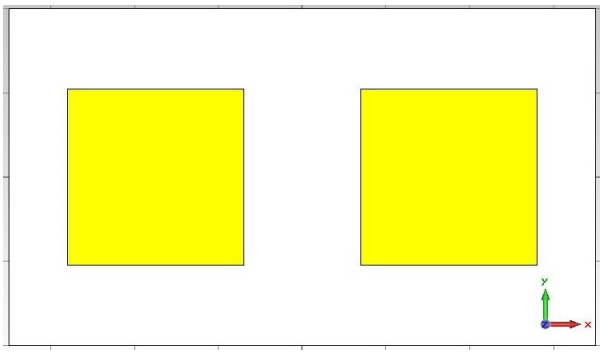

**Figure B.42:** 1 x 2 array printed on a Preperm L440 substrate with a permittivity of $\epsilon_r$ = 4.4

| Frequency [GHz] | 1.525 | 1.544 | 1.559 | 1.626 | 1.644 | 1.660 |
|---|---|---|---|---|---|---|
| Realized Gain [dBi] | 6.02 | 5.44 | 4.59 | 4.5 | 5.4 | 6.24 |
| Radiation Efficiency [dB] | -0.4 | -0.39 | -0.36 | -0.28 | -0.38 | -0.6 |
| Total Efficiency [dB] | -1.2 | -1.85 | -2.7 | -3.11 | -2.26 | -1.47 |
| Axial Ratio [dB] | 6 | 5 | 4 | 3.5 | 4 | 4 |

**Table B.16:** Results for 1 x 2 array simulated with a substrate Preperm 400, $\epsilon_r = 4.4$

### B.3.2 2 x 2 array, $1^{st}$ design

One of the cause of mutual coupling is surface waves which propagate within the substrate [31]. Therefore, cutting a part of the substrate between the array elements could represent a way of decreasing the mutual coupling.

In the first case, represented in Figure B.43, the values for the transmissions coefficients before and after the slot in the substrate are given in Table . Only the transmission coefficient of the ports that have shown high mutual coupling in the beginning (above - 10 dB) are given in the table.

| | S_{15} | S_{37} | S_{26} | S_{48} |
|---|---|---|---|---|
| Before | -7.26 | -7.26 | -6 | -6 |
| After | -7.76 | -7.76 | -6.46 | -6.46 |

**Table B.17:** Transfer coefficients for 2 x 2 array when a part of the dielectric is removed on the $x - axis$

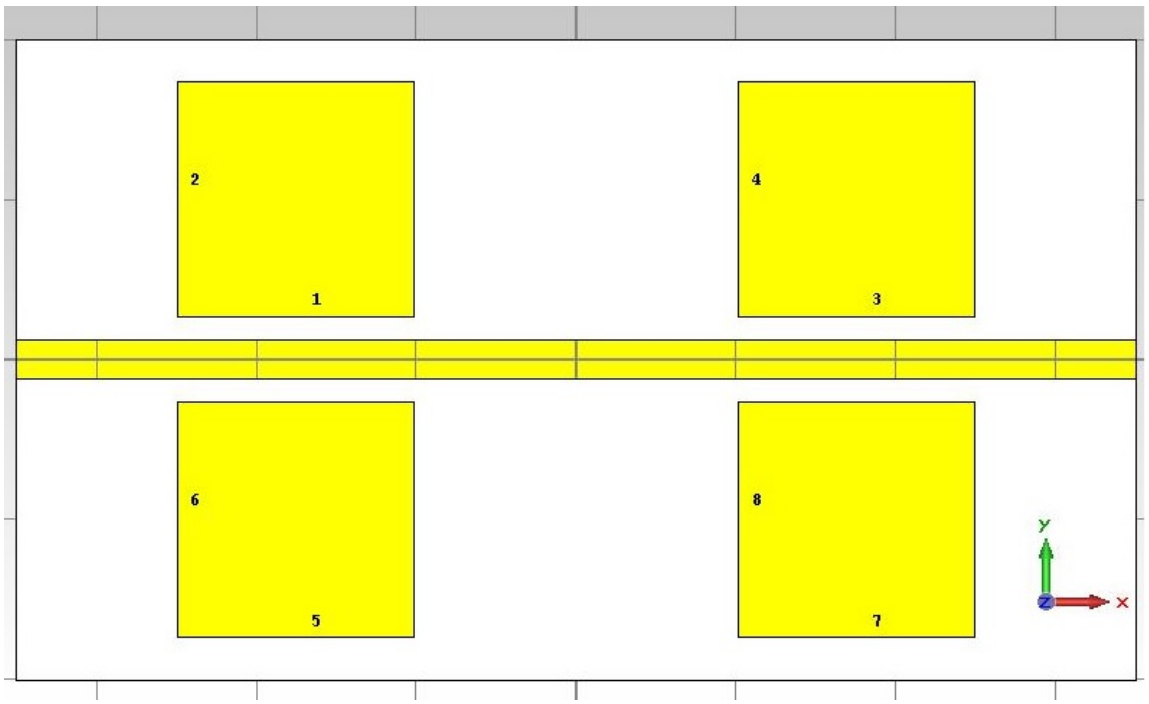


**Figure B.43:** Horizontal cut in the substrate for reducing mutual coupling

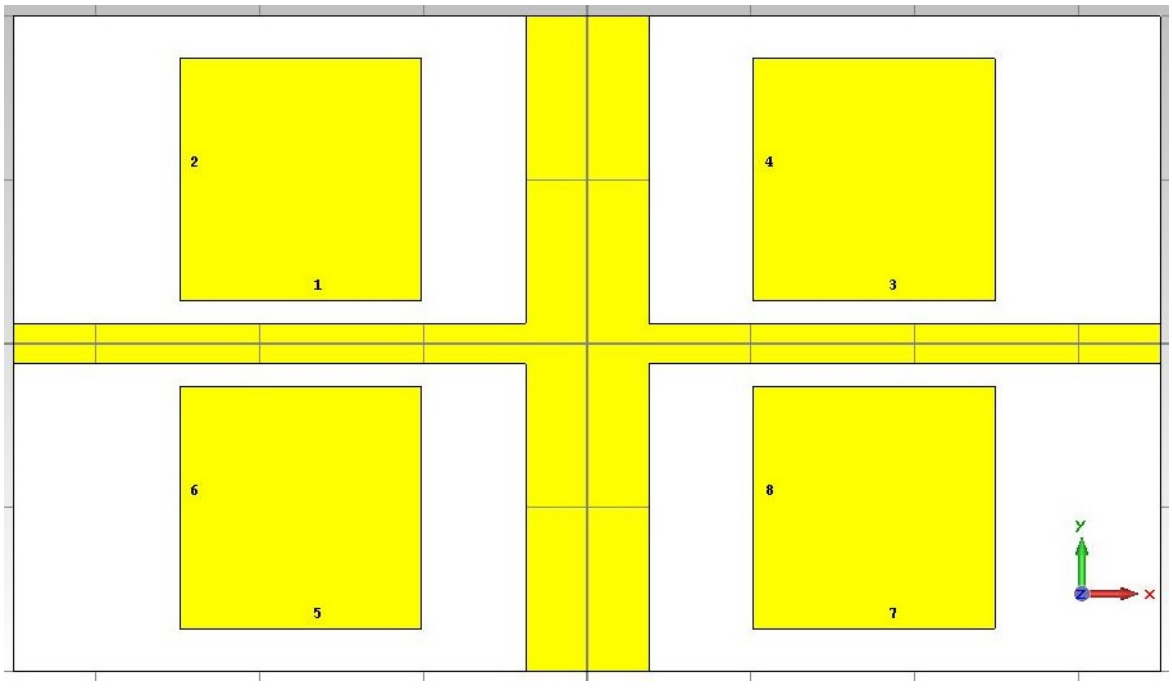


**Figure B.44:** Horizontal and vertical cut in the substrate for reducing mutual coupling

| | S_{15} | S_{37} | S_{26} | S_{48} |
|---|---|---|---|---|
| Before | -7.26 | -7.26 | -6 | -6 |
| After | -7.9 | -7.9 | -6.5 | -6.5 |

**Table B.18:** Transfer coefficients for 2 x 2 array when two parts of the dielectric is removed on the $x - axis$ and $y - axis$

## B.4 Mutual coupling

Figures B.45 and B.46 show the mutual coupling between two patches while varying the substrate permittivity from 5 to 10. The position of the patches is the one of the elements 1 and 3 from the 2x2 array, $1^{st}$ layout, with an edge to edge separation of 10.5 mm. It can be seen that for a substrate permittivity lower that 8, the mutual coupling is higher for the E-plane. From values greater than 8, the E-plane mutual coupling settles while the H-plane mutual coupling increases.

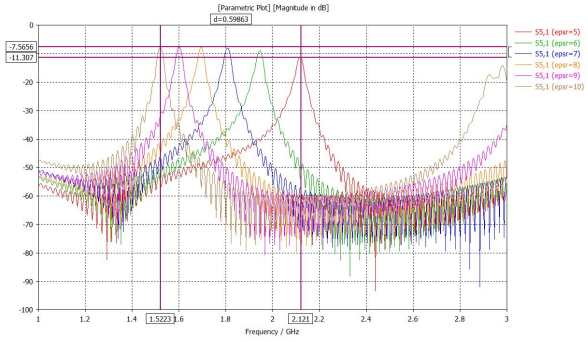


**Figure B.45:** Coupling coefficients between ports in E-plane with an edge to edge separation of 10.5 mm for different values of the substrate permittivity ($h_s = 3mm$)

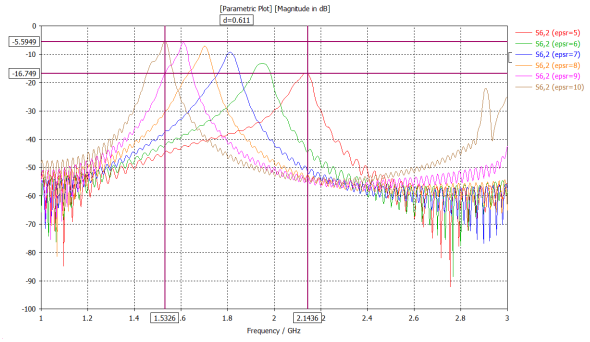


**Figure B.46:** Coupling coefficients between ports in H-plane with an edge to edge separation of 10.5 mm for different values of the substrate permittivity ($h_s = 3mm$)

## B.5 Circuit Modeling

The circuit modeling is performed in CST Design Studio, which imports automatically the model designed in CST Microwave studio and allows implementation of different subsystem. The matching, optimization and parameters sweep have been performed in this part of the simulation software. For the components of the matching circuit, the modeling can be performed in different ways. The blocks that are analyzed in this project, are only the one used in simulation *port*,*capacitor* and *inductor*.

The port block allows definition of the input impedance, which in this project was set to 50Ω.

The capacitor block has two model types. The first model is *Parasitic 1st Order Model*, which takes as input the values of the capacitance, the parasitic resistance and the parasitic inductance. The second model is *Parasitic SMD Model*, which is used in this project. This takes as input the values of the capacitance, the parasitic resistance, the parasitic inductance, the pad resistance and the pad capacitance. The equivalent circuit as modeled by the program is shown in Figure (put draw and reference.) In all the simulations the parasitic inductance and the capacitance of the pad are considered to have the value 0, while the pad resistance is the default one given by the program with a value of $1M\Omega$.

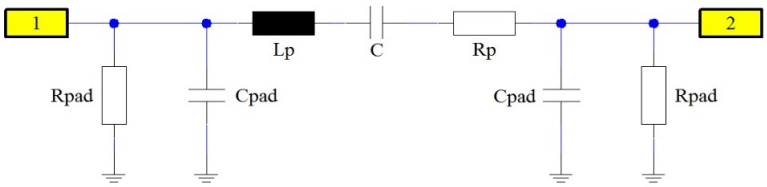


**Figure B.47:** SMD Model for capacitor (Source: [68])

The inductor block has three model types. The first model is *Parasitic 1st Order Model*, which takes as input the values of the inductance, the parasitic resistance and the parasitic capacitance. The second model is *Parasitic SMD Model*, which is almost the same as described for the capacitor block. This takes as input the values of the inductance, the parasitic resistance, the parasitic capacitance, the pad resistance and the pad capacitance. The equivalent circuit as modeled by the program is shown in Figure (put draw and reference). In all the simulations the parasitic capacitance and the capacitance of the pad are considered to have the value 0, while the pad resistance is the default one given by the program with a value of $1M\Omega$. The third model of the inductor is the *Parasitic Q model*, which takes as inputs the value of the Q and the definition frequency of the Q. Given these inputs, the program computes the parasitic resistance as follows:

$$R_p = \frac{2\pi f_d}{Q_f} \tag{B.1}$$

where $f_d$ is the definition frequency, $R_p$ is the parasitic resistance and $Q_f$ is the quality factor at the defined frequency. As seen from the formula, it is important that the specified $Q_f$ to be defined at a frequency as close as possible to the working frequency as the program doesn't assume frequency variation. However, this occurs for real components and it will influence the radiation efficiency and thus the whole result. In this project, the models used for the inductor are the Parasitic SMD Model and the Parasitic Q model. It is very important that

the inputs of the components are considered for the working frequency as the program does not seem to make a frequency variation of these values.

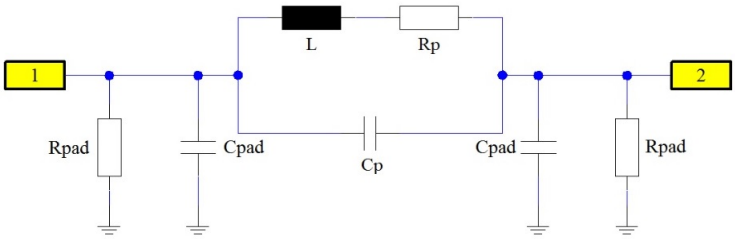


**Figure B.48:** SMD Model for inductor (Source: [68])

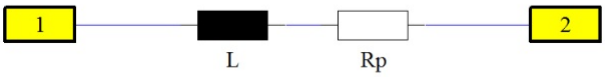


**Figure B.49:** Q Model for inductor (Source: [68])

As an example, for an inductor of $12nH$, in the general data sheet (ref to murata), the specifications are $R_p = 0.04\Omega$ and $Q = 80$. If the resistance is taken as the minimum one, of 0.04, by using equation B.1 at the working frequency of 1.6 GHz, this will result in an approximate $Q = 3000$, very far from the specified value of 80. Having a second look at a more detailed datasheet (put site description) and the Spice description of the component, see Figure B.50, assuming the frequency variation, the resistance increases $R_p = 1\Omega$ and $Q_f = 130$ for the working frequency of 1.6 GHz.

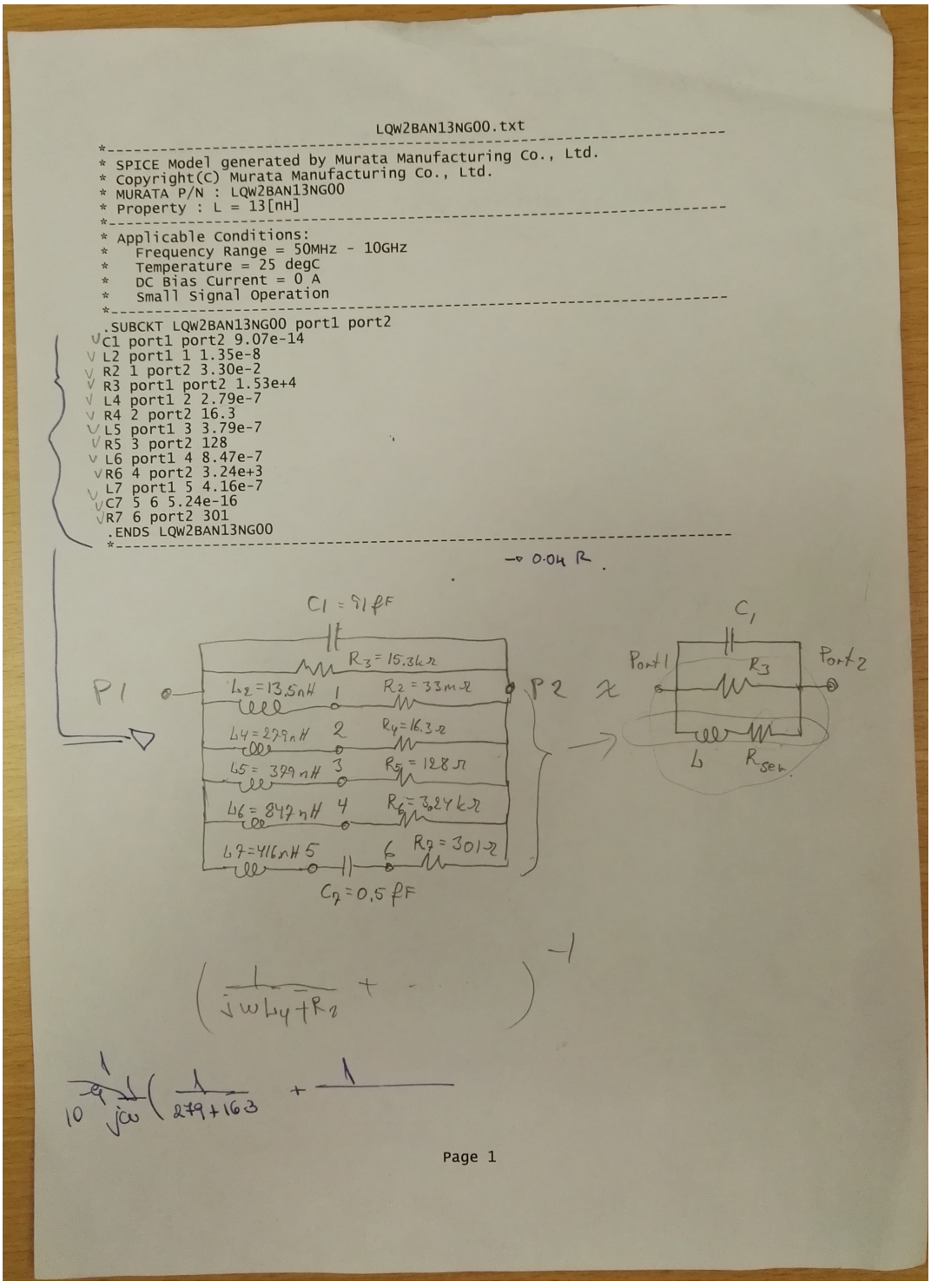


**Figure B.50:** Murata inductor equivalent circuit

## B.6 Yiled analysis

The yield analysis test the performance of the antenna in case of materials and components variations. In case of the material, the dielectric constant can vary, changing the resonance frequency, while in the case of the components, a variance in their values will result in poor matching.

### B.6.1 Dielectric constant variation

Both substrates used in this simulations report a variation of their dielectric constant. According to the data sheet, Preperm 900HF has an estimated tolerance of $\pm 0.45$ , while Rogers RO3006 has an estimated tolerance of $\pm 0.15$.

**First layout**

| Frequency [GHz] | 1.525 | 1.544 | 1.559 | 1.626 | 1.644 | 1.660 |
|---|---|---|---|---|---|---|
| Realized Gain [dBi] | 1.39 | 4.4 | 5.64 | 4.21 | 5.23 | 6.04 |
| Radiation Efficiency [dB] | -2 | -1.68 | -1.43 | -0.47 | -0.45 | -0.62 |
| Total Efficiency [dB] | -5.64 | -2.86 | -1.73 | -3.3 | -2.4 | -1.67 |
| Axial Ratio [dB] | 6 | 4.5 | 3 | 2.5 | 3 | 3.5 |

**Table B.19:** Results for 2x2 array , $1^{st}$ layout, $\epsilon_{Preperm}$ = 8.55, f=1.644

| Frequency [GHz] | 1.525 | 1.544 | 1.559 | 1.626 | 1.644 | 1.660 |
|---|---|---|---|---|---|---|
| Realized Gain [dBi] | 6.36 | 5.51 | 4.6 | 5.9 | 3.06 | -0.871 |
| Radiation Efficiency [dB] | -0.5 | -0.41 | -0.38 | -1.6 | -2.5 | -3.49 |
| Total Efficiency [dB] | -0.91 | -1.85 | -2.8 | -1.77 | -4.63 | -8.53 |
| Axial Ratio [dB] | 6 | 4.5 | 3 | 2.5 | 3 | 3.5 |

**Table B.20:** Results for 2x2 array , $1^{st}$ layout, $\epsilon_{Preperm}$ = 9.45, f=1.566

| Frequency [GHz] | 1.525 | 1.544 | 1.559 | 1.626 | 1.644 | 1.660 |
|---|---|---|---|---|---|---|
| Realized Gain [dBi] | 3.86 | 6.23 | 6.39 | 5.77 | 6.56 | 5.11 |
| Radiation Efficiency [dB] | -1.15 | -0.86 | -0.65 | -0.64 | -1.02 | -1.58 |
| Total Efficiency [dB] | -3.29 | -1.09 | -1 | -1.87 | -1.17 | -2.68 |
| Axial Ratio [dB] | 6 | 4.5 | 3 | 2.5 | 3 | 3.5 |

**Table B.21:** Results for 2x2 array , $1^{st}$ layout, $\epsilon_{Rogers}$ = 6, f=1.6

| Frequency [GHz] | 1.525 | 1.544 | 1.559 | 1.626 | 1.644 | 1.660 |
|---|---|---|---|---|---|---|
| Realized Gain [dBi] | 5.09 | 6.25 | 5.71 | 6.39 | 5.82 | 2.63 |
| Radiation Efficiency [dB] | -1.2 | -0.93 | -0.70 | -0.68 | -1.13 | -1.82 |
| Total Efficiency [dB] | -2.13 | -1.08 | -1.66 | -1.24 | -1.91 | -5.16 |
| Axial Ratio [dB] | 6 | 4.5 | 3 | 2.5 | 3 | 3.5 |

**Table B.22:** Results for 2x2 array , $1^{st}$ layout, $\epsilon_{Rogers}$ = 6.3, f=1.6

**Second layout**

| Frequency [GHz] | 1.525 | 1.544 | 1.559 | 1.626 | 1.644 | 1.660 |
|---|---|---|---|---|---|---|
| Realized Gain [dBi] | 1.42 | 4.49 | 5.67 | 4.04 | 4.78 | 5.77 |
| Radiation Efficiency [dB] | -1.95 | -1.62 | -1.41 | -0.51 | -0.43 | -0.51 |
| Total Efficiency [dB] | -5.74 | -2.87 | -1.77 | -3.5 | -2.89 | -2.03 |
| Axial Ratio [dB] | 6 | 4.5 | 3 | 2.5 | 3 | 3.5 |

**Table B.23:** Results for 2x2 array , $2^{nd}$ layout, $\epsilon_{Preperm}$ = 8.55, f=1.65

| Frequency [GHz] | 1.525 | 1.544 | 1.559 | 1.626 | 1.644 | 1.660 |
|---|---|---|---|---|---|---|
| Realized Gain [dBi] | 6.39 | 6.01 | 5.14 | 6.12 | 3.82 | 0.226 |
| Radiation Efficiency [dB] | -0.63 | -0.44 | -0.37 | -1.45 | -2.23 | -3.08 |
| Total Efficiency [dB] | -0.99 | -1.42 | -2.31 | -1.61 | -3.9 | -7.45 |
| Axial Ratio [dB] | 6 | 4.5 | 3 | 2.5 | 3 | 3.5 |

**Table B.24:** Results for 2x2 array , $2^{nd}$ layout, $\epsilon_{Preperm}$ = 9.45, f=1.566

| Frequency [GHz] | 1.525 | 1.544 | 1.559 | 1.626 | 1.644 | 1.660 |
|---|---|---|---|---|---|---|
| Realized Gain [dBi] | 3.72 | 6.16 | 6.56 | 5.79 | 6.71 | 5.79 |
| Radiation Efficiency [dB] | -1.14 | -0.87 | -0.70 | -0.52 | -0.88 | -01.39 |
| Total Efficiency [dB] | -3.55 | -1.25 | -0.92 | -1.89 | -1.09 | -2.08 |
| Axial Ratio [dB] | 6 | 4.5 | 3 | 2.5 | 3 | 3.5 |

**Table B.25:** Results for 2x2 array , $1^{st}$ layout, $\epsilon_{Rogers}$ = 6, f=1.6

| Frequency [GHz] | 1.525 | 1.544 | 1.559 | 1.626 | 1.644 | 1.660 |
|---|---|---|---|---|---|---|
| Realized Gain [dBi] | 6.36 | 5.51 | 4.6 | 5.9 | 3.06 | -0.871 |
| Radiation Efficiency [dB] | -0.5 | -0.41 | -0.38 | -1.6 | -2.5 | -3.49 |
| Total Efficiency [dB] | -0.91 | -1.85 | -2.8 | -1.77 | -4.63 | -8.53 |
| Axial Ratio [dB] | 6 | 4.5 | 3 | 2.5 | 3 | 3.5 |

**Table B.26:** Results for 2x2 array (FDTD simulation), $1^{st}$ layout, $\epsilon_{Rogers}$ = 6.3, f=

## B.6.2 Components tolerance

**First layout**

| Frequency [GHz] | 1.525 | 1.544 | 1.559 | 1.626 | 1.644 | 1.660 |
|---|---|---|---|---|---|---|
| Realized Gain [dBi] | 3.95 | 6.24 | 6.45 | 6.01 | 6.58 | 4.92 |
| Radiation Efficiency [dB] | -1.17 | -0.87 | -0.66 | -0.64 | -1.03 | -1.61 |
| Total Efficiency [dB] | -3.2 | -1.09 | -0.95 | -1.63 | -1.15 | -2.87 |
| Axial Ratio [dB] | 6 | 4.5 | 3 | 2.5 | 3.5 | 4 |

**Table B.27:** Results for 2x2 array , $1^{st}$ layout,all components $-2\%$, f=1.6

| Frequency [GHz] | 1.525 | 1.544 | 1.559 | 1.626 | 1.644 | 1.660 |
|---|---|---|---|---|---|---|
| Realized Gain [dBi] | 5.09 | 6.28 | 5.64 | 6.24 | 5.91 | 2.76 |
| Radiation Efficiency [dB] | -1.24 | -0.92 | -0.70 | -0.67 | -1.11 | -1.79 |
| Total Efficiency [dB] | -2.13 | -1.05 | -1.73 | -1.39 | -1.81 | -5.02 |
| Axial Ratio [dB] | 6 | 4.5 | 3 | 2.5 | 3.5 | 4 |

**Table B.28:** Results for 2x2 array , $1^{st}$ layout,all components +2%, f=1.6

# Appendix C

# Implementation and Prototype manufacturing

## C.1 First prototype

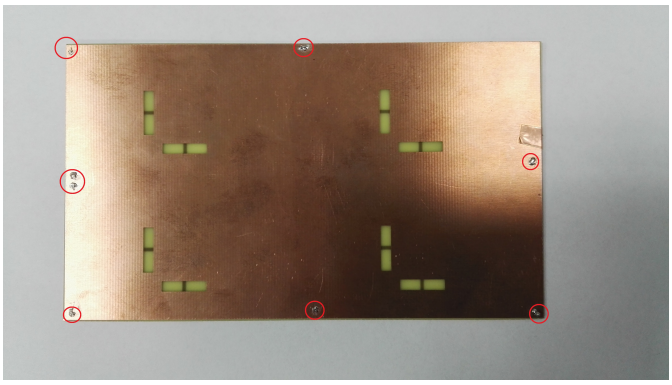

**Figure C.1:** Prototype feeding board, FR4, 140 x 80 mm (top view)

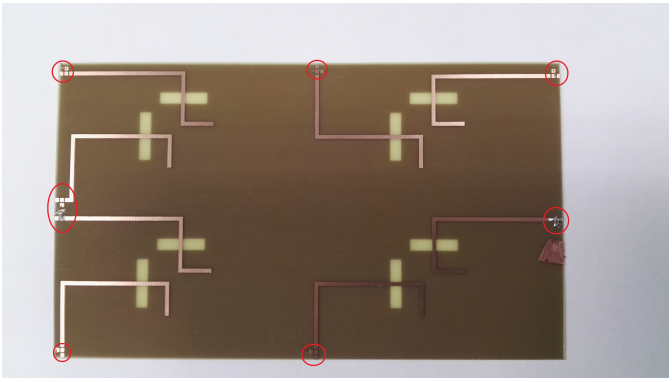

**Figure C.2:** Prototype feeding board, FR4, 140 x 80 mm (bottom view)

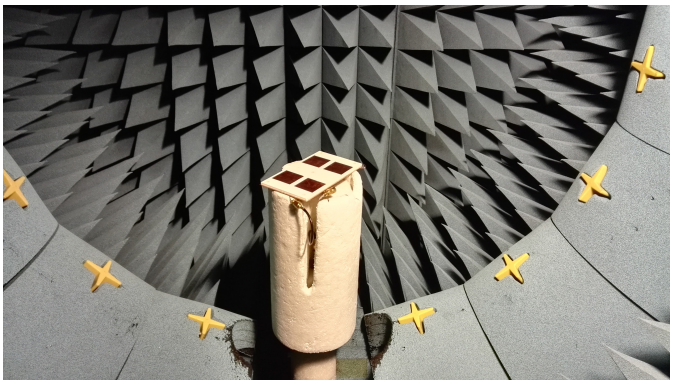

**Figure C.3:** Prototype measurement